PEOPLE'S DEMOCRATIC REPUBLIC OF ALGERIA

MINISTRY OF HIGHER EDUCATION

AND SCIENTIFIC RESEARCH

University of Echahid Hamma Lakhdar - El Oued

FACULITY OF EXACT SCIENCES

DEPARTMENT OF PHYSICS

Thesis Submitted in Partial Fulfilment of the Requirement for the Degree of

LMD Doctorate in Physics

Specialty: Applied Physics

Optical Properties of some Nonlinear Optical Materials

Presented by

AYACHI Mohammed Lakhdar

Thesis defended on

16/12/2023

Before the jury composed of

Pr. A. Medjouri	Echahid Hamma Lakhdar University (El Oued)	President
Dr. N. Meftah	Echahid Hamma Lakhdar University (El Oued)	Examiner
Dr. B. Tioua	Echahid Hamma Lakhdar University (El Oued)	Examiner
Pr. S. Douis	Kasdi Merbah University (Ouargla)	Examiner
Pr. A. Kaddour	CDER (Ghardaïa)	Examiner
Pr. M. Difallah	Echahid Hamma Lakhdar University (El-Oued)	Supervisor

2023-2024

Contents

List of Figures

List of Tables

Acknowledgments

I am immensely grateful to my advisor, Prof. Difallah Mosbah, for his unwavering support throughout my doctoral study and research. His patience, motivation, and profound knowledge have been invaluable to my academic journey. Furthermore, I extend my heartfelt appreciation to the Algerian Ministry of Higher Education and Scientific Research for their generous support, which has played a crucial role in the advancement of my studies.

I am deeply grateful for the invaluable support and encouragement I have received from Prof. Benhaoua Boubaker and Dr. Rahal Achour. Their contributions have been of immense significance to the completion of this work. Special thanks to the members of the discussion committee, including Professor Abdelkader Medjouri, Chairman, and Drs. Tioua Belkheir, Nassima Meftah, Professor Al-Said Douis, and Professor Abdelmajid Kaddour, for graciously accepting to discuss my thesis with utmost confidence and honesty.

I would also like to extend my sincere gratitude to the late Dr. Athman Benhaoua, whose guidance and constant feedback have been instrumental in shaping this project. Though no longer with us, his impact on my research will always be remembered with utmost respect and appreciation.

Lastly, I would like to thank all the members of the VTRS lab for their support throughout this journey. Their assistance and guidance have been indispensable, and I am truly thankful for their collective efforts in helping me accomplish this endeavor.

Finally, I express my heartfelt gratitude to my parents and brothers for their unwavering support and encouragement throughout all aspects of my life. Their love and backing have been instrumental in shaping who I am today, and I am truly blessed to have them by my side.

Abstract

This study explores the linear and nonlinear optical characteristics of undoped and cobalt-doped tin oxide. We initially discuss electromagnetic wave propagation in vacuum and diverse media, emphasizing the material's response to external electromagnetic fields. Using the dipole oscillator model, we establish Kramers-Kronig relations, gaining a comprehensive understanding of linear optical susceptibility in the frequency domain. Subsequently, we investigate second and third-order nonlinear optical processes using the dipole oscillator model. After this theoretical examination, thin films of cobalt-doped tin oxide are fabricated via spray pyrolysis, with cobalt doping levels ranging from (0-5 at.% Co/Sn). X-ray diffraction analysis reveals a tetragonal crystalline structure consistent with the rutile type, particularly in the (211) plane. Linear spectroscopy in the 300-900 nm range shows a direct band gap energy between 3.74 to 3.79 eV and Urbach energy in the 0.64 1.1 eV range. The estimation of the non-linear refractive index n_2 and third-order nonlinear susceptibility ($\chi^{(3)}(\omega)$)is achieved through the self-Kerr effect. Results demonstrate a photon energy-dependent nonlinear susceptibility. The Sheik-Bahae model illustrated that nonlinear refractive index (NRI), $n_2 = 6.91 \times 10^{-8}$ cm^2/W, and two-photon absorption coefficient (TPA), $\beta = 3.63$ cm/W, have high values.

Keywords: Tin oxide, Electric dipole model, Nonlinear absorption coefficient, Nonlinear refractive index, Nonlinear optical susceptibility.

الملخص

في هذا العمل درسنا الخصائص الضوئية الخطية وغير الخطية لأكسيد القصدير المطعم وغير المطعم بالكوبالت.
حيث تم أولا دراسة انتشار الأمواج في الفراغ و المادة و التطرق لأهم المقادير الفيزيائية المهمة, وركزنا الدراسة على استجابة المادة للحقول الكهرومغناطيسية الخارجية بالاستخدام نموذج ثنائي القطب المهتز الذي يوضح علاقات كرامر و كرونش التي عرفنا من خلالها صيغة الاستجابة الكهربائية الضوئية للمادة في فضاء التواترات. ثم تعرفنا على عمليات مختلفة من الاستجابة غير الخطية للمادة من الرتبة الثانية و الثالثة في فضاء التواترات. بعد هذه الدراسة النظرية تم تحضير شرائح أكسيد القصدير المطعم بالكوبالت من (0-5 at.% Co/Sn)انعراج الأشعة السينية بين أن للشرائح بنية من نوع روتيل مع اتجاه نمو تفضيلي (211). أما الخصائص الضوئية حددت بمطيافية UV-VIS في المجال $300-900$ nm حيث كان العرض الطاقوي للحزمة الممنوعة يتراوح بين 3.74 إلى 3.79 eV وطاقة أورباخ تتراوح بين 0.64 إلى 1.1 eV . كما تم رسم منحنى تغيرات كل من قرينة الانكسار غير الخطية n_2 و الاستجابة غير الخطية من الرتبة الثالثة ($\chi^3(\omega)$) بدلالة طاقة الفوتونات اعتمادا على (*kerr sefl effect*). وبين نموذج (*Sheik-Bahae*) أن هذه المادة لديها معامل امتصاص غير خطي (TPA) $\beta = 3.63$ cm/W وقرينة انكسار غير خطية (*NRI*) ($n_2 = 6.91 \times 10^{-8}$ cm^{-2}/W) عاليتين في المجال المرئي.

الكلمات المفتاحية: أكسيد القصدير; نموذج ثنائي القطب المهتز; معامل الامتصاص غير الخطي; قرينة الانكسار غير الخطية; الاستجابة الضوئية غير الخطية.

Résumé

Cette étude explore les caractéristiques optiques linéaires et non linéaires de l'oxyde d'étain non dopé et dopé au cobalt. Nous discutons initialement de la propagation des ondes électromagnétiques dans le vide et divers milieux, en mettant l'accent sur la réponse du matériau aux champs électromagnétiques externes. En utilisant le modèle d'oscillateur dipolaire, nous établissons les relations de Kramers-Kronig, acquérant une compréhension approfondie de la susceptibilité optique linéaire dans le domaine fréquentiel. Ensuite, nous étudions les processus optiques non linéaires du deuxième et du troisième ordre en utilisant le modèle d'oscillateur dipolaire. Après cet examen théorique, des films minces d'oxyde d'étain dopé au cobalt sont fabriqués par pyrolyse par pulvérisation, avec des niveaux de dopage en cobalt allant de (0-5 % at. Co/Sn). L'analyse par diffraction des rayons X révèle une structure cristalline tétragonale conforme au type rutile, notamment dans le plan (211). La spectroscopie linéaire dans la plage de 300 à 900 nm montre une énergie de bande interdite directe entre 3.74 et 3.79 eV et une énergie d'Urbach dans la plage de 0.64 à 1.1 eV. L'estimation de l'indice de réfraction non linéaire n_2 et de la susceptibilité non linéaire du troisième ordre ($\chi^{(3)}(\omega)$) est réalisée grâce à l'effet auto-Kerr. Les résultats démontrent une susceptibilité non linéaire dépendante de l'énergie des photons. Le modèle de Sheik-Bahae illustre que l'indice de réfraction non linéaire (NRI), $n_2 = 6,91 \times 10^{-8}$ cm^2/W, et le coefficient d'absorption à deux photons (TPA), $\beta = 3.63$ cm/W, ont des valeurs élevées.

Mots clés: L'oxyde d'étain, Le modèle d'oscillateur dipolaire, Le coefficient d'absorption non linéaire, L'indice de réfraction non linéaire, Susceptibilité optique non linéaire.

General Introduction

In the ever-evolving realm of modern science and technology, a silent yet profound revolution has been quietly reshaping the landscape of optics and photonics. This revolution, known as nonlinear optics, represents humanity's unwavering pursuit of understanding the intricate dance between light and matter [1]. Its origins date back to the early 1960s, and since then, it has broken free from the constraints of conventional optics to explore a world where the behavior of light transcends linear expectations [2]. Nonlinear optics is an interdisciplinary discipline that intersects physics, engineering, and mathematics, fundamentally altering our perception of light's capabilities [3]. At its core, it delves into the intriguing interplay between light and matter, uncovering a plethora of astonishing phenomena that go beyond the simple linear relationship between incident light and its response [4]. The seeds of nonlinear optics were sown in the pioneering experiments of Arthur Schawlow and Charles Townes during the 1950s, laying the groundwork for laser development [5]. However, it wasn't until the 1960s that systematic exploration of nonlinear phenomena truly began, leading to the formulation of fundamental principles and groundbreaking applications [6]. A pivotal discovery in this field was second harmonic generation, where photons combine to generate new photons with unique properties [7]. This revelation challenged our understanding of optics, paving the way for diverse applications such as frequency-doubling lasers and coherent light sources across the electromagnetic spectrum [8].

Nonlinear optics has since evolved into a multifaceted discipline, giving rise to phenomena like optical parametric amplification, four-wave mixing, and soliton propagation [9]. These innovations have revolutionized fields ranging from telecommunications to quantum information processing and biomedical imaging [10]. The creation of ultra-short laser pulses has enabled advancements in ultrafast spectroscopy and the study of ultrafast processes in atomic and molecular systems [11].

Beyond its practical applications, nonlinear optics has found a profound place in the burgeoning field of quantum optics [12]. It enables the manipulation of individual photons and quantum states of light, fostering progress in quantum information

processing, cryptography, and sensing [13].

As we stand on the cusp of a new era, the revolution of nonlinear optics continues to unfold [14]. Researchers are relentlessly pushing the boundaries of what is achievable with light and matter, with ongoing developments in nonlinear photonic materials, novel optical configurations, and advanced theoretical frameworks [15]. The future holds the promise of even deeper impacts on diverse fields, including materials science, medicine, and renewable energy, as nonlinear optics continues to illuminate the path to unprecedented possibilities [16].

Semiconductor nonlinear optics in thin films is an intriguing and highly specialized field of research that focuses on understanding and harnessing nonlinear optical phenomena within the context of thin semiconductor layers [17]. In this unique realm, semiconductors are meticulously engineered into ultra-thin films, often just a few nanometers thick, to exploit their nonlinear optical properties. These thin films serve as a versatile platform for manipulating and controlling light-matter interactions, offering precise control over the intensity and propagation of light. Researchers in this field investigate phenomena such as nonlinear absorption, Kerr effect, and two-photon processes within these thin semiconductor layers [18]. The ability to engineer the thickness and composition of these films allows for tailoring their nonlinear response to specific applications. Semiconductor nonlinear optics in thin films has found applications in a wide range of areas, including integrated photonic devices, optical modulators, and sensors. Its unique properties and adaptability make it a promising avenue for advancing the field of optoelectronics and enabling innovative technologies for optical signal processing and communication [19].

The aims of this research lies in the utilization of a semi-empirical formula to investigate the nonlinear optical parameters of both undoped and cobalt-doped tin oxide. It is widely acknowledged that most materials exhibit third-order nonlinear susceptibility, as evidenced by the optical Kerr effect, even in a vacuum [20]. The selection of tin oxide was motivated by its ready availability in our laboratory and its classification within the Transparent Conductive Oxides (TCOs) family, known for its extensive applications in photonics. Furthermore, cobalt, as a transitional element, possesses three electrons in its outer shell that can be excited by incident light, making it an intriguing addition to our study. our work organized as follows:

The first chapter will commence by studying topics, beginning with electromagnetic waves in a vacuum, and then delving into the concept of polarization, including an exploration of its three types. Furthermore, we will examine the monochromatic nature of light and delve into the concept of energy density. Building on this foundational knowledge, we will then proceed to explore Maxwell's equations and

their applications in wave propagation across different media. In particular, our primary focus will be on how matter responds to external electromagnetic fields, and for this purpose, we will employ the dipole oscillator model to gain valuable insights from Kramers Kronig relations. This approach will enable us to comprehend optical susceptibility in the frequency domain and also investigate the intricate characteristics of laser pulses during their propagation through dispersive media. Throughout this chapter, we will encounter and meticulously analyze pivotal solutions for the wave equations within this contextual framework.

In the upcoming second chapter, we will delve into various aspects of nonlinear optical phenomena and processes. We will commence by discussing the concept of nonlinear susceptibility, which will be based on the classical anharmonic oscillator. Subsequently, our attention will shift to nonlinear optical processes in the frequency domain, where we will explore topics, including second harmonic generation, optical rectification, and the Pockels effect. We will strongly emphasize the importance of phase matching in the context of nonlinear phenomena and will introduce the optical parametric oscillation (OPO) effect, along with its applications. Towards the end of the chapter, we will delve even further into third-order nonlinear processes in the frequency domain, where we will investigate phenomena such as the Optical Kerr Effect, Intensity-Dependent Refractive Index, and related effects, including self-focusing, self-phase modulation, chirp frequency, four-wave mixing, and third harmonic generation, both within the framework of phase matching condition.

In the fourth chapter, we will delve into the experimental phase of our study. We will prepare thin films of tin oxide doped with varying percentage of cobalt and subsequently study their linear and nonlinear properties, by employ specific approximations.

In the end general conclusion summarize all important results in this work.

Bibliography

[1] Boyd, R. W. Nonlinear Optics (3rd ed.). Academic Press. (2008).

[2] Bloembergen, N. Nonlinear Optics. World Scientific. (1965).

[3] Sutherland, R. L. Handbook of Nonlinear Optics. CRC Press. (2003).

[4] Shen, Y. R. The Principles of Nonlinear Optics. Wiley .(1984).

[5] Schawlow, A. L., and Townes, C. H. Infrared and Optical Masers. Physical Review, 112(6), 19401949. (1958).

[6] Maker, P. D., and Terhune, R. W. Study of Optical Effects Due to an Induced Polarization Third Order in the Electric Field Strength. Physical Review, 137(3A), A801A818. (1965).

[7] Franken, P. A., Hill, A. E., Peters, C. W., and Weinreich, G. Generation of Optical Harmonics. Physical Review Letters, 7(4), 118119. (1961).

[8] Boyd, R. W., and Kleinman, D. A. Parametric Interaction of Focused Gaussian Light Beams. Journal of Applied Physics, 39(8), 35973639. (1968).

[9] Boyd, R. W. Nonlinear Optics: Second Harmonic Generation, Parametric Down-Conversion, and Optical Kerr Effect. Academic Press. (1986).

[10] Yariv, A., and Yeh, P. Photonics: Optical Electronics in Modern Communications. Oxford University Press. (1984).

[11] Weiner, A. M. (2011). Ultrafast Optics. Wiley.

[12] Walls, D. F., and Milburn, G. J. Quantum Optics (2nd ed.). Springer. (2008).

[13] Kok, P., Lee, H., and Dowling, J. P. Creation of Large Photon-Number Path Entanglement Conditional on Photodetection. Physical Review A, 65(5), 052104. (2007).

[14] Agrawal, G. P. Nonlinear Fiber Optics (4th ed.). Academic Press. (2006).

[15] Boyd, R. W. Nonlinear Optics: A Lecture Note and Reprint Volume. National Academies. (2003).

[16] Sipe, J. E., and Sheng, P. Properties of the Nonlinear Susceptibility in the Dynamical Theory of Nonlinear Light Scattering. Physical Review A, 33(4), 26342647.(1986).

[17] Kauranen, M., and Zayats, A. V. Nonlinear plasmonics. Nature Photonics, 6(11), 737748. (2012).

[18] Butet, J., and Martin, O. J. F. Optical second harmonic generation in plasmonic nanostructures: from fundamental principles to advanced applications. ACS Nano, 8(11), 1122211247. (2014).

[19] Kauranen, M., and Uchida, K. Nonlinear plasmonics. Nature Photonics, 8(7), 512513. (2014).

[20] S. Robertson, Optical Kerr efect in vacuum, Phys. Rev. A, vol. 100, no. 6, 063831, 2019.

Chapter 1

Electromagnetic Waves in Arbitrary Media

By 1831, many experiments had been performed to reveal electromagnetic interactions with matter. Among them, Faraday's experiments were significant. He observed that changing the magnetic induction field with time, such as the motion of a magnet, near a conductor wire can create a time-varying electric field [1]. Moreover, Ampere illustrated the opposite phenomenon, where a changing electric field in time, such as the motion of an electric charge in a conductor, generates an induction field. Scientists assert that both electric and magnetic induction fields are vector quantities that change in time and position and can be expressed mathematically in the following form: $\mathbf{B}(\mathbf{r}, t)$ and $\mathbf{E}(\mathbf{r}, t)$. However, the mathematical link between electricity and magnetism remained unknown until Maxwell's appearance [2].

In 1847, James Clerk Maxwell became fascinated by the actions of polarized lenses, and this sparked research activities that resulted in one of the most important discoveries of his time. He mathematically explained Faraday's and Ampere's observations and established the exact relationship between electricity and magnetism [3]. Maxwell asserted that light, electricity, and magnetism are of the same nature, which means that light is only an electromagnetic wave. One of the most significant achievements of eighteenth-century physics was Maxwell's formulation of a unified mathematical formula for electromagnetic waves in four partial differential equations that are local in fields and sources, implying a constant velocity in a vacuum, as demonstrated by experimental studies [4].

This chapter encompasses a comprehensive study of various aspects of electromagnetism. It begins by examining Maxwell's equations in a vacuum, which form the foundation of electromagnetic theory. The properties of light and the description of its propagation inside dielectric media are then explored, including Maxwell's equations adapted to the material's properties. Moreover, the chapter introduces an

electric dipole model that describes the material's response to light, shedding light on its behavior under electromagnetic fields. Additionally, it covers the Kramers-Kronig relations, which are essential in understanding the connection between the real and imaginary parts of the material's refractive index. Lastly, the chapter delves into the significant solutions of the wave equation in free space, offering valuable insights into the behavior of light as it interacts with matter. This discussion enriches our understanding of how electromagnetic waves propagate and interact in various environments. The four Maxwell's equations have following integral form

$$\oint \mathbf{E} \cdot \mathbf{ds} = \frac{Q}{\varepsilon_0} \tag{1.1}$$

$$\oint_c \mathbf{E} \cdot \mathbf{dl} = -\frac{d}{dt} \int_{S(c)} \mathbf{B}.\mathbf{ds} \tag{1.2}$$

$$\oint_s \mathbf{B} \cdot \mathbf{ds} = \mathbf{0} \tag{1.3}$$

$$\oint_c \mathbf{B} \cdot \mathbf{dl} = \mu_0 \mathbf{I} + \varepsilon_0 \mu_0 \frac{d}{dt} \int_{S(c)} \mathbf{E}.\mathbf{ds}. \tag{1.4}$$

Equations 1.1 and 1.3 are known as Gauss's laws, while equations 1.2 and 1.4 are associated with Faraday's and Ampere's laws, respectively. The symbols Q, ε_0, μ_0, and I represent electric charge, vacuum permittivity, magnetic permeability, and electric current, respectively [5]. Together, these four equations, with the equation describing the motion of a charge in an electromagnetic field

$$\mathbf{F} = q(\mathbf{E} + \mathbf{v} \times \mathbf{B}) \tag{1.5}$$

constitute the fundamental equations of classical electromagnetism.
Maxwell's equations describe the behavior of electric and induction fields and their interactions with charges and currents. In their integral form, the equations relate the fields to the sources of the fields (i.e., the charges and currents) through a set of four equations: Gauss's law for electric fields, Gauss's law for magnetic induction fields, Faraday's law, and Ampere's law.
In their local form, the integral equations are substituted by pure differential equations which describe the behavior of the fields at each point in space and time. To derive the local form of Maxwell's equations, we introduce charge and current densities which describe the distribution of charges and currents within a given region of space, respectively, [6]

$$Q = \int_V \rho(\mathbf{r}, t) dv, \tag{1.6}$$

$$\mathbf{I} = \int_s \mathbf{J}(\mathbf{r}, t) \mathbf{ds} \tag{1.7}$$

The symbol $\rho(\mathbf{r}, t)$ denotes the charge density which represents the amount of charge per unit volume at a given point in space and time. The symbol $\mathbf{J}(\mathbf{r}, t)$ denotes the current density which represents the flow of charge per unit surface area at a given point in space and time.
To obtain the local form of Maxwell's equations we substitute the charge and current densities into the integral equations and apply Gauss's and Stokes' theorems. Specifically, we take the divergence of Gauss's law for electric fields (equation 1.1) and Gauss's law for induction fields (Eq. 1.3), and apply Stokes' theorem to Faraday's law (Eq.1.2) and Ampere's law (Eq.1.4) [7].

$$\nabla \cdot \mathbf{E} = \frac{Q}{\varepsilon_0} \tag{1.8}$$

$$\nabla \times \mathbf{E} = -\frac{\partial \mathbf{B}}{\partial t} \tag{1.9}$$

$$\nabla \cdot \mathbf{B} = \mathbf{0} \tag{1.10}$$

$$\nabla \times \mathbf{B} = \mu_0 \mathbf{J} + \varepsilon_0 \mu_0 \frac{\partial \mathbf{E}}{\partial t} \tag{1.11}$$

Through these equations we can calculate the electric and induction fields from the charge and current densities. If we take the divergence of equation 1.11, we obtain the charge continuity equation

$$\nabla \cdot \mathbf{J} + \frac{\partial \rho}{\partial t} = 0 \tag{1.12}$$

This equation expresses the conservation of electric charge, stating that the rate of change of charge density at a point in space and time is equal to the divergence of the current density at that point. This continuity equation is a fundamental principle in electromagnetism and is important for understanding the behavior of electric circuits and electromagnetic waves.

1.1 Electromagnetic Waves in Vacuum

Maxwell's equations in vacuum, where there are no charges and currents densities, can be written as [8]

$$\nabla \cdot \mathbf{E} = 0 \tag{1.13}$$

$$\nabla \times \mathbf{E} = -\frac{\partial \mathbf{B}}{\partial t} \tag{1.14}$$

$$\nabla \cdot \mathbf{B} = 0 \tag{1.15}$$

$$\nabla \times \mathbf{B} = \varepsilon_0 \mu_0 \frac{\partial \mathbf{E}}{\partial t} \tag{1.16}$$

Applying curl to 1.14 and 1.16, we obtain

$$\nabla^2 \mathbf{E} - \mu_0 \varepsilon_0 \frac{\partial^2 \mathbf{E}}{\partial t^2} = \mathbf{0} \tag{1.17}$$

$$\nabla^2 \mathbf{B} - \mu_0 \varepsilon_0 \frac{\partial^2 \mathbf{B}}{\partial t^2} = \mathbf{0} \tag{1.18}$$

These are the wave equations for the electric and magnetic induction fields in vacuum. They show that the electric and magnetic induction fields propagate at the speed of light, which is equal to $1/\sqrt{\mu_0 \varepsilon_0}$. These wave equations have the plane wave solutions (linearly polarized)

$$\mathbf{B}(\mathbf{r}, t) = \tilde{B} \exp i(\mathbf{k}.\mathbf{r} - \omega t)\epsilon \tag{1.19}$$

$$\mathbf{E}(\mathbf{r}, t) = \tilde{E} \exp i(\mathbf{k}.\mathbf{r} - \omega t)\epsilon \tag{1.20}$$

where $\tilde{B}, \tilde{E}, \mathbf{k}, \omega, \epsilon$ denote the induction and electric amplitudes, wave vector, wave frequency and polarization vector, respectively. When we substitute these solutions into equations 1.19 and 1.20, we obtain the dispersion relation

$$-k^2 + \frac{\omega^2}{c^2} = 0. \tag{1.21}$$

1.1.1 Polarization

The wave equation of the electromagnetic field is a linear differential equation, and therefore, it obeys to the superposition principle

$$E_0 = E_1 e_1 + E_2 e_2, \tag{1.22}$$

where E_1, E_2 complex amplitudes take the following form

$$E_1 = |E_1| e^{i\delta_1}, E_2 = |E_2| e^{i\delta_2} \tag{1.23}$$

The kind of Polarization know from both phase difference δ_1, δ_2

1.1.1.1 Elliptic Polarization

$$\delta_1 \neq \delta_2$$

The real part of the electric field, $\mathbf{Re}(\mathbf{E}(\mathbf{r}, t))$ at r on an ellipse spanned by unit vectors e_1 and e_2.

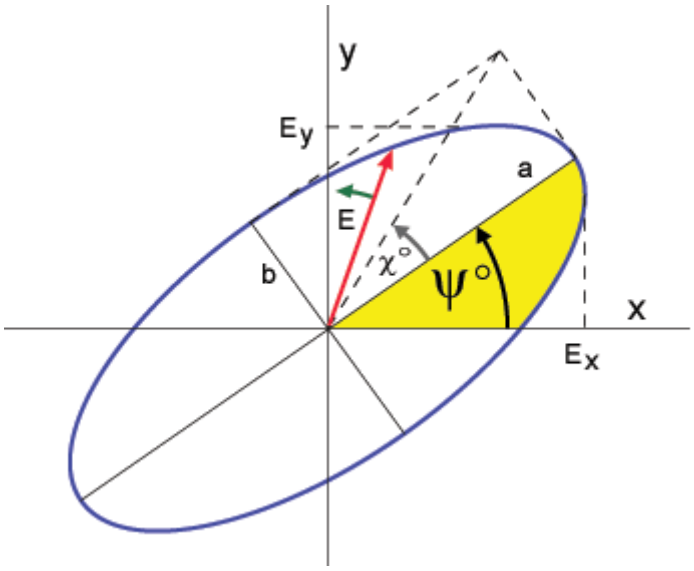

Fig.}1.1: Elliptical polarization [13]

where ψ is the angle between x direction and a axis and χ is the angle between a axis and the electric filed vector

1.1.1.2 Circular Polarization

$$\delta_1 = \delta_2 \pm \frac{\pi}{2}$$

The real part of the electric field, $\mathbf{Re}(\mathbf{E}(\mathbf{r}, t))$, can be rotating at r with a circular trajectory.

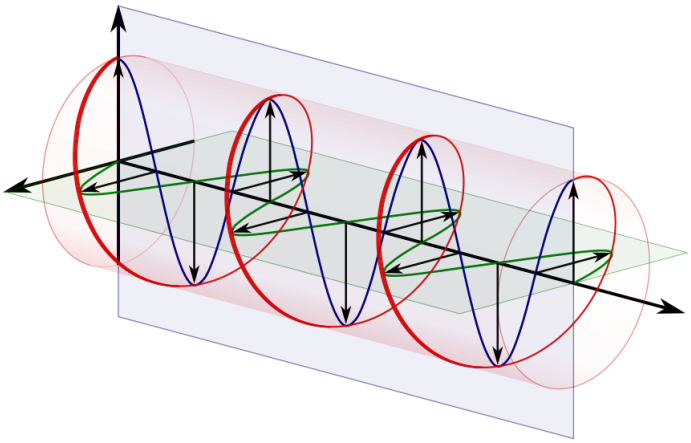

Fig.}1.2: Circular polarization [17].

1.1.1.3 Linear Polarization

The real part of the electric field $\mathbf{Re}(\mathbf{E}(\mathbf{r},t))$ may oscillate in a linear form without exhibiting any rotation so we fined.

$$\delta_1 = \delta_2 + n\pi$$

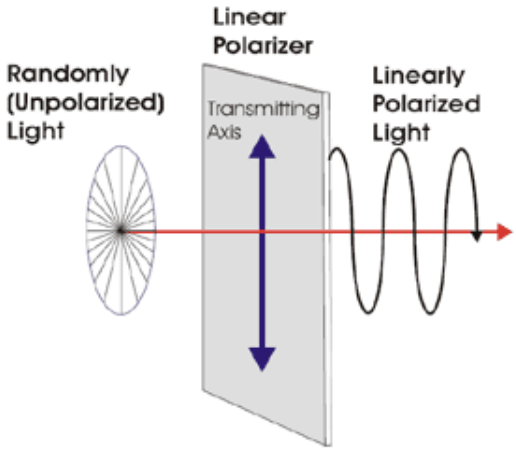

Fig.}1.3: Linear polarization [19].

1.1.2 Monochromatic Plane Waves in Vacuum

Rewriting the the solution of the wave equation as

$$\mathbf{E}(\mathbf{z},t) = \tilde{E}_0 \exp i(\mathbf{k}\cdot\mathbf{z} - \omega_0 t)\epsilon = \tilde{E}_0 \exp(i\phi(\mathbf{z},t)) \tag{1.24}$$

Here the frequency ω_0 is very specific and can be extracted from the phase $\phi(z,t)$. In general, the harmonic waves such as sinusoidal waves have ω frequency, where the differences in frequency value in visible range identical with different colors, this wave called monochromatic.

$$\text{frequency} = -\frac{\partial \phi}{\partial t} = \omega_0. \tag{1.25}$$

There exist other kind of wave having non-monochromatic, in this case the phase $\phi(z,t)$ contain other therm depend with time. So the solution of wave equation becomes.

$$\mathbf{E}(\mathbf{z},t) = \tilde{E}_0 \exp i(\mathbf{k}\cdot\mathbf{z} - \omega_0 t + \delta(t))\epsilon = \tilde{E}_0 \exp(i\phi(\mathbf{z},t)) \tag{1.26}$$

meaning that the frequency depend with time.

$$\text{frequency} = -\frac{\partial \phi}{\partial t} = \omega_0 \pm \frac{\partial \delta(t)}{\partial t} \tag{1.27}$$

Assuming monochromatic wave move over "z" direction and independent with "x, y" directions, so write the following form.

$$\mathbf{B}(\mathbf{z},t) = \tilde{B}_0 \exp i(\mathbf{k}.\mathbf{z} - t)\epsilon = \tilde{B}_0 \exp(i\phi(\mathbf{z},t)) \tag{1.28}$$
$$\mathbf{E}(\mathbf{z},t) = \tilde{E}_0 \exp i(\mathbf{k}.\mathbf{z} - \omega t)\epsilon = \tilde{E}_0 \exp(i\phi(\mathbf{z},t)) \tag{1.29}$$

where $\tilde{B}, \tilde{E}$ complex induction and electric amplitudes, respectively. Maxwell equations imposes additional conditions on $\tilde{B}_0, \tilde{E}_0$ given that

$$\begin{aligned}
\nabla\cdot\mathbf{E} &= 0, && (1.30)\\
\nabla\cdot\mathbf{B} &= 0 && (1.31)\\
\nabla\cdot\mathbf{E}(\mathbf{z},t) &= \tilde{E}_{0z}(ik\cdot\epsilon)\exp i(\mathbf{k}\cdot\mathbf{z} - \omega t) = 0 && (1.32)\\
\nabla\cdot\mathbf{B}(\mathbf{z},t) &= \tilde{B}_{0z}(ik\cdot\epsilon)\exp i(\mathbf{k}\cdot\mathbf{z} - \omega t) = 0 && (1.33)
\end{aligned}$$

which means that the electromagnetic wave is transverse to the propagation direction. Also can shows that electric and induction field waves and the wave vector form an orthogonal trihedron 1.9. Moreover, the following expression

$$\mathbf{B}(\mathbf{z},t) = \frac{\tilde{E}_0}{\omega}(k\times\epsilon)\sin(\mathbf{k}\cdot\mathbf{z} - \omega t + \delta), \tag{1.34}$$

via Eq (1.33), shows the amplitude of induction field is $\mathbf{B}(\mathbf{z},t) = \tilde{E}_0/c$.

1.1.3 Energy density of electromagnetic waves

Electromagnetic waves contain energy that flows as they propagate. The energy density of electromagnetic fields in a vacuum can be calculated using the following formula [12]

$$u = \frac{1}{2}\left[\epsilon_0|\mathbf{E}|^2 + \frac{1}{\mu_0}|\mathbf{B}|^2\right] \tag{1.35}$$

$$= \epsilon_0\tilde{E}_0^2\sin^2(\mathbf{k.z} - \omega t + \delta). \tag{1.36}$$

Taking the average of the fast oscillations (i.e., $\langle\sin^2\rangle = \frac{1}{2}$), we can rewrite the time-averaged energy density.

$$\langle u\rangle = \frac{1}{2}\epsilon_0\tilde{E}_0^2. \tag{1.37}$$

We can also express the time-averaged energy density as a function of the photon density n_{ph} (number of photons per unit volume)

$$n_{ph} = \frac{dN_{ph}}{dV}. \tag{1.38}$$

Since each photon carries an amount of energy that is equal to $\hbar\omega$, we can write

$$\langle u\rangle = n_{ph}\hbar\omega. \tag{1.39}$$

By comparing equation 1.37 with equation 1.39, we can obtain the absolute value of the electric field amplitude.

$$|\tilde{E}| = \sqrt{\frac{2n_{ph}\hbar\omega}{\epsilon_0}} \tag{1.40}$$

Calling the Poynting vector which describes the instantaneous transport of energy in space

$$\mathbf{S} = \frac{1}{\mu_0}\mathbf{E}\times\mathbf{B} = \epsilon_0 c\frac{\mathbf{k}}{k}\tilde{E}^2\sin^2(\mathbf{k}\cdot\mathbf{r} - \omega t + \delta). \tag{1.41}$$

We take its time average which is used to quantify radiation intensity

$$I = \frac{1}{2}\epsilon_0 c\tilde{E}^2 = cn_{ph}\hbar\omega \tag{1.42}$$

This result is directly proportional to the photon flux intensity (cn_{ph}). The radiation intensity is the amount of field energy transported per unit area per unit time.

1.1.4 Important Approximate Solutions to Wave Equations

Starting from the wave equation (1.17) and assuming that the electric field is monochromatic, ie has a time dependence $e^{i\omega t}$. Then the wave equation collapses into the Helmholtz equation, Now we will study some important cases in wave propagation [13].

$$\left(\nabla^2 + \frac{1}{c^2}\frac{\partial^2}{\partial t^2}\right)\mathbf{E}(\mathbf{r},t) = 0. \tag{1.43}$$

Consider that the electric field is monochromatic

$$\mathbf{E}(\mathbf{r},t) = \mathbf{E}(\mathbf{r})\, e^{i\omega t} \tag{1.44}$$

with

$$\mathbf{E}(\mathbf{r}) = E_0 e^{i(\mathbf{k}\cdot\mathbf{r}+\phi_0)} \tag{1.45}$$

for plane waves. Plugging (1.45) into 1.44 gives the Helmoholtz equation

$$\left(\nabla^2 + k^2\right)\mathbf{E}(\mathbf{r}) = 0, \quad k = \frac{\omega}{c} \tag{1.46}$$

which is equivalent to an eigenvalue equation in quantum mechanics

$$\left(-\nabla^2\right)\mathbf{E}(\mathbf{r}) = \frac{\omega^2}{c^2}\mathbf{E}(\mathbf{r}). \tag{1.47}$$

The plane waves $e^{i\mathbf{k}\cdot\mathbf{r}}\mathbf{e}_\sigma$ are special solutions to the equation (1.46). If we focus on one polarization, the scalar Helmholtz equation follows for the field amplitude

$$\left(\nabla^2 + k^2\right)\mathbf{E}_0(\mathbf{r}) = 0. \tag{1.48}$$

In spherical coordinates the Laplacian reads

$$\nabla^2 = \frac{1}{r^2}\frac{\partial}{\partial r}\left(r^2\frac{\partial}{\partial r}\right) + \frac{1}{r^2\sin\theta}\frac{\partial}{\partial\theta}\left(\sin\theta\frac{\partial}{\partial\theta}\right) + \frac{1}{r^2\sin^2\theta}\frac{\partial^2}{\partial\phi^2}$$

The solution to the wave equation takes the form of a spherical wave

$$\mathbf{E}_0(\mathbf{r}) = A\frac{e^{ikr}}{r} \tag{1.49}$$

with a constant A satisfies the scalar Helmholtz equation in spherical coordinates. The wave fronts are spherical shells with a radial distance of $\lambda = 2\pi/k$, which propagate radially with the phase velocity c. The spherical waves can be simplified under certain circumstances. To do this, we consider a spherical wave that propagates

from the origin of coordinates at a location near the z-axis, so that the condition $\rho = \sqrt{x^2 + y^2} \ll z$ is fulfilled.

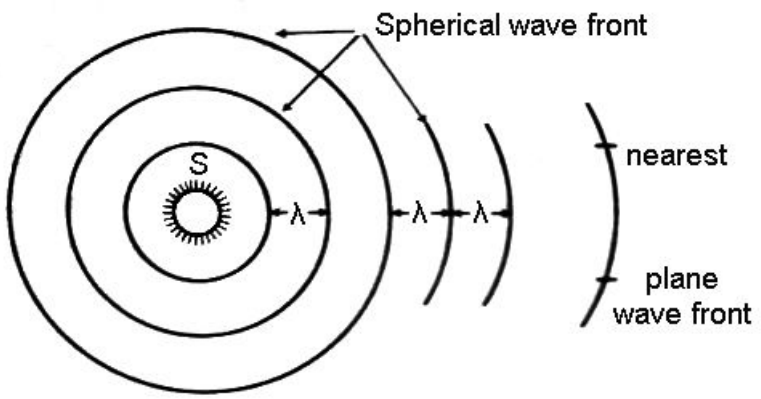

Fig.}1.4: Spherical wave front [22].

Then we develop

$$r = \sqrt{\rho^2 + z^2} \approx z \left(1 + \frac{\rho^2}{2z^2}\right) = z + \frac{\rho^2}{2z} \tag{1.50}$$

and then we substitute in the expression for the spherical wave. For the amplitude we consider that $\rho \simeq z$ and we get with

$$\mathbf{E}(\mathbf{r}) = \frac{A}{z} e^{i\mathbf{k}z} e^{ik\frac{\rho^2}{2z}} \tag{1.51}$$

the so-called Fresnel approximation. Herein, the wave fronts are paraboloids, so that one also speaks of parabolic waves here. If the distance z becomes much larger, the spherical wave finally turns into a plane wave.

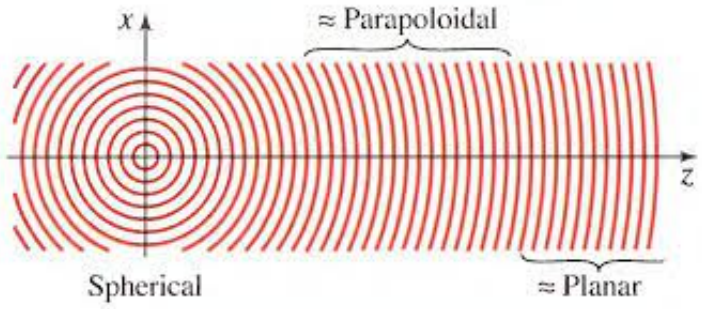

Fig.}1.5: Paraxial Helmholtz [31]

1.1.4.1 Paraxial Helmholtz equation

If the wave fronts change only slightly along z-direction, we may in good approximation consider it as a plane wave. We therefore start from a plane wave

$$\mathbf{E}_0(\mathbf{r}) = A(\mathbf{r})e^{ikz} \tag{1.52}$$

with slowly varying amplitude $A(\mathbf{r})$ of the position. By this we mean that the envelope $A(\mathbf{r})$ and its derivative with respect to z do not vary much within a wavelength $\lambda = 2\pi/k$ (this is the so-called slowly varying envelope approximation, or SVEA)

$$\frac{\partial A}{\partial z} \ll kA \quad \text{and} \quad \frac{\partial^2 A}{\partial z^2} \ll k^2 A \tag{1.53}$$

Inserting into Helmholtz equation

$$\begin{aligned}
\left(\nabla^2 + k^2\right) A(\mathbf{r})e^{ikz} &= \nabla_{\mathrm{T}}^2 A(\mathbf{r})e^{ikz} + \left(\frac{\partial^2}{\partial z^2} + k^2\right) A(\mathbf{r})e^{ikz} \\
&= \nabla_{\mathrm{T}}^2 A(\mathbf{r})e^{ikz} + \left(\frac{\partial^2 A}{\partial z^2} - k^2 A + 2ik\frac{\partial A}{\partial z} + k^2 A\right) e^{ikz} \\
&\overset{\text{SVEA}}{\simeq} \nabla_{\mathrm{T}}^2 A(\mathbf{r})e^{ikz} + 2ik\frac{\partial A}{\partial z}e^{ikz}.
\end{aligned}$$

Thus we obtain the paraxial Helmholtz equation

$$\left(\frac{\partial^2}{\partial x^2} + \frac{\partial^2}{\partial y^2}\right) A(\mathbf{r}) + +2ik\frac{\partial}{\partial z}A(\mathbf{r}) = 0. \tag{1.54}$$

It also possible to verify that the parabolic waves (1.51) are even solutions of paraxial Helmholtz equation (1.54).

1.1.4.2 Gaussian Beams

Another class of solutions to the paraxial Helmholtz equation is found by replacing $z \to q(z) = z - iz_0$, with a constant z_0, in the parabolic wave

$$\mathbf{E}_0(\mathbf{r}) = \frac{A}{q(z)}e^{i\mathbf{k}(z-iz_0)}e^{i\mathbf{k}\frac{\rho^2}{q(z)}}. \tag{1.55}$$

The function $1/q(z)$ can be divided into real and imaginary parts,

$$\frac{1}{q(z)} = \frac{1}{R(z)} + i\frac{\lambda}{\pi\omega^2(z)} \tag{1.56}$$

where

$$W(z) = W_0\sqrt{1+\left(\frac{z}{z_0}\right)^2}, \quad W_0^2 = \frac{\lambda z_0}{\pi}, \quad R(z) = z\left[1+\left(\frac{z}{z_0}\right)^2\right]. \tag{1.57}$$

With the redefinition of the constant $A \longmapsto A/(iz_0)$ and the Gouy phase $\xi(z) = -\arctan\left(\frac{z}{z_0}\right)$, we then find for the complex amplitude

$$\mathbf{E}_0(\mathbf{r}) = \frac{AW_0}{W(z)}.e^{-\frac{\rho^2}{q(z)}}\exp\left[ikz + ik\frac{\rho^2}{2R(z)} + i\xi(z)\right] \tag{1.58}$$

so intensity take the following form

$$I(\rho, z) = |A|^2\left(\frac{W_0}{W(z)}\right)^2\exp\left[-\frac{2\rho^2}{W^2(z)}\right] \tag{1.59}$$

which is Gaussian function of ρ for every z. The width of the beam is determined by $W(z)$, where at $z = 0$: $W(z = 0) = W_0$ the beam is narrowest with waist radius W_0, i.e., the spot size of the beam is $2W_0$. The Gaussian beam diverges during the propagation, where z_0 is the Rayleigh length characterizes the defocusing. The focal length at which the ray increases by a factor of $\sqrt{2}$ is twice the Rayleigh length

$$2z_0 = \frac{2\pi W_0^2}{\lambda}. \tag{1.60}$$

The wave fronts of the Gaussian beam are defined by the phase in (1.58), neglecting the z-dependence in $R(z)$ and $\xi(z)$, then the wave fronts are given by the relation $z + \rho^2/(2R) \approx$ const. This is an equation of a parabolic surface with radius of curvature R. The wave fronts are shown in Fig. 1.6.

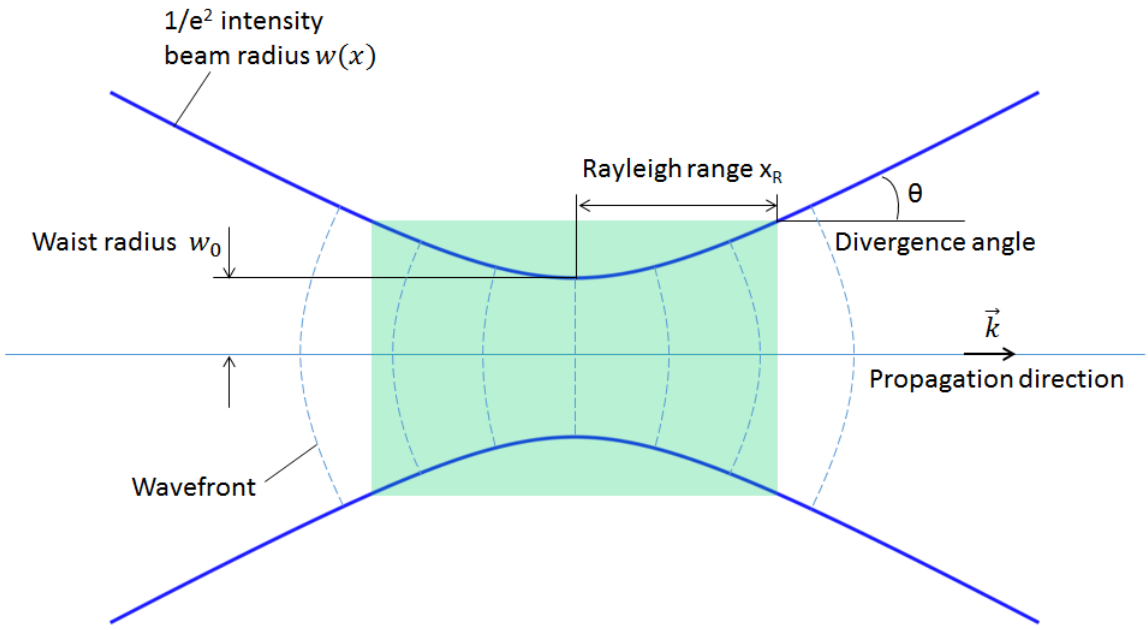

Fig.}1.6: Wave fronts of a Gaussian beam [36].

1.2 Maxwell's Equations in Media

The Maxwell's equations have different formulas in presence of matter, as the medium contains positive and negative charges, as well as current densities ρ and J [17]

$$\nabla \cdot \mathbf{E} = \frac{\rho}{\varepsilon_0} = \frac{\rho_b + \rho_f}{\varepsilon_0} \tag{1.61}$$

$$\nabla \times \mathbf{E} = -\frac{\partial \mathbf{B}}{\partial t} \tag{1.62}$$

$$\nabla \cdot \mathbf{B} = 0 \tag{1.63}$$

$$\nabla \times \mathbf{B} = \mu \mathbf{J} + \epsilon\mu \frac{\partial \mathbf{E}}{\partial t} \tag{1.64}$$

Here, ρ_b and ρ_f are the densities of bound and free charges, respectively, and J is the current density. The interaction of radiation with matter is determined by considering that matter is atomic. Atoms and molecules respond to electromagnetic fields by creating electric and magnetic dipoles, which arise from the separation of positive and negative charges in atoms. Magnetic dipoles arise from the orbital and spinning motion of electrons in atoms. When we sum up a huge number of atoms in a small volume we obtain the macroscopic quantities known as polarization field $\mathbf{P}(\mathbf{r}, t)$ and a magnetization field $\mathbf{M}(\mathbf{r}, t)$ (the electric and magnetic dipole moments per unit volume).

$$\rho_b = -\nabla \cdot \mathbf{P} \tag{1.65}$$

where ρ_b is the density of bound charges. Substituting the equation 1.65 in 1.61 yields

$$\begin{aligned} \varepsilon_0 \nabla \cdot \mathbf{E} &= -\nabla.\mathbf{P} + \rho_f & (1.66)\\ \nabla \cdot (\varepsilon_0 \mathbf{E} + \mathbf{P}) &= \rho_f & (1.67)\\ \nabla \cdot \mathbf{D} &= \rho_f, & (1.68) \end{aligned}$$

where **D** is electric displacement field. In addition the current can written as

$$J = J_f + J_b + J_p. \tag{1.69}$$

Here, $\mathbf{J}_f$ is the free current produced from free charges, and $\mathbf{J}_b = \nabla \times \mathbf{M}$ is the bound current produced by the density of magnetic dipoles. $\mathbf{J}_p = \dfrac{\partial \mathbf{P}}{\partial t}$ is produced from the variation of polarization with time when charges shift. We can, therefore, rewrite the Maxwell's equations as follows

$$\begin{aligned} \nabla \cdot \mathbf{D} &= \rho & (1.70)\\ \nabla \times \mathbf{E} &= -\frac{\partial \mathbf{B}}{\partial t} & (1.71)\\ \nabla \cdot \mathbf{B} &= 0 & (1.72)\\ \nabla \times \mathbf{H} &= \mathbf{J}_f + \frac{\partial \mathbf{D}}{\partial t} & (1.73) \end{aligned}$$

Here $\mathbf{H} = \dfrac{\mathbf{B}}{\mu_0} - \mathbf{M}$ being the magnetic field, and the polarization vector is proportional to the electric field [18].

$$\mathbf{P} = \epsilon_0 \chi \mathbf{E} \tag{1.74}$$

Here, χ is the electric susceptibility. Using this definition, we can write the displacement field as

$$\begin{aligned} \mathbf{D} &= (\epsilon_0 \mathbf{E} + \epsilon_0 \chi^{(1)} \mathbf{E}) \Rightarrow \mathbf{D} = \epsilon_0 (1 + \chi^{(1)}) \mathbf{E} & (1.75)\\ \epsilon_r &= (1 + \chi^{(1)}) = n^2 & (1.76)\\ \mathbf{D} &= \epsilon_0 \epsilon_r \mathbf{E} = \epsilon \mathbf{E}, & (1.77) \end{aligned}$$

where ϵ_r is the relative permittivity and n is the refractive index of the dielectric. Applying curl to Equation 1.71 we obtain

$$\begin{aligned} \nabla \times (\nabla \times \mathbf{E}) &= -\mu_0 \frac{\partial (\nabla \times \mathbf{H})}{\partial t} & (1.78)\\ \nabla(\nabla.\mathbf{E}) - \nabla^2 \mathbf{E} &= -\mu_0 \epsilon \frac{\partial^2 \mathbf{E}}{\partial t^2} & (1.79)\\ \nabla^2 \mathbf{E} &= \mu_0 \epsilon_0 \epsilon_r \frac{\partial^2 \mathbf{E}}{\partial t^2} & (1.80)\\ \nabla^2 \mathbf{E} &= \frac{n^2}{c^2} \frac{\partial^2 \mathbf{E}}{\partial t^2} & (1.81) \end{aligned}$$

So, using these equations, we can eventually obtain a wave equation that looks exactly the same as the previous case in vacuum, except for the addition of the n^2 term. This term arises because the medium is not free, and therefore n is not equal to 1. The solution to Equation 1.81 can be expressed using the following ansatz

$$\mathbf{E}(\mathbf{r},t) = \mathbf{E}_0(\mathbf{r})e^{i\phi(\mathbf{r},t)} \tag{1.82}$$

$$\phi(\mathbf{r},t) = n\mathbf{k}.\mathbf{r} - \omega t \tag{1.83}$$

Plugging this ansatz into the previous equation yields

$$\{\nabla^2\mathbf{E}(\mathbf{r}) - (\nabla\phi)^2\mathbf{E}_0(\mathbf{r}) + n^2\mathbf{k}^2\mathbf{E}_0(\mathbf{r}) + i\left[(\nabla^2\phi)\mathbf{E}_0(\mathbf{r}) + 2(\nabla\phi)(\nabla\mathbf{E}_0(\mathbf{r}))\right]\}e^{i\phi(\mathbf{r},t)} = 0, \tag{1.84}$$

which can be split into two parts real and imaginary. Assuming that the length scale over which the refractive index varies is much greater than the wavelength, and that the amplitude $\mathbf{E}_0(\mathbf{r})$ changes only slighltly. In this approximation we can omit the term $\mathbf{E}_0$ and arrive at the eikonal equation of geometric optics

$$(\nabla\phi)^2 = \frac{n\omega}{c}. \tag{1.85}$$

1.3 Propagation in Linear and Nonlinear Media

In linear media, the polarization field is linearly proportional to the electric field of the wave, with the proportionality factor called the linear susceptibility. However, in nonlinear media, the polarization field is nonlinearly proportional to the electric field of the wave, with the proportionality factor called the nonlinear susceptibility [19]. Therefore, Maxwell's equations take the following form in media [20]:

$$\nabla\cdot\mathbf{D} = 0 \tag{1.86}$$

$$\nabla\times\mathbf{E} = -\frac{\partial\mathbf{B}}{\partial t} \tag{1.87}$$

$$\nabla\cdot\mathbf{B} = 0 \tag{1.88}$$

$$\nabla\times\mathbf{H} = \epsilon_0\frac{\partial}{\partial t}\left(\mathbf{E} + \chi^{(1)}\mathbf{E} + \chi^{(2)}\mathbf{E}\mathbf{E} + \chi^{(3)}\mathbf{E}\mathbf{E}\mathbf{E} + ...\right) \tag{1.89}$$

where the last equation can be written in the form

$$\nabla\times\mathbf{H} = \frac{\partial}{\partial t}\left(\mathbf{P}_L + \mathbf{P}_{NL}\right) \tag{1.90}$$

$$\mathbf{P}_L = \epsilon_0(1+\chi^{(1)}).\mathbf{E} \tag{1.91}$$

$$\mathbf{P}_{NL} = \epsilon_0(\chi^{(2)}\mathbf{E}\mathbf{E} + \chi^{(3)}\mathbf{E}\mathbf{E}\mathbf{E} + \dots) \tag{1.92}$$

Here $\chi^{(1)}$ is second rank tensor and $\chi^{(2)}, \chi^{(3)}$ are tensors whith higher order. In this part we are interested in the linear matter polarization field $\mathbf{P}_L$ (low field intensity) where the application of electric field on dielectric material causes the flux density to be greater than it would be in free space. In general, there is a causal (response) relation between the dielectric material and the applied electric field . The material for which **D** and **E** are in the same direction is isotropic (properties are the same at all points in different directions). For anisotropic materials **D**, **E** , and are not parallel ϵ is a tensor. Because the dielectric response can be anisotropic, meaning that the electrical properties of the material can vary with direction. In such cases, a tensor dielectric constant is used to describe the material's electrical properties in different directions [21]

$$\begin{pmatrix} \mathbf{D}_x \\ \mathbf{D}_y \\ \mathbf{D}_z \end{pmatrix} = \begin{pmatrix} \epsilon_{xx} & \epsilon_{xy} & \epsilon_{xz} \\ \epsilon_{yx} & \epsilon_{yy} & \epsilon_{yz} \\ \epsilon_{zx} & \epsilon_{zy} & \epsilon_{zz} \end{pmatrix} . \begin{pmatrix} \mathbf{E}_x \\ \mathbf{E}_y \\ \mathbf{E}_z \end{pmatrix} \tag{1.93}$$

An example of a material with optical anisotropy is the perovskite which is a cristal of cubic structure as depicted in the following figure A tensor is a mathematical

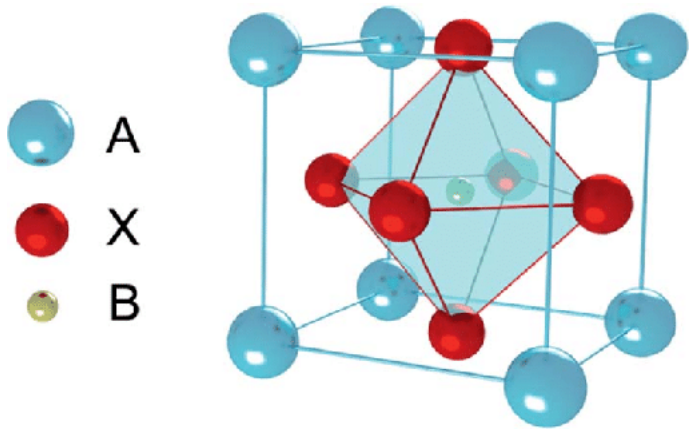

Fig.}1.7: Structure of perovskite [22].

object that describes how a physical quantity changes with direction. In our case of the dielectric tensor can be used to describe how the electrical properties of a material change depending on the orientation of the electric field with respect to the crystallographic axes of the material. The dielectric tensor is represented by a 3x3 matrix, where each element of the matrix describe the electrical properties of the material in a particular direction. In general, the permittivity tensor will have six independent components, since it is symmetric, i.e., it can be diagonalized by an

orthogonal matrix (rotation matrix), to find out the principle axes system.

$$\begin{pmatrix} \epsilon_x & 0 & 0 \\ 0 & \epsilon_y & 0 \\ 0 & 0 & \epsilon_z \end{pmatrix} \tag{1.94}$$

where ϵ_x, ϵ_y and ϵ_z are the principal dielectric permittivity components. The electric energy density inside a material reads

$$\begin{aligned} 2W_{\text{el}} &= \mathbf{D} \cdot \mathbf{E} \\ &= \epsilon_0 \frac{D_x^2}{\epsilon_x} + \epsilon_0 \frac{D_y^2}{\epsilon_y} + \epsilon_0 \frac{D_z^2}{\epsilon_z}. \end{aligned} \tag{1.95}$$

Hence

$$\frac{D_x^2}{n_x^2} + \frac{D_y^2}{n_y^2} + \frac{D_z^2}{n_z^2} = \frac{2W_{\text{el}}}{\epsilon_0}, \tag{1.96}$$

which can be written as follows

$$\frac{x^2}{n_x^2} + \frac{y^2}{n_y^2} + \frac{z^2}{n_z^2} = 1, \tag{1.97}$$

where $x^2 = \frac{\epsilon_0 D_x^2}{2W_{\text{el}}}$, $y^2 = \frac{\epsilon_0 D_y^2}{2W_{\text{el}}}$, $z^2 = \frac{\epsilon_0 D_z^2}{2W_{\text{el}}}$. The equation (1.97) is known as the index ellipsoid.

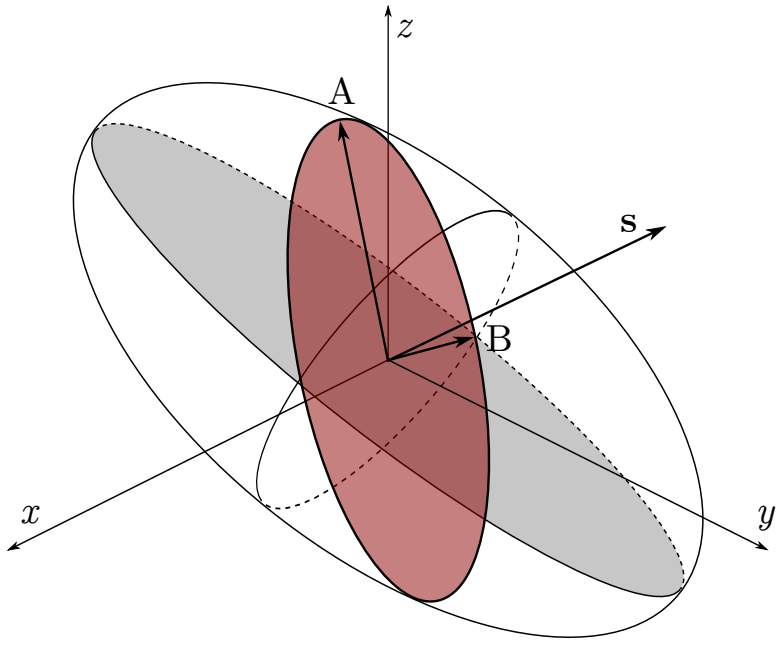

Fig.}1.8: The index ellipsoid, **s** is the unit vector along the propagation direction, the two points A and B determine the major and minor semiaxes, respectively [23].

Moreover, the optic axis is defined as the wave-normal direction in which the refractive index is independent of the direction of polarization, i.e, the direction perpendicular to the circular cross section of the index ellipsoid. In general, there are two optical axis not parallel to semi-axis of the ellipsoid at angles $\sin\theta = \frac{n_x}{n_y}\sqrt{\frac{n_y^2-n_x^2}{n_z^2-n_x^2}}$. According to the number of optic axes we can distinguish three main types of crystals:

1. Isotropic: $\epsilon_x = \epsilon_y = \epsilon_z \quad (n_x = n_y = n_z)$ which has a cubic symmetry

2. Uniaxial: $\epsilon_x = \epsilon_y \neq \epsilon_z \quad (n_x = n_y \neq n_z)$ which has trigonal, tetragonal and hexagonal symmetry (one optic axis).

3. Biaxial: $\epsilon_x \neq \epsilon_y \neq \epsilon_z \quad (n_x \neq n_y \neq n_z)$ which has orthorhombic, monoclinic and triclinic symmetry (two optic axes).

1.3.1 Light Propagation in Uniaxial Media

For uniaxial medium where $n_x = n_y \neq n_z$, the index ellipsoid is an ellipsoid of revolution (spheroid). We define two refractive indices:

1. Ordinary index of refraction n_o where the wave normal is parallel to the optic axis.

2. Extraordinary index of refraction n_e where the wave normal is perpendicular to the optic axis.

The dispersion relation reads

$$\left(\frac{k_x^2}{n_o^2} + \frac{k_y^2}{n_o^2} + \frac{k_y^2}{n_o^2} - \frac{\omega^2}{c^2}\right)\left(\frac{k_x^2}{n_e^2} + \frac{k_y^2}{n_e^2} + \frac{k_y^2}{n_o^2} - \frac{\omega^2}{c^2}\right) = 0 \tag{1.98}$$

Since one of the brackets in right-hand side of Eq.(1.98) has to be equal zero, the left brackets represent an equation of sphere where the ordinary rays behave like in isotropic media and see a refractive index n_o independent of $\mathbf{k}$, whereas the right brackets is an ellipsoid of revolution (spheroid) where the extraordinary rays have an effective refractive index which depends on the direction of $\mathbf{k}$ and interpolates somewhere between n_o and n_e. The velocity of light in any medium is related to

the refractive index, so we can notice in isotropic materials the same refractive index along all directions. But in uniaxial medium is the same but two different directions, and in biaxial medium is different for all directions. The refractive index in dielectric materials is defined to be

$$n_i = \sqrt{\epsilon_i}. \tag{1.99}$$

In isotropic materials, the index of refraction $n = \sqrt{\epsilon}$ is the same in all directions, i.e, $\epsilon_x = \epsilon_y = \epsilon_z = \epsilon$, but in uniaxial media, where $\epsilon_x = \epsilon_y \neq \epsilon_z$, we have two distinct indices of refraction the ordinary refractive index $n_o = \sqrt{\epsilon_x} = \sqrt{\epsilon_x}$ and the extra-ordinary refractive index $n_e = \sqrt{\epsilon_z}$.
For positive uniaxial, $n_e > n_o$, the effective refractive index has the form

$$n(\theta) = \frac{n_e n_o}{(n_o^2 \sin^2\theta + n_e^2 \cos^2\theta)^{1/2}}, \tag{1.100}$$

where

$$k_x = k\cos\theta \tag{1.101}$$
$$k_y = k\sin\theta \tag{1.102}$$
$$k_z = 0, \tag{1.103}$$

and θ is the angle between the wave normal and the optic axis. Here two distinct wave vectors $\mathbf{k}$ are allowed corresponding to the polarizations of ordinary and extra-ordinary rays.

1.3.2 Birefringence

If one looks at the refraction at an interface between isotropic (vacuum) and anisotropic media (uniaxial crystal) with two refractive indices, two refracted waves with different wave numbers show up. The effect of double refraction is known as birefringence . Two distinct types are:
If $\epsilon_x = \epsilon_y < \epsilon_z$, this corresponds to positive birefringence.
If $\epsilon_x = \epsilon_y > \epsilon_z$, this is the case of negative birefringence.
For example, two diffrent uniaxial crystals like quartz and calcite:
Quartz, $n_e - n_o > 0$, $n_o = 1.5443 \quad n_e = 1.5534$, positive birefringence.
Calcite, $n_e - n_o < 0$, $n_o = 1.6584 \quad n_e = 1.4864$, negative birefringence.

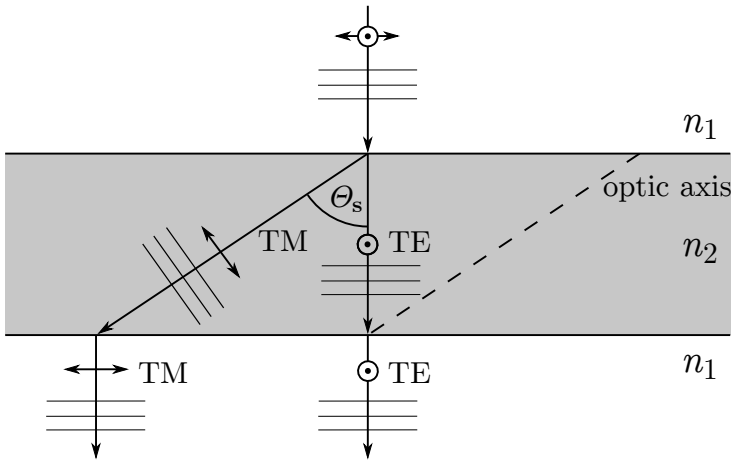

Fig.}1.9: Birefringence, one incident TE or TM waves is refracted into ordinary or extraordinary waves [24].

The birefringence can be applied to construct optical devices such as polarizing beam splitter. where TE and TM is transverse electric mode and transverse magnetic mode respectively.

1.3.3 Dipole Model for Linear Polarization

In the dipole model, the polarization of the material is determined by the polarizability of the individual atoms or molecules in the material, as well as the strength of the applied electric field. The dipole model is a simplified description of the behavior of real materials, but it provides a useful framework for understanding the behavior of linear materials in electric fields. This model is widely used for studying matter polarization, because it's clear and simple. We will apply this model to determine the susceptibility formula or response function at external electric field exerted on matter [25].

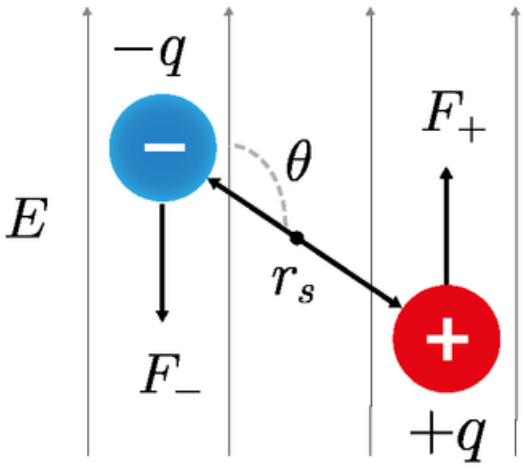

Fig.}1.10: Electric dipole model [26]

To construct a simple model that contains the essential properties of the linear susceptibility we consider a dipole consisting of two oppositely elementary charges $\pm e$ separated with distance $\mathbf{r}$ from each other. Newton's equations of motion for charged point masses with charge q_i and position $\mathbf{r}_i$ have the form

$$m_i \ddot{\mathbf{r}}_i = q_i \left[\mathbf{E}(\mathbf{r}_i, t) + \dot{\mathbf{r}}_i \times \mathbf{B}(\mathbf{r}_i, t)\right] + \mathbf{F}_{\text{diss}} + \sum_j \mathbf{F}_{ij}, \tag{1.104}$$

where the individual forces denote the Lorentz force, possible dissipative (friction) forces and conservative binding forces between the charges. Let $q_i = \pm e$ and the electric field is polarized along x direction (dipole direction), .i.e, $\mathbf{E} = E\mathbf{e}_x$. The equation of motion reads

$$m\ddot{x} = F_{\text{driv}} + F_{\text{diss}} + F_{\text{cons}}. \tag{1.105}$$

Plugging $F_{\text{driv}} = e\mathbf{E}_x, F_{\text{diss}} = -m\gamma\dot{x}$, and $\quad F_{\text{cons}} = -m\omega_0^2 x$ into (1.105) yields

$$m\ddot{x} - m\gamma\dot{x} + m\omega_0^2 x = F_{\text{driv}} \tag{1.106}$$

where γ is the coefficient of friction and ω_0 being the natural frequency that arises from the conservative binding force. Let us consider a harmonic wave for the driver

$$E(t) = E_0 e^{-i\omega t} \tag{1.107}$$

and with the ansatz

$$x(t) = x_0 e^{-i\omega t} \tag{1.108}$$

we get the solution

$$(-\omega^2 + i\gamma\omega + \omega_0^2)x(t) = \frac{e}{m}E_0 e^{-i\omega t}, \tag{1.109}$$

hence

$$x(t) = \frac{\frac{e}{m}E(t)}{\omega^2 - \omega_0^2 - i\gamma\omega}. \tag{1.110}$$

Moreover, the induced dipole moment is

$$p = ex(t) = \alpha(\omega)E(t) \tag{1.111}$$

where $\alpha(\omega)$ is the polarizability which tells how well this dipole interacts with the electromagnetic field. From Eq.(1.110) we obtain that

$$\alpha(\omega) = \frac{e^2/m}{\omega^2 - \omega_0^2 - i\gamma\omega}. \tag{1.112}$$

Defining the number density n, the linear susceptibility reads

$$\begin{aligned} \chi^{(1)}(\omega) &= n\alpha(\omega) \\ &= \frac{ne^2/m}{\omega^2 - \omega_0^2 - i\gamma\omega} \end{aligned} \tag{1.113}$$

which is a complex function. Dividing the linear susceptibility into real and imaginary parts gives

$$\mathrm{Re}\,\chi^{(1)}(\omega) = \frac{ne^2}{m}\frac{(\omega_0^2 - \omega^2)}{(\omega_0^2 - \omega^2)^2 + \gamma^2\omega^2} \tag{1.114}$$

$$\mathrm{Im}\,\chi^{(1)}(\omega) = \frac{ne^2}{m}\frac{\gamma\omega^2}{(\omega_0^2 - \omega^2)^2 + \omega^2\gamma^2} \geq 0. \tag{1.115}$$

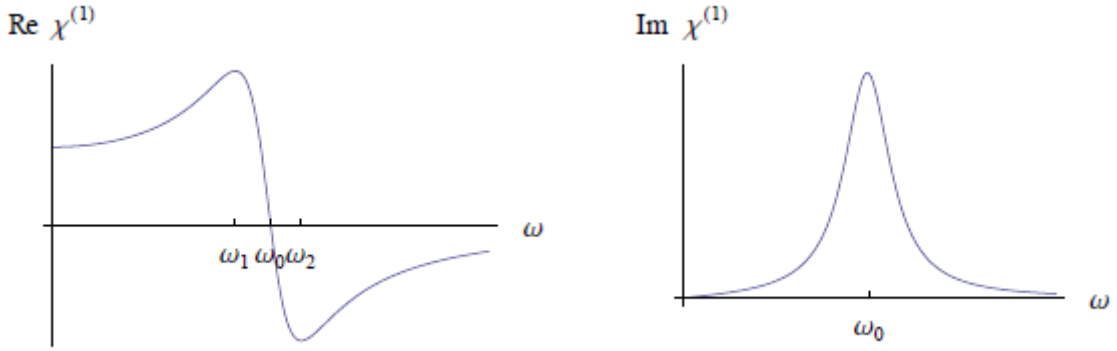

Fig.}1.11: Real and imaginary parts of linear susceptibility.

Both functions are shown schematically in Fig. 1.11. In the intervals of $\omega < \omega_1$ and $\omega > \omega_2$, the light is refracted more with increasing frequency (normal dispersion). In the interval $\omega_1 < \omega < \omega_2$, on the other hand, an anomalous dispersion occurs. The imaginary part has its maximum at the resonance frequency ω_0. One can also see that absorption takes place over the entire frequency range. One can explicitly check that the susceptibility obtained in this way actually satisfies the KramersKronig relations. In general, a medium consists of many oscillators with different resonance frequencies and oscillator strengths. Even within an atom there is a large number of dipole transitions whose transition matrix elements follow from a quantum mechanical treatment. So we can model a more general medium by a susceptibility

$$\chi^{(1)}(\omega) = \frac{ne^2}{m} \sum_k \frac{f_k}{\omega^2 - \omega_k^2 - i\gamma_k\omega}, \tag{1.116}$$

where the sum is taken over all possible dipole transitions with oscillator strengths f_k, resonance frequencies ω_k and damping γ_k. Equation (1.116) is the DrudeLorentz model of a dielectric medium, with the help of which the wave propagation can be described very well, in particular for low intensities or energy densities. Moreover, the absorption spectra can fitted to the imaginary part of equation (1.116) where the peaks take place at the frequencies ω_k. The maxima are determined by oscillator strengths f_k and widths by the damping parameters γ_k.

1.3.4 Dispersion and Absorption

When an electromagnetic field impinges on a medium, consisting of (generally bound) distributions of charges. The latter will be shifted by this field, resulting in an induced polarization field (and also magnetization if the medium is magnetic). In general, we can write the constitutive equations as

$$\mathbf{D}(\mathbf{r},t) = \epsilon_0\mathbf{E}(\mathbf{r},t) + \mathbf{P}[\mathbf{E}(\mathbf{r},t)] \tag{1.117}$$

$$\mathbf{H}(\mathbf{r},t) = \frac{1}{\mu_0}\mathbf{B}(\mathbf{r},t) - \mathbf{M}[\mathbf{B}(\mathbf{r},t)], \tag{1.118}$$

which means that the polarization $\mathbf{P}$ and the magnetization $\mathbf{M}$ are functionals that depend on the fields $\mathbf{E}$ and $\mathbf{B}$, respectively. Of course, in electro-optics and magneto-optics the polarization $\mathbf{P}$ and the magnetization $\mathbf{M}$ can also depend on $\mathbf{B}$ and $\mathbf{E}$, respectively, but this is not of interest here in this thesis. The exact dependency still has to be specified according the medium properties. In linear media we can assume that the polarization is directly proportional to the applied electric field and the magnetization is directly proportional to the magnetic induction. That is, we

assume a linear dependence, .i.e,

$$\mathbf{P} \propto \mathbf{E} \tag{1.119}$$
$$\mathbf{M} \propto \mathbf{B}, \tag{1.120}$$

hence

$$\mathbf{D}(\mathbf{r},t) = \epsilon\mathbf{E}(\mathbf{r},t) \tag{1.121}$$
$$\mathbf{H}(\mathbf{r},t) = \frac{1}{\mu}\mathbf{B}(\mathbf{r},t), \tag{1.122}$$

where ϵ and μ represent the permittivity and the permeability of the medium, respectively. This leads to the wave equation for the electric field as

$$-\Delta\mathbf{E}(\mathbf{r},t) + \epsilon\mu\ddot{\mathbf{E}}(\mathbf{r},t) = 0. \tag{1.123}$$

A comparison with the wave equation (1.17) in vacuum shows that we can relate the expression $\epsilon\mu$ to the speed of light in the medium,

$$\epsilon\mu = \frac{1}{c^2} \Rightarrow c = \frac{1}{\epsilon\mu}. \tag{1.124}$$

If we designate the speed of light in a vacuum with c_0, then the ratio

$$\frac{c_0}{c} = \sqrt{\frac{\epsilon\mu}{\epsilon_0\mu_0}} = n \tag{1.125}$$

define the index of refraction n of the medium. In reality, the assumption of a constant response to the externally applied field over all frequencies cannot be useful as it neglects all the details of material response. In particular, it is assumed that the medium still has the same refractive index even at very high frequencies, in extreme cases X-rays or gamma rays, which obviously contradicts with the fact that any material is perfectly transparent for very high frequencies, i.e., $n = 1$.
We now want to set up a more realistic model of the linear response of a medium, which as we shall see, can be linked to the polarization of a dipole or an ensemble of dipoles. We first assume for the sake of simplicity that the medium is not magnetic, so that the magnetic material equation in the vacuum, $\mathbf{H} = \frac{1}{\mu_0}\mathbf{B}$ remains valid. In fact, in most natural media, the magnetic effects are irrelevant to light propagation. A general linear relationship between polarization and electric field can be given as as [27]:

$$\mathbf{P}(\mathbf{r},t) = \epsilon_0 \int d^3r' \int_{-\infty}^{t} dt' \overleftrightarrow{\chi}^{(1)}(\mathbf{r},\mathbf{r}',t-t') \cdot \mathbf{E}(\mathbf{r}',t'). \tag{1.126}$$

Here $\chi(\mathbf{r}, \mathbf{r}', t - t')$ denotes the tensorial linear susceptibility. The structure of (1.126) is that of a temporal causal response of polarization to an external electric field. The raison behind causality is that only electric fields at times before t contribute to the polarization. On the other hand, the possibility is also provided that the response of the material takes place at a different point than the excitation (spatial dispersion). As a rule, this effect can be neglected. Furthermore, in (1.126) the possibility is provided that the material is birefringent, so that a tensorial description is necessary.
We want to focus here on a simplified description, in which the effects of anisotropy and spatial dispersion are neglected. From now on we will use the linear susceptibility

$$\overleftrightarrow{\chi}^{(1)}(\mathbf{r}, \mathbf{r}', t - t') = \chi^{(1)}(\mathbf{r}, t)\delta_{ij}\delta(\mathbf{r} - \mathbf{r}') \tag{1.127}$$

of an isotropic media whose polarization is

$$\begin{aligned} \mathbf{P}(\mathbf{r}, t) &= \epsilon_0 \int_{-\infty}^{t} dt' \chi^{(1)}(\mathbf{r}, t - t')\mathbf{E}(\mathbf{r}, t') \\ &= \epsilon_0 \int_{0}^{\infty} dt' \chi^{(1)}(\mathbf{r}, t')\mathbf{E}(\mathbf{r}, t - t'). \end{aligned} \tag{1.128}$$

The Equation ((1.128)) has the mathematical structure of a convolution. Hence Fourier transforming the equation yields the following formula

$$\mathbf{P}(\mathbf{r}, \omega) = \epsilon_0 \chi^{(1)}(\mathbf{r}, \omega)\mathbf{E}(\mathbf{r}, \omega) \tag{1.129}$$

in frequency space with the relation

$$\chi^{(1)}(\mathbf{r}, \omega) = \chi^{(1)^*}(\mathbf{r}, -\omega^*), \tag{1.130}$$

which implies that the frequency components of the susceptibility are complex numbers.

1.3.5 Kramers-Kronig Relations

The Fourier components $\chi^{(1)}(\mathbf{r}, \omega)$ of the linear susceptibility satisfy an important integral relation, which we now want to derive. To do this, we go back to Equation (1.128) and first state that this is only a one-sided Fourier transformation. In order to be able to extend the integration to the whole time axis and at the same time to take into account the causality of the dielectric response, we have to require that the susceptibility vanishes at negative times. This can be achieved by Firstly define

$$\chi^{(1)}(t) = \theta(t)\chi^{(1)}(t), \tag{1.131}$$

where $\theta(t)$ is the Heaviside step function. We now transform both sides of equation (1.131) using the relations

$$\chi^{(1)}(\omega) = \int_{-\infty}^{\infty} dt\, e^{i\omega t}\chi^{(1)}(t), \quad \chi^{(1)}(t) = \frac{1}{2\pi}\int_{-\infty}^{\infty} d\omega\, e^{-i\omega t}\chi^{(1)}(\omega) \tag{1.132}$$

to obtain

$$\begin{aligned}
\chi^{(1)}(\omega) &= \int_{-\infty}^{\infty} dt\, e^{i\omega t}\theta(t)\chi^{(1)}(t) \\
&= \int_{-\infty}^{\infty} dt\, e^{i\omega t}\theta(t)\frac{1}{2\pi}\int_{-\infty}^{\infty} d\omega'\, e^{i\omega' t}\chi^{(1)}(\omega') \\
&= \frac{1}{2\pi}\int_{-\infty}^{\infty} d\omega'\, \chi^{(1)}(\omega')\int_{0}^{\infty} dt\, e^{-i(\omega-\omega')t} \\
&= \frac{1}{2\pi i}\int_{-\infty}^{\infty} d\omega'\, \chi^{(1)}(\omega')\left[\pi\delta(\omega-\omega') - \mathcal{P}\frac{1}{\omega-\omega'}\right] \\
&= \frac{1}{2}\chi^{(1)}(\omega') - \frac{1}{2\pi}\mathcal{P}\int_{-\infty}^{\infty} d\omega'\frac{\chi^{(1)}(\omega')}{\omega-\omega'}.
\end{aligned} \tag{1.133}$$

Here $\mathcal{P}$ is the principal value. Finally the linear susceptibility reads

$$\chi^{(1)}(\omega) = -\frac{1}{i\pi}\mathcal{P}\int_{-\infty}^{\infty} d\omega'\frac{\chi^{(1)}(\omega')}{\omega-\omega'}$$

which is a complex function that contains real and imaginary parts

$$\mathrm{Re}\,\chi^{(1)}(\omega) = -\frac{1}{\pi}P\int_{-\infty}^{+\infty}\frac{\mathrm{Im}\,\chi^{(1)}(\omega')}{\omega-\omega'}d\omega', \quad \mathrm{Im}\,\chi^{(1)}(\omega) = \frac{1}{\pi}P\int_{-\infty}^{+\infty}\frac{\mathrm{Re}\,\chi^{(1)}(\omega')}{\omega-\omega'}d\omega'. \tag{1.134}$$

From (1.134) it is obvious that it is impossible to generate a purely real susceptibility in the frequency domain.

The consequences of Kramers-Kronig relations become particularly clear when one calculates the energy dissipated in the medium. For this we have to remember that the source term for the electromagnetic field energy is $-\mathbf{j}\cdot\mathbf{E}$. We now interpret the current density $\mathbf{j}$ as the current density induced by the electric field in the medium

$$\mathbf{j}_{\mathrm{ind}} = -\dot{\mathbf{P}}(\mathbf{r},t) + \nabla\times\mathbf{M}(\mathbf{r},t) \tag{1.135}$$

and calculate the total energy supplied to the electromagnetic field as

$$\begin{aligned} W &= -\int dt \int d^3r\, \mathbf{j}_{\text{ind}}(\mathbf{r},t)\cdot\mathbf{E}(\mathbf{r},t) \\ &= -\int d\omega \int \frac{d^3k}{(2\pi)^3}\text{Re}\left[\mathbf{j}_{\text{ind}}(\mathbf{k},\omega)\cdot\mathbf{E}^*(\mathbf{k},\omega)\right] \\ &= -\int d\omega \int \frac{d^3k}{(2\pi)^3}\frac{1}{2}\left[\mathbf{j}_{\text{ind}}(\mathbf{k},\omega)\cdot\mathbf{E}^*(\mathbf{k},\omega)+\mathbf{j}^*_{\text{ind}}(\mathbf{k},\omega)\cdot\mathbf{E}(\mathbf{k},\omega)\right] \\ &= -\int d\omega \int \frac{d^3k}{(2\pi)^3}\omega\text{Im}\,\chi^{(1)}(\omega)\left|\mathbf{E}(\mathbf{k},\omega)\right|^2, \end{aligned} \tag{1.136}$$

where we have substituted the Fourier transform of the induced current density via the polarization, and then used the relation (1.129).
The equation (1.136) ensures that the total energy of the electromagnetic field decreases as a function of the imaginary part of the susceptibility. Accordingly, the imaginary part describes the dissipative part of the dielectric response of the medium, whereas the real part reveals the reactive part of the response. From Kramers-Kronig relations (1.134), we see that both parts are directly linked. Any medium that responds to an external electromagnetic field must necessarily also absorb radiation. However, one can imagine materials in which the absorption in limited frequency intervals is negligibly small (e.g. glasses), but this is not true outside of these regions (e.g. ultraviolet frequencies) glasses are not particularly transparent media and must absorb electromagnetic radiation [28].

1.3.6 Dispersion and Optical Pulses

Dispersion means that the refractive index depends on frequency through the electric susceptibility. This has a direct impact on the propagation of electromagnetic waves through dielectric media. The refractive index is now also frequency dependent as given by the following formula

$$n(\omega) = \sqrt{1+\chi^{(1)}(\omega)} \tag{1.137}$$

Assuming a light linearly polarized propagating in the z-direction, it can be described by an electric field wave

$$\mathbf{E}(z,t) = \frac{1}{2}\left[E_0(z,t)e^{-i\omega_0 t}+\text{c.c.}\right] \tag{1.138}$$

The envelope $E_0(z,t)$ at $z=0$ position can be given by the Gaussian profile

$$E(0,t) = Ae^{-t^2/(2t_0)^2}. \tag{1.139}$$

Apply Fourier transform on $E(0,t)$ gives

$$\begin{aligned} E(0,\omega) &= \int_{-\infty}^{+\infty} dt\, e^{i(\omega-\omega_0)t} E_0(0,t) \\ &= \sqrt{2\pi} A t_0 e^{-(\omega-\omega_0)t_0^2/2} \end{aligned} \tag{1.140}$$

which is also a Gaussian function. This field at location z is now determined via $E_0(z,\omega) = E_0(0,\omega)e^{ik(\omega)z}$. Let us expand the wave number $k(\omega)$ in a Taylor series around the frequency ω_0 of the carrier wave,

$$k(\omega) = k_0(\omega) + \beta_1(\omega-\omega_0) + \frac{1}{2}\beta_2(\omega-\omega_0)^2 + \cdots . \tag{1.141}$$

Here

$$\beta_1 = \left.\frac{dk}{d\omega}\right|_{\omega=\omega_0} = \frac{1}{v_g} = \frac{\tau_g}{z}, \quad \beta_2 = \left.\frac{d^2k}{d\omega^2}\right|_{\omega=\omega_0} = \frac{1}{z}\frac{d\tau_g}{d\omega} = \frac{1}{z}\frac{d\tau_g}{d\lambda}\frac{d\lambda}{d\omega} \tag{1.142}$$

where v_g is the group velocity and τ_g is the group delay time. In a dispersive medium, the wave number depends on the refractive index through the relation $k = \frac{2\pi n}{\lambda}$, therefore

$$\frac{dk}{d\lambda} = \frac{2\pi}{\lambda^2}\left(\lambda\frac{dn}{d\lambda} - n\right) \tag{1.143}$$

$$\frac{d\lambda}{d\omega} = \frac{d}{d\omega}\left(\frac{2\pi c}{\omega}\right) = -\frac{2\pi c}{\omega^2}. \tag{1.144}$$

This enables us to write τ_g as

$$\tau_g = \frac{z}{c}\left(n - \lambda\frac{dn}{d\lambda}\right) \tag{1.145}$$

$$\frac{d\tau_g}{d\lambda} = -\frac{z}{c}\lambda\frac{d^2n}{d\lambda^2} = D_\lambda z \tag{1.146}$$

where D_λ is the dispersion parameter. Through this analysis, we can find the formula for β_2 reads

$$\beta_2 = -\frac{D_\lambda \lambda^2}{2\pi c}. \tag{1.147}$$

We thus find that the Taylor expansion of the wave number $k(\omega)$ around $\omega = \omega_0$ up to second order can be written as

$$k(\omega) = k(\omega_0) + \frac{\tau_g}{z}(\omega-\omega_0) - \frac{D_\lambda\lambda^2}{4\pi c}(\omega-\omega_0)^2 \tag{1.148}$$

Transforming back into the time space we obtain

$$E_0(z,t)e^{-i\omega_0 t} = \frac{A}{\sqrt{1+i\xi}} e^{-i\omega_0\left(t-z/v_p\right)} e^{-\frac{(t-\tau_g)^2}{t_0^2(1+\xi^2)}} e^{-\frac{i\xi(t-\tau_g)^2}{2t_0^2(1+\xi^2)}}, \tag{1.149}$$

where $v_p = \omega_0/k$ is the phase velocity and $\xi = \left(\frac{\beta_2 z}{t_0^2}\right) z$ is the normalized propagation length.
Equation (1.149) reveals the following properties of the pulse propagation:

- the carrier wave propagates with phase velocity v_p.
- the envelope moves with group velocity v_g.
- the pulse is broadened by a factor $\sqrt{1+\xi^2}$.
- the peak intensity of the pulse reduced by the factor $1+\xi^2$.
- the carrier frequency changes along the pulse (chirp).

The frequency chirp is obtained from the last term in equation (1.149), which we write as $e^{i\psi(t)}$ and remember that $d\psi/dt$ represents the carrier frequency shift. The chirp, i.e., the frequency shift, is then

$$\frac{d\omega}{dt} = \frac{d^2\psi(t)}{dt^2} = \frac{\xi}{t_0^2(1+\xi^2)} \overset{|\xi|\gg 1}{\approx} \frac{1}{t_0^2\xi} = \frac{1}{\beta_2 t_0^2} \tag{1.150}$$

If β_2 is positive, that is, the group time delay increases with frequency, then the chirp is also positive. As a result, lowest frequencies occur first and highest frequencies last. This behavior is shown in Fig. 4.3, which shows the electric field of an originally Gaussian pulse before and after propagation through a linear dispersive medium with $\xi = +3$.

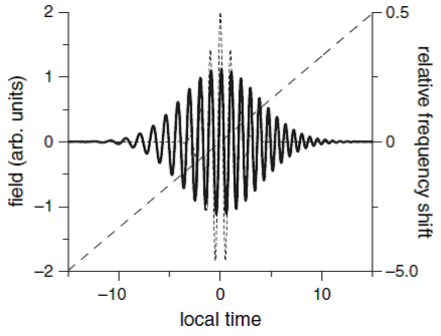

Fig.}1.12: Profile of chirped Gaussian pulse with $\xi = +3$. The dotted curse represents the original pulse. The Slanting dotted line shows the relative frequency shift and confirms the linearity of the chirp. [29]

1.4 Conclusion

Throughout this chapter, we covered a range of topics starting with electromagnetic waves in a vacuum and delving into the concept of polarization, exploring its three types. Furthermore, we examined the monochromatic nature of light and energy density. Building on this foundation, we then explored Maxwell's equations and their applications in wave propagation across different media. In particular, our focus was on matter response to external electromagnetic fields, wherein we utilized the dipole oscillator model to gain insights from Kramers-Kronig relations. This approach allowed us to understand optical susceptibility in the frequency domain and also explore the characteristics of laser pulses during the propagation through dispersive media. Throughout the chapter, we encountered and analyzed crucial solutions for the wave equations within this context.The following chapter will discuss the propagation of high light intensity in birefringent materials.

Bibliography

[1] Ampere, A. M. Memoire sur la determination des forces magnetiques et des lois que ces forces suivent dans leurs variations. Annales de chimie et de physique, 34, 233-261.(1827).

[2] Faraday, M. Experimental Researches in Electricity. Volume I. Royal Society of London.(1832).

[3] Maxwell, J. C. A Dynamical Theory of the Electromagnetic Field. Philosophical Transactions of the Royal Society of London, 155, 459-512. (1865).

[4] Whittaker, E. T. A History of the Theories of Aether and Electricity: From the Age of Descartes to the Close of the Nineteenth Century.(1951).

[5] D. J. Griffiths and C. Inglefield, Introduction to Electrodynamics , Am. J. Phys., vol. 73, no. 6, pp. 574574, doi: 10.1119/1.4766311, 2005.

[6] L. I. and A. Fisher, The Mathematical Theory of Probabilities., J. R. Stat. Soc., vol. 87, no. 4, p. 617, doi: 10.2307/2341466,1924.

[7] J. D. Jackson, Classical Electrodynamics, 3rd edition, Wiley, New York, 1999.

[8] F. Lacava, Classical Electrodynamics From Image Charges to the Photon Mass and Magnetic Monopoles. 2016.

[9] https://shorturl.at/FMOZ9

[10] https://shorturl.at/bCIN9

[11] https://shorturl.at/cdozE

[12] D. Colton and R. Kress. Inverse Acoustic and Electromagnetic Scattering Theory.Springer, New York etc, third edition, 2013.

[13] M. E. Thomas, Optical propagation in linear media: atmospheric gases and particles, solid-state components, and water. Johns Hopkins University Appli, 2006.

[14] https://shorturl.at/foIQ5

[15] https://t.ly/mEmxZ

[16] https://t.ly/Trhr1

[17] J. Schwinger, L. L. DeRaad Jr, K. Milton, and W. Tsai, Classical electrodynamics. CRC Press, 2019.

[18] E. M. Purcell, Electricity and magnetism, Berkeley Univ., vol. 2, 1963.

[19] R. Menzel, "Photonics : linear and nonlinear interactions of laser light and matter", Berlin Springer, 2007.

[20] I. Lindell, A. Sihvola, S. Tretyakov, and A. J. Viitanen, Electromagnetic waves in chiral and bi-isotropic media. Artech House, 1994.

[21] V. M. Agranovich and V. L. Ginzburg, Crystal optics with spatial dispersion, vol. 9, no. C. 1971.

[22] https://t.ly/jPZ0n

[23] https://t.ly/no5p3

[24] https://t.ly/CDOjD

[25] K. E. Oughstun and N. A. Cartwright, On the Lorentz-Lorenz formula and the Lorentz model of dielectric dispersion, Opt. Express, vol. 11, no. 13, pp. 15411546, 2003.

[26] https://shorturl.at/HSY69

[27] P. Hertel, Lectures on Theoretical Physics: Linear Response Theory, Univ. Osnabruck, Ger., p. 59, 2001, [Online]. Available: http://grk.physik.uni-osnabrueck.de/lecture/lrt.pdf.

[28] T. Kamiya, F. Krausz, B. Monemar, H. Venghaus, H. Weber, and H. Weinfurter, Kramers-Kronig Relations and Sum Rules in Nonlinear Optics. 2005.

[29] G. New, "Introduction to nonlinear optics", Cambridge University Press, 2011.

Chapter 2

Propagation of Light in Nonlinear Media

Nonlinear optical response refers to the phenomenon where the optical properties of a material change nonlinearly with the intensity of light. This effect arises from the interaction of light with the electrons in the material, and it can be used for various applications, such as frequency conversion [1], optical switching [2], and signal processing. The history of nonlinear optics can be traced back to the early 20th century, when researchers first observed nonlinear optical effects in various materials. However, it was absent until the development of lasers in the 1960s that the field of nonlinear optics began to flourish [3]. In 1961, the American physicist Frank J. Murray proposed the idea of using nonlinear optical effects to create laser sources at new wavelengths [4]. The following year, the Soviet physicist Aleksandr Prokhorov independently proposed a similar idea. Both researchers shared the Nobel Prize in Physics in 1964 for their contributions to the development of laser technology. In the 1970s, researchers began to investigate the use of nonlinear optics for signal processing and communication. In 1973, the American physicist Peter Franken and his colleagues demonstrated the first optical parametric oscillator, a device that generates coherent light at new wavelengths using nonlinear optical effects [6]. In the 1980s [5], the field of nonlinear optics continued to advance, with the development of new materials and devices for manipulating light. One important breakthrough was the discovery of second harmonic generation in optical fibers, which paved the way for the development of all-optical communication systems. Today, nonlinear optics is a mature field with many applications in science and technology. It has contributed to the development of laser technology, optical communication, spectroscopy, microscopy, and many other areas [7, 8]. The wave equation in a dielectric

medium can be written as

$$\begin{aligned} \nabla^2\mathbf{E}(\mathbf{r},t) - \frac{1}{c^2}\ddot{\mathbf{E}}(\mathbf{r},t) &= \mu_0\ddot{\mathbf{P}}(\mathbf{r},t) \\ &= \mu_0\ddot{\mathbf{P}}_L(\mathbf{r},t) + \mu_0\ddot{\mathbf{P}}_{NL}(\mathbf{r},t) \end{aligned} \tag{2.1}$$

where $\ddot{\mathbf{P}}_L$ and $\ddot{\mathbf{P}}_{NL}$ are the linear and nonlinear driving fields of polarization. In general, the optical response can often be described by expressing the polarization as a Taylor expansion in the field strength as

$$P_i = \epsilon_0 \left[\chi_{ij}^{(1)} E_j + \chi_{ijk}^{(2)} E_j E_k + \chi_{ijkl}^{(3)} E_j E_k E_l + \cdots\right]. \tag{2.2}$$

Here $\chi_{ijk}^{(2)}$ and $\chi_{ijkl}^{(3)}$ are second and third order nonlinear susceptibilities, where $\chi^{(3)}$ is tensor of rank 4 that has 81 components and $\chi^{(2)}$ is tensor of rank 3 which has 27 components. The number of independent components depends strongly on the symmetry of crystals, e.g, for centrosymmetric materials $\chi_{ijk}^{(2)} = 0$. The expansion (2.2) also shows that nonlinear effects in polarization only become visible with larger field strengths [9]. It was only with the development of the laser in the 1960s that it was possible to generate fields with sufficiently high spatial and spectral energy densities. This laid to the emergence of the field of nonlinear optics [10].

2.1 Nonlinear Susceptibility of a Classical Anharmonic Oscillator

To see how such nonlinearities can occur, let us go back to our dipole model of a dielectric medium, in which we write the equation of motion of the dipole in a harmonic approximation as

$$m(\ddot{x} + \gamma\dot{x} + \omega_0^2 x) = eE. \tag{2.3}$$

We have assumed that the conservative binding force is linear in displacement (Hooke's law). The associated potential must, therefore, be quadratic (harmonic) [11]. This is certainly only correct to a first approximation. For example, consider the potential of an electron as it moves around the nucleus [12]. The effective potential is the sum of Coulomb potential and the centrifugal barrier

$$W(r) = -\frac{e^2}{4\pi\epsilon_0 r} + \frac{L^2}{2mr^2}$$

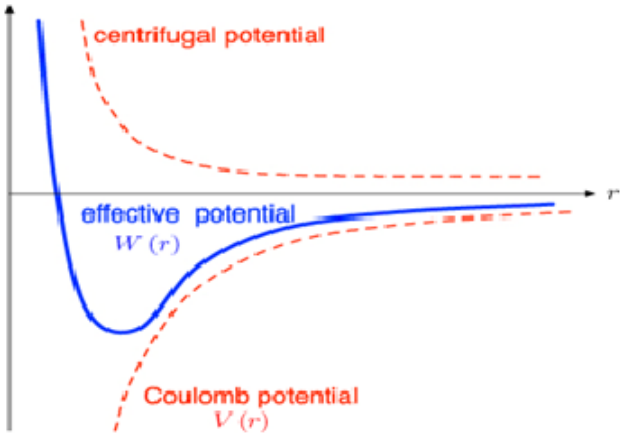

Fig.}2.1: The Effective potential of an electron moving around the atomic nucleus [13].

The potential can only be approximated by a parabola for very small displacements from the equilibrium position x_0. Now let us write Taylor expansion close to x_0

$$V(x) = V(x_0) + \frac{1}{2!}V''(x_0)x^2 + \frac{1}{3!}V'''(x_0)(x-x_0)^3 + \cdots \tag{2.4}$$

To obtain the first nonlinear order, substitute the third term in Eq 2.4 and solve for the resulting expression.

$$m(\ddot{x} + \gamma\dot{x} + \omega_0^2 x) = eE - \frac{1}{2}V'''x^2. \tag{2.5}$$

This is a nonlinear differential equation which can be solved according to this anzats

$$x(t) = x_1(t) + x_2(t) + \cdots = \tilde{x}_1 e^{-i\omega t} + \tilde{x}_2 e^{-2i\omega t} + \cdots \tag{2.6}$$

and the electric field as a monochromatic wave $E(t) = E_0 e^{-i\omega t}$. Substituting in Eq 2.5 yields two different equations for Fourier coefficients $e^{-i\omega t}$ and $e^{-2i\omega t}$, respectively

$$m(\ddot{x}_1 + \gamma\dot{x}_1 + \omega_0^2 x_1) = eE_0 e^{-i\omega t} \tag{2.7}$$

$$m(\ddot{x}_2 + \gamma\dot{x}_2 + \omega_0^2 x_2) = -\frac{1}{2}V'''x_1^2. \tag{2.8}$$

The solution x_1 of Eq 2.7 can be obtained in similar way to the linear theory

$$x_1(t) = \frac{\frac{e}{m}E_0}{\omega_0^2 - \omega^2 - i\gamma\omega}e^{-i\omega t}. \tag{2.9}$$

Substituting this solution into Equation 2.8, we find that

$$m(\ddot{x}_2 + \gamma\dot{x}_2 + \omega_0^2 x_2) = -\frac{V'''}{2m}\frac{\left(\frac{e}{m}E_0\right)^2}{(\omega_0^2 - \omega^2 - i\gamma\omega)^2}e^{-2i\omega t} \tag{2.10}$$

This is in agreement with the hypothesis that $x_2(t) \propto e^{-2i\omega t}$. Finally, the solution to nonlinear differential equation 2.5 reads

$$x_2(t) = -\frac{V'''}{2m}\left(\frac{e}{m}\right)^2 E_0^2 \frac{1}{\left[\omega_0^2 - \omega^2 - i\gamma\omega\right]^2\left[\omega_0^2 - (2\omega)^2 - 2i\gamma\omega\right]} e^{-2i\omega t}. \tag{2.11}$$

In addition to the already known resonance denominator (which appears squared here), a new resonance denominator with the resonance frequency $\propto 2\omega$ appears here. The frequency dependence of this part of the solution is $e^{-2i\omega t}$, although it was only irradiated with an electric field of frequency $e^{-i\omega t}$. As expected, the amplitude of the electric field appears square as E_0^2. Therefore, we can write the electric dipole moment in the following form [14]

$$p(t) = \alpha^{(1)}E(t) + \alpha^{(2)}E^2(t). \tag{2.12}$$

Here, $\alpha^{(1)}$ and $\alpha^{(2)}$ represent the linear and nonlinear polarizabilities, respectively

$$\alpha^{(1)} = \frac{e^2}{m}\frac{1}{\omega_0^2 - \omega^2 - i\gamma\omega} \tag{2.13}$$

$$\alpha^{(2)} = -\frac{V'''e^3}{2m^3}\frac{1}{\left[\omega_0^2 - \omega^2 - i\gamma\omega\right]^2\left[\omega_0^2 - (2\omega)^2 - 2i\gamma\omega\right]}. \tag{2.14}$$

The first term corresponds to a linear polarization $\mathbf{P}_L$, the second a nonlinear polarization $\mathbf{P}_{NL}$. In frequency space, the equation (2.1) transforms to the Helmholtz equation

$$\nabla^2\mathbf{E}(\mathbf{r},\omega) + \frac{\omega^2}{c^2}\ddot{\mathbf{E}}(\mathbf{r},\omega) = -\mu_0\omega^2\mathbf{P}_L(\mathbf{r},\omega) - \mu_0\omega^2\mathbf{P}_{NL}(\mathbf{r},\omega). \tag{2.15}$$

Introducing the linear polarization $\mathbf{P}_L(\mathbf{r},\omega) = \epsilon_0\chi^{(1)}(\omega)\mathbf{E}(\mathbf{r},\omega)$, the equation (2.15) becomes

$$\nabla^2\mathbf{E}(\mathbf{r},\omega) + \frac{\omega^2}{c^2}\epsilon(\omega)\mathbf{E}(\mathbf{r},\omega) = -\mu_0\omega^2\mathbf{P}_{NL}(\mathbf{r},\omega), \tag{2.16}$$

where $\epsilon(\omega) = 1 + \chi^{(1)}(\omega)$ is the dielectric permittivity. The right hand side of the equation (2.16) serves as a source term of the electric field applied to the linear medium. Until now it is unclear how the frequency components of nonlinear polarization look like. Later on we will concentrate on second and third order of the optical responses.

2.2 Second Order Nonlinearities

We have seen that every linear response can be written as a time convolution integral over the susceptibility, which reflects the causality principle (1.126). Any nonlinear

response can be written in the same way. If we limit ourselves to homogeneous media [15], we can omit the location arguments for the sake of simplicity

$$\mathbf{P}_{NL}^{(2)}(t) = \epsilon_0 \int_0^\infty d\tau_1 \int_0^\infty d\tau_2 \bar{\bar{\chi}}^{(2)}(\tau_1, \tau_2) : \mathbf{E}(t-\tau_1)\mathbf{E}(t-\tau_2) \tag{2.17}$$

or, in component notation,

$$P_{NL,i}^{(2)}(t) = \epsilon_0 \int_0^\infty d\tau_1 \int_0^\infty d\tau_2 \chi_{ijk}^{(2)}(\tau_1, \tau_2) E_j(t-\tau_1) E_k(t-\tau_2) \tag{2.18}$$

The Fourier transform reduces the number of integrals by one, but a convolution remains,

$$P_{NL}^{(2)}(\omega) = \epsilon_0 \int_{-\infty}^\infty d\omega' \chi_{ijk}^{(2)}(\omega, \omega', \omega-\omega') E_j(\omega') E_k(\omega-\omega') \tag{2.19}$$

We now suppose that the electric fields are monochromatic fields with discrete frequencies !n. This approximation is permissible when it comes to stationary fields in narrow frequency bands. Let's assume the electric field can be as

$$\mathbf{E}(t) = \tilde{\mathbf{E}}(\omega_1)e^{-i\omega_1 t} + \tilde{\mathbf{E}}(\omega_2)e^{-i\omega_2 t} + \tilde{\mathbf{E}}^*(\omega_1)e^{i\omega_1 t} + \tilde{\mathbf{E}}^*(\omega_2)e^{i\omega_2 t} \tag{2.20}$$

In the frequency space we get

$$\mathbf{E}(\omega) = \tilde{\mathbf{E}}(\omega_1)\delta(\omega-\omega_1) + \tilde{\mathbf{E}}(\omega_2)\delta(\omega-\omega_2) + \tilde{\mathbf{E}}^*(\omega_1)\delta(\omega+\omega_1) + \tilde{\mathbf{E}}^*(\omega_2)\delta(\omega+\omega_2). \tag{2.21}$$

Multiplying the two fields $E_j(\omega')E_k(\omega-\omega')$ and integrating over ω' then yields the nonlinear polarization (2.19).

2.2.1 Second Harmonic Generation

As an example, let's look at the term

$$E_j(\omega')E_k(\omega-\omega') = \tilde{E}_j(\omega_1)\tilde{E}_k(\omega_1)\delta(\omega'-\omega_1)\delta(\omega-\omega'-\omega_1) + 15\,\text{terms}. \tag{2.22}$$

The product of the delta functions is equivalent to

$$\delta(\omega'-\omega_1)\delta(\omega-\omega'-\omega_1) = \delta(\omega'-\omega_1)\delta(\omega-2\omega_1), \tag{2.23}$$

thus

$$E_j(\omega')E_k(\omega-\omega') = E_j(\omega_1)E_k(\omega_1)\delta(\omega'-\omega_1)\delta(\omega-2\omega_1) \tag{2.24}$$

Substituting this result into $P_{NL,i}^{(2)}(\omega)$ leads to

$$P_{NL,i}^{(2)}(\omega) = \epsilon_0 \chi_{ijk}^{(2)}(\omega; \omega_1, \omega_1) E_j(\omega_1) E_k(\omega_1) \delta(\omega-2\omega_1) + \cdots \tag{2.25}$$

or

$$P^{(2)}_{NL,i}(2\omega_1) = \epsilon_0 \chi^{(2)}_{ijk}(2\omega_1;\omega_1,\omega_1)E_j(\omega_1)E_k(\omega_1)\delta(\omega - 2\omega_1) + \cdots \tag{2.26}$$

The nonlinear polarization here only has a component at twice the frequency of one of the monochromatic field modes, $\omega = 2\omega_1$. This contribution is linked to frequency doubling (second-harmonic generation, SHG) [16]. The term $P^{(2)}_{NL,i}(2\omega_1)$ drives a wave of frequency $2\omega_1$ in the wave equation (2.1). Analogously, there is of course another term $P^{(2)}_{NL,i}(2\omega_2)$ that drives a wave at frequency $2\omega_2$. The process of frequency doubling is illustrated schematically in Figure 2.2.

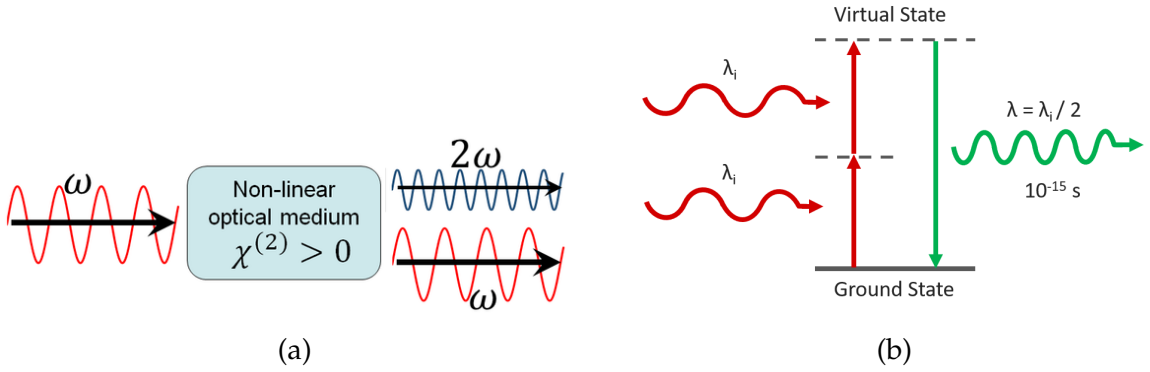

(a) (b)

Fig.}2.2: (a) Second harmonic generation schema. (b) Energy-level diagram describing second-harmonic generation [17].

2.2.2 Optical Rectification

Further processes can be obtained by multiplying out the nonlinear polarization. This is how you find, for example

$$E_j(\omega')E_k(\omega - \omega') = \tilde{E}_j(\omega_1)\tilde{E}^*_k(\omega_1)\delta(\omega' - \omega_1)\delta(\omega - \omega' + \omega_1) \tag{2.27}$$

The product of the delta functions yields

$$\delta(\omega' - \omega_1)\delta(\omega - \omega' + \omega_1) = \delta(\omega' - \omega_1)\delta(\omega), \tag{2.28}$$

hence

$$\tilde{E}_j(\omega_1)\tilde{E}_k(\omega - \omega_1) = \tilde{E}_j(\omega_1)\tilde{E}^*_k(\omega_1)\delta(\omega' - \omega_1)\delta(\omega) \tag{2.29}$$

Substituting this result in $P^{(2)}_{NL}(\omega)$ gives

$$P^{(2)}_{NL,i}(\omega) = \epsilon_0 \chi^{(2)}_{ijk}(0;\omega_1,-\omega_1)\tilde{E}_j(\omega_1)\tilde{E}^*_k(\omega_1)\delta(\omega) + \cdots, \tag{2.30}$$

i.e., a contribution that is frequency independent. This process is called optical rectification. It causes a DC voltage to be generated during the propagation of intense

radiation through a non-linear medium. Conversely, applying a static electric field to a nonlinear crystal produces a polarization that oscillates with frequency ω. From the equation (2.29), we note that this process does not depend on frequency, which means that a nonlinear medium can produce a static electric field. Therefore, consider an electric field $\mathbf{E}(t) = \mathbf{E}_0 + \tilde{\mathbf{E}}(\omega_1)e^{-i\omega_1 t} + \tilde{\mathbf{E}}^*(\omega_1)e^{i\omega_1 t}$. The nonlinear polarization drives a wave of frequency ω_1 whose strength depends on the constant field $\mathbf{E}_0$, i.e., DC voltage. This is the Pockel's effect, which causes the refractive index to depend on the amplitude $\mathbf{E}_0$. For the sake of simplicity assume that the direction of propagation is in one dimension, then the refractive index becomes a Pockel's element

$$n = \sqrt{1 + \chi^{(1)} + 2\chi^{(2)}E_0}. \tag{2.31}$$

2.2.3 Sum and Difference Frequency Generation

Sum frequency generation (SFG) or up conversion is a type of nonlinear optical process in which two or more input laser beams of different frequencies interact with a material or interface, and generate a new beam at the sum of their frequencies, approximately very similar with second harmonic generation, but in sum frequency generation the two input waves different frequencies [18]. The remaining terms in (2.22) that contain contributions from the two monochromatic fields

$$E_j(\omega')E_k(\omega - \omega') = \tilde{E}_j(\omega_1)\tilde{E}_k(\omega_2)\delta(\omega' - \omega_1)\delta(\omega - \omega' - \omega_2), \tag{2.32}$$

hence

$$P^{(2)}_{NL}(\omega) = \epsilon_0\chi^{(2)}_{ijk}(\omega_1 + \omega_2; \omega_1, \omega_2)E_j(\omega_1)E_k(\omega_2)\delta(\omega - \omega_1 - \omega_2) \tag{2.33}$$

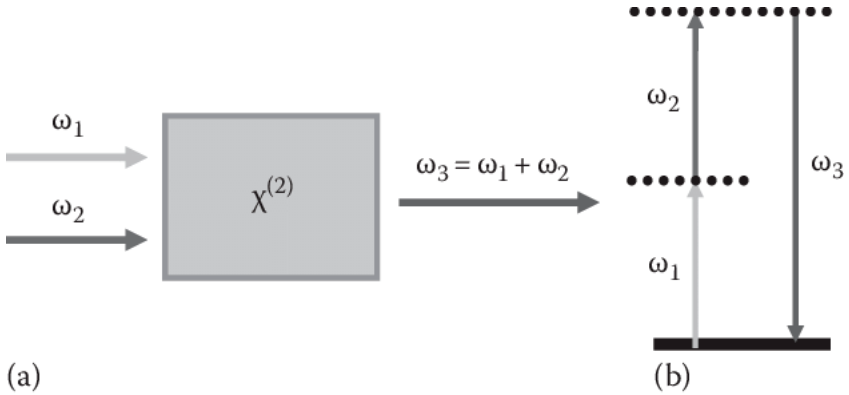

Fig.}2.3: Sum frequency generation and energy level diagram, two laser beams with frequencies ω_1 and ω_2 ($\omega_1 < \omega_2$) are impinging on a nonlinear medium, the SFG process produces a new beam with a frequency of $\omega_3 = \omega_1 + \omega_2$ [19].

SFG is widely used in surface science and materials science to study molecular structures, surface chemistry, and interfacial phenomena such as adsorption, desorption, and surface reactions. It is also used in spectroscopy [20], microscopy, and imaging techniques to investigate biological membranes, liquid interfaces, and other complex systems. The difference frequency generation (DFG) or down conversion is another type of nonlinear optical process that is similar to sum frequency generation (SFG), but instead of generating a new beam at the sum of the frequencies, it generates a new beam at the difference of the frequencies [21].

$$E_j(\omega')E_k(\omega-\omega') = \tilde{E}_j(\omega_1)\tilde{E}_k(\omega_2)\delta(\omega'-\omega_1)\delta(\omega-\omega'+\omega_2), \tag{2.34}$$

thus

$$P^{(2)}_{NL}(\omega) = \epsilon_0\chi^{(2)}_{ijk}(\omega_1-\omega_2;\omega_1,\omega_2)E_j(\omega_1)E_k(\omega_2)\delta(\omega-\omega_1+\omega_2) \tag{2.35}$$

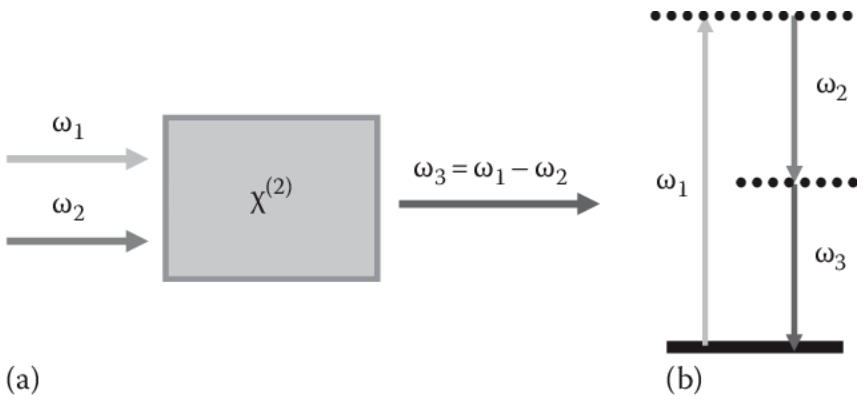

Fig.}2.4: Difference frequency generation and energy level diagram, two input laser beams with frequencies ω_1 and ω_2 ($\omega_1 > \omega_2$) are incident on a material, the DFG process produces a new beam with a frequency of $\omega_3 = \omega_1 - \omega_2$ [22].

DFG is also a powerful tool for studying material properties and interfacial phenomena, and is particularly useful for investigating molecular vibrations and energy transfer processes in condensed phase systems such as liquids, solids, and biological materials. It has applications in various fields such as spectroscopy, microscopy, and imaging techniques [23].
Compared to SFG, DFG is more sensitive to bulk properties of materials, as it can probe bulk vibrations and energy transfer processes, while SFG is more sensitive to surface and interfacial structures and dynamics.
Since the effect of two monochromatic waves with frequencies ω_1 and ω_2 results the generation of new waves with the frequencies

$$\omega_+ = \omega_1 \pm \omega_2. \tag{2.36}$$

The frequencies are either converted up or down (frequency up-conversion and frequency down-conversion). But also should be noted here that all nonlinear optical processes happen if energies and momenta are conserved. Lets now take a closer look at the up-conversion process. The relation

$$\omega_1 + \omega_2 = \omega_3 = \omega_+ \tag{2.37}$$

reflects the energy conservation of the process. For propagating waves, the spatial factors must also be taken into account. The combination of two waves entering the medium

$$e^{i(\mathbf{k}_1 \cdot \mathbf{r} - \omega_1 t)} e^{i(\mathbf{k}_2 \cdot \mathbf{r} - \omega_2 t)} = e^{i(\mathbf{k}_+ \cdot \mathbf{r} - \omega_+ t)} \tag{2.38}$$

implies the momentum conservation condition

$$\mathbf{k}_1 + \mathbf{k}_2 = \mathbf{k}_3 = \mathbf{k}_+. \tag{2.39}$$

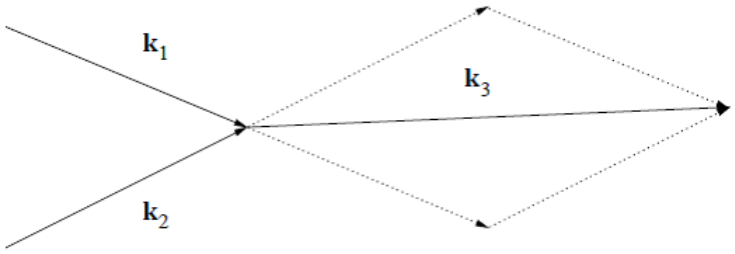

Fig.}2.5: Phase matching in three-wave mixing.

This phase matching means that special processes can be selected out of possible nonlinear processes. This is particularly important when dispersion in the medium has to be taken into account because the refractive index is frequency dependent. To fulfill phase matching condition, birefringence crystals are good candidate for instance (Zinc dioxide, LBO, BBO) [24], [25].
Now let's imagine light with frequencies ω_1 and ω_2 are mixed into a wave with frequency $\omega_3 = \omega_1 + \omega_2$ using phase matching. This new wave with ω_3 can now generate a wave with the difference frequency $\omega_2 = \omega_3 - \omega_1$ in addition to the existing wave frequency ω_1, since this process is also phase-matched. The radiation generated at ω_3 can also produce a difference frequency ω_1 with ω_2. All three waves are mutually coupled to one another within the framework of a three-wave mixing. Such a process is also known as parametric interaction. These parametric processes are involved in

- Optical frequency conversion (OFC): Sum and difference frequency generation ($\omega_3 = \omega_1 + \omega_2$ or $\omega_2 = \omega_3 - \omega_1$) and frequency doubling ($\omega_3 = 2\omega_2$)

- Optical parametric amplification (OPA): A process in which a high-energy pump laser beam is used to generate two lower-energy daughter beams, typically referred to as the signal and idler beams, in a nonlinear optical crystal. This process is based on the phenomenon of parametric amplification, where the energy of the pump beam is converted into the energy of the signal and idler beams, while preserving the overall energy and momentum of the system [26]. The signal and idler beams are generated at frequencies that are lower than the frequency of the pump beam, and the amount of energy transferred from the pump to the signal and idler beams depends on the properties of the nonlinear crystal and the characteristics of the pump beam. OPA can be used to amplify weak signals, to generate new frequencies for use in spectroscopy or imaging, or to produce ultrafast pulses for use in laser-based applications such as microscopy or femtosecond spectroscopy [27].

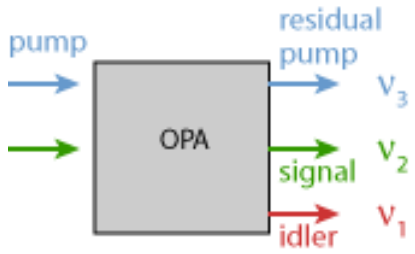

Fig.}2.6: Optical parametric amplification [28]

- Optical parametric oscillator (OPO): OPA with feedback (resonator), produces coherent radiation.

- Spontaneous Parametric Down-Conversion (SPDC): Spontaneous Parametric Down-Conversion (SPDC) is a nonlinear optical process where a single photon is split into two photons of lower frequency (longer wavelength), known as signal and idler photons. The conservation of energy and momentum is maintained during this process, hence the term "down-conversion" [29].
The SPDC process occurs in a nonlinear crystal, where the crystal lattice structure interacts with the incoming photon to generate two new photons. The polarization and direction of the signal and idler photons are correlated or entangled [30].

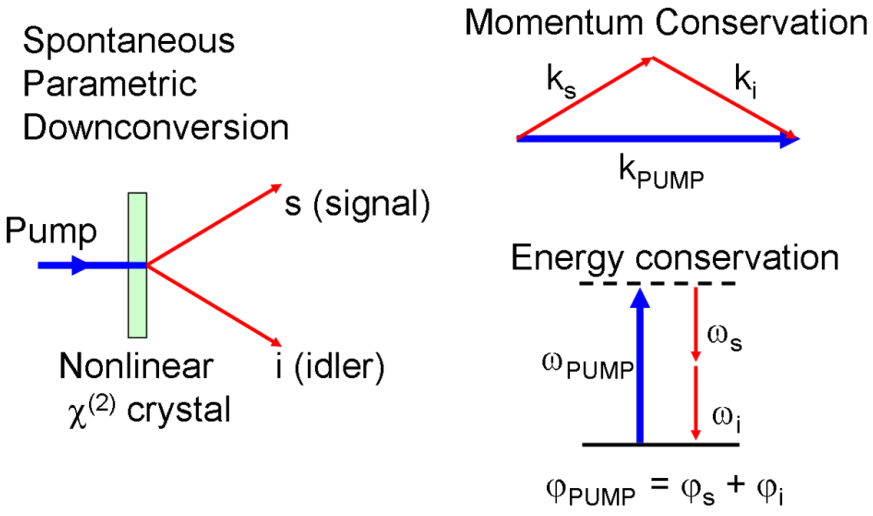

Fig.}2.7: Spontaneous Parametric Down-Conversion [31]

SPDC has been widely used in quantum optics research and applications, including quantum cryptography, quantum teleportation, and quantum computing.

2.3 Third Order Nonlinear Processes

Second-order nonlinearities are not particularly common because they are often excluded by symmetry. In our potential model, for example, this means that the molecular potential is symmetrical and therefore the first correction to the harmonic potential is the form

$$V(x) = V(x_0) + \frac{1}{2!}V''(x_0)x^2 + \frac{1}{4!}V''''(x_0)(x-x_0)^4 + \cdots \tag{2.40}$$

In the phenomenological description, this means that the non-linearity is denoted as [32]:

$$\mathbf{P}^{(3)}_{NL} = \epsilon_0 \int_0^\infty d\tau_1 \int_0^\infty d\tau_2 \int_0^\infty d\tau_3 \vdots\mathbf{E}(t-\tau_1)\mathbf{E}(t-\tau_2)\mathbf{E}(t-\tau_3) \tag{2.41}$$

and in component notation,

$$\mathbf{P}^{(3)}_{NL,i} = \epsilon_0 \int_0^\infty d\tau_1 \int_0^\infty d\tau_2 \int_0^\infty d\tau_3 \chi^{(3)}_{ijkl}(\tau_1,\tau_2,\tau_3)E_j(t-\tau_1)E_k(t-\tau_2)E_l(t-\tau_3) \tag{2.42}$$

We note here that $\chi^{(3)}$ is third rank tensor, and after using Fourier transformation the third order nonlinear optical susceptibility becomes [33]

$$\mathcal{P}^{(3)}_{NL}(\omega) = \epsilon_0 \int_{-\infty}^{\infty} d\omega_1 \int_{-\infty}^{\infty} d\omega_2 \chi^{(3)}_{ijkl}(\omega;\omega_1,\omega_2,\omega_3) E_j(\omega_1) E_k(\omega_2) E_l(\omega_3), \tag{2.43}$$

where the energy conservation $\omega = \omega_1 + \omega_2 + \omega_3$ holds.

2.3.1 Optical Kerr Effect and Intensity-Dependent Refractive Index

We now look at some important special cases and start with a monochromatic wave propagating in a given direction through homogeneous $\chi^{(3)}$ nonlinear medium. [34] Among many nonlinear processes we investigate the contribution where $\mathbf{E}(t) = \tilde{\mathbf{E}}(\omega_0)e^{-i\omega_0 t} + \tilde{\mathbf{E}}^*(\omega_0)e^{i\omega_0 t}$, and its Fourier transform $\mathbf{E}(\omega) = \tilde{\mathbf{E}}(\omega_0)\delta(\omega-\omega_0) + \tilde{\mathbf{E}}^*(\omega_0)\delta(\omega+\omega_0)$. Droping all vector indices we write

$$\mathbf{P}^{(3)}_{NL}(t) = \frac{3}{4}\epsilon_0 \chi^{(3)}(\omega;\omega,\omega,-\omega)|\tilde{E}(\omega)|^2 \tilde{E}(\omega) \tag{2.44}$$

which oscillates at the same frequency as the irradiated monochromatic wave. Substituting this term in wave equation (2.1) and using Fourier Transformation we found

$$\Delta\tilde{E} + \frac{\omega^2}{c^2}\left[1 + \chi^{(1)}(\omega) + \frac{3}{4}\epsilon_0\chi^{(3)}(\omega;\omega,\omega,-\omega)|\tilde{E}(\omega)|^2\right]\tilde{E}(\omega) = 0, \tag{2.45}$$

so the light propagates in medium having effective refractive index

$$n = \sqrt{1 + \chi^{(1)}(\omega) + \frac{3}{4}\epsilon_0\chi^{(3)}(\omega;\omega,\omega,-\omega)|\tilde{E}(\omega)|^2}. \tag{2.46}$$

The index of refraction is now dependent on the intensity. Therefore the propagation of light inside the medium depends on its (instantaneous) intensity. We can write for small nonlinearities

$$n(\omega, I) = n_L(\omega) + \Delta n I(\omega) \quad n_L = \sqrt{1 + \chi^{(1)}(\omega)} \tag{2.47}$$

where the change in refractive index is given by

$$\Delta n = \frac{3\epsilon_0}{8 n_L}\chi^{(3)}(\omega;\omega,\omega,-\omega) \tag{2.48}$$

This is the case of self-Kerr effect, i.e. the intensity-dependent refractive index due to the same monochromatic wave. This effect is responsible for self-phase modulation and self-focusing.

2.3.1.1 Self Focusing

Self-focusing is a phenomenon that occurs when a beam of light or another type of wave (such as a sound wave or a plasma wave) propagates through a medium and focuses on itself due to nonlinearity. This means that the beam of light or wave is able to change the refractive index of the medium during propagation, causing more self-focusing to occur [35]. It is a result of the nonlinear interaction between the wave and the medium, and it can lead to a number of interesting effects, such as the formation of solitons, which are self-contained wave packets that propagate through the medium without changing their shape. Self-focusing can also lead to the generation of intense, localized beams of light or other waves, which have important applications in areas such as laser physics, nonlinear optics, and plasma physics.

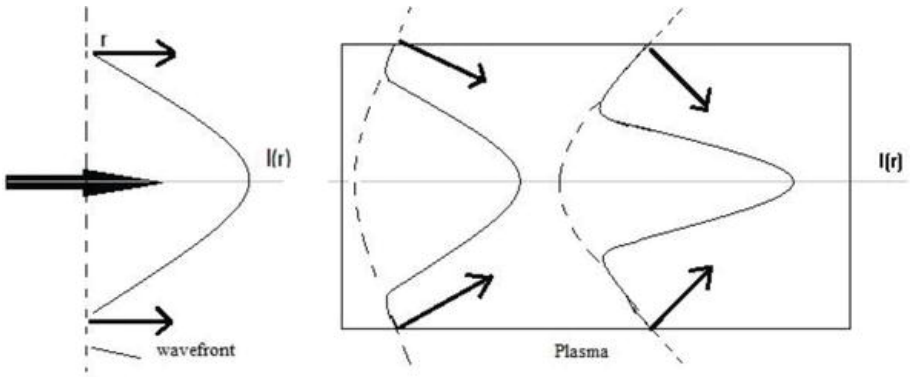

Fig.}2.8: Self focusing wave in nonlinear media [36].

Self-focusing can occur in a variety of media, including gases, liquids, and solids, and it is typically observed at high intensities or powers. It is an important phenomenon in many areas of science and engineering.

2.3.1.2 Self Phase Modulation

Self-phase modulation (SPM) is a nonlinear optical phenomenon that occurs when a high-intensity laser beam propagates through a transparent material, such as an optical fiber or a crystal. In SPM, the intensity of the laser beam changes the refractive index of the material, causing a phase shift in the beam [37].

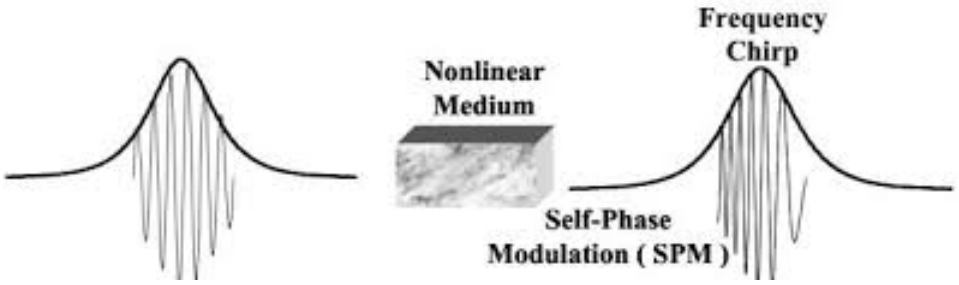

Fig.}2.9: Self phase modulation [38].

The phase velocity v_p of a wave propagating in $z-$direction is defined as

$$\phi(z,t) = -\omega \Delta n I(t) \frac{z}{c} \tag{2.49}$$

whose time derivative is the instantaneous pulse frequency

$$\frac{d\phi}{dt} = -\frac{z\omega\Delta n}{c}\frac{dI}{dt} \tag{2.50}$$

where the chirp frequency is

$$\frac{d\omega}{dt} = -\frac{z\omega\Delta n}{c}\frac{d^2I}{dt^2}. \tag{2.51}$$

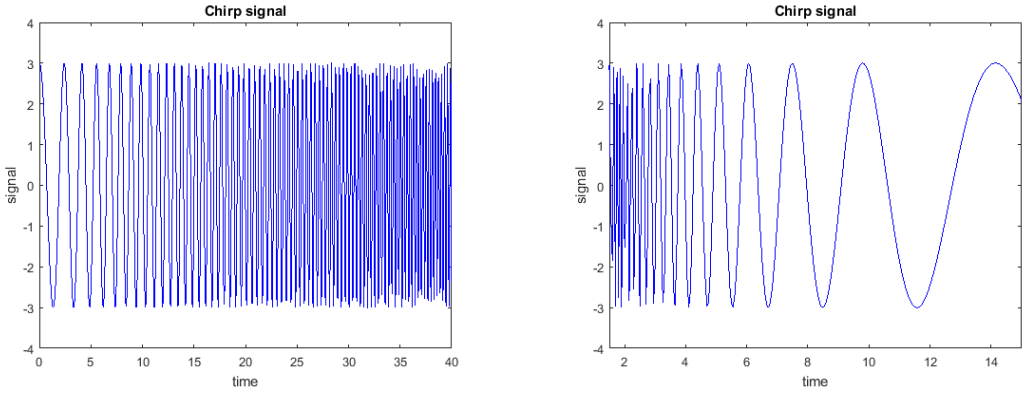

(a) (b)

Fig.}2.10: (a) positive chirp in the case $\frac{d\omega}{dt} > 0$. (b) negative chirp in the case $\frac{d\omega}{dt} < 0$.

When both effects are combined with the properties of propagation in a linear dispersive medium, the frequency dependence of the group time delay leads to a chirp. If you combine the positive chirp of the self-phase modulation of the Kerr effect with a negative linear dispersion, we achieve that both chirps compensate each other and a stable pulse shape, a temporal optical soliton, is generated.

2.3.1.3 Four Wave Mixing

Four-wave mixing (FWM) is a nonlinear optical process that occurs in a medium has $\chi^3(\omega)$ when multiple input laser beams interact with each other. In FWM, three input beams with frequencies ω_1, ω_2 and ω_3 are combined in a nonlinear medium to generate a fourth beam at frequency ω_4. This effect produce nonlinear polarization has the following formula [39]

$$\mathbf{P}^{(3)}_{NL,i}(\omega) = \epsilon_0 \chi^{(3)}_{ijkl}(\omega_4; \omega_1, \omega_2, \omega_3) \tilde{E}_j(\omega_1) \tilde{E}_k(\omega_2) \tilde{E}_l(\omega_3) \tag{2.52}$$

The FWM effect is a type of nonlinear mixing, which means that the output signal is not simply a linear combination of the input signals. Instead, the FWM process involves the conservation of energy and momentum

$$\omega_4 + \omega_3 = \omega_1 + \omega_2 \tag{2.53}$$

$$\mathbf{k}_1 + \mathbf{k}_2 = \mathbf{k}_3 + \mathbf{k}_4 \tag{2.54}$$

from the input beams to the generated output beam, which can have a different frequency, phase, and polarization compared to the input beams. The nonlinearity of the vacuum is responsible for the interaction of four photons, which in free-space quantum electrodynamics is hardly to occur since its probability depends on the factor α^2 (α is the fine structure constant). The FWM effect is often used in optical communication systems to generate new wavelengths for wavelength division multiplexing (WDM) applications. It is a key process in optical fiber amplifiers and in optical signal processing, such as wavelength conversion and signal regeneration. The FWM effect is also used in various other applications, such as in the generation of ultrashort laser pulses [40], quantum information processing [41], and spectroscopy.

2.3.2 Conclusion

In this chapter we presented the main second and third nonlinear optical processes that occur in crystals, so can sum up this processes in the following tables

Second order nonlinear optical processes	
Second harmonic generation [42]	$\omega, \omega \rightarrow 2\omega$ (frequency doubling)
Pockel's effect [43]	$\omega, 0 \rightarrow \omega$ apply static electric field on crystal
Optical rectification [44]	$\omega, -\omega \rightarrow 0$ modulation and switching
Up or down conversion [45]	$\omega_1, \omega_2 \rightarrow \omega_1 \pm \omega_2$ sum or difference frequency conversion

Table}2.1: Second order nonlinear optical processes.

Third order nonlinear optical processes	
Third harmonic generation [46]	$\omega, \omega, \omega \rightarrow 3\omega$ (frequency doubling)
Kerr effect [34]	$\omega, 0, 0 \rightarrow \omega$ Intensity dependent refractive index
Four-wave mixing [41]	$\omega_1, \omega_2, -\omega_3 \rightarrow \omega_4$ (free-space QED)

Table}2.2: Third order nonlinear optical processes.

Bibliography

[1] M. Galletti et al., High efficiency second harmonic generation of nanojoule-level femtosecond pulses in the visible based on bibo, High Power Laser Sci. Eng., vol. 7, pp. 18, doi: 10.1017/hpl.2018.72, 2019.

[2] V. Sasikala and K. Chitra, All optical switching and associated technologies: a review, J. Opt., vol. 47, no. 3, pp. 307317, 2018.

[3] G. New, Introduction to nonlinear optics. Cambridge University Press, 2011.

[4] P. A. Franken, A. E. Hill, C. W. el Peters, and G. Weinreich, Generation of optical harmonics, Phys. Rev. Lett., vol. 7, no. 4, p. 118, 1961.

[5] D. E. Watkins, C. R. Phipps, and S. J. Thomas, Determination of the third-order nonlinear optical coefficients of germanium through ellipse rotation, Opt. Lett., vol. 5, no. 6, pp. 248249, 1980.

[6] H. Kildal and J. C. Mikkelsen, The nonlinear optical coefficient, phasematching, and optical damage in the chalcopyrite AgGaSe2, Opt. Commun., vol. 9, no. 3, pp. 315318, 1973.

[7] A. Krasnok, M. Tymchenko, and A. Alù, Nonlinear metasurfaces: a paradigm shift in nonlinear optics, Mater. Today, vol. 21, no. 1, pp. 821, doi:10.1016/j.mattod.2017.06.007, 2018.

[8] V. Pasiskevicius, Nonlinear Optical Methods for Biophotonics Applications, 2016.

[9] T. Kobayashi, Nonlinear Optics, vol. 45, no. 2. 1989.

[10] M. Joffre, Master Physique et Applications -seconde année (M2) Concepts Fondamentaux de la Physique Optique non-linéaire en régimes continu et femtoseconde, 2014.

[11] F. Zernike and J. E. Midwinter, Applied nonlinear optics. Courier Corporation, 2006.

[12] M. Wegener, Extreme nonlinear optics: an introduction. Springer Science & Business Media, 2005.

[13] T. H. Cooke and J. L. Wood, An algebraic method for solving central force problems, Am. J. Phys., vol. 70, no. 9, pp. 945950, doi: 10.1119/1.1491262, 2002.

[14] R. Wortmann and D. M. Bishop, Effective polarizabilities and local field corrections for nonlinear optical experiments in condensed media, J. Chem. Phys., vol. 108, no. 3, pp. 10011007, 1998.

[15] Y. V. G. S. Murti and C. Vijayan, Physics of Nonlinear Optics. 2021.

[16] A. I. Ferguson, The Elements of Nonlinear Optics, vol. 38, no. 6. 1991.

[17] https://rb.gy/t74e1q

[18] Y. R. Shen, Basic theory of surface sum-frequency generation, J. Phys. Chem. C, vol. 116, no. 29, pp. 1550515509, 2012.

[19] M. Abdullah, F. T. M. Noori, and A. H. Al-Khursan, Second-order nonlinear susceptibility in quantum dot structure under applied electric field, Superlattices Microstruct., vol. 82, pp. 219233, 2015.

[20] F. Vidal and A. Tadjeddine, Sum-frequency generation spectroscopy of interfaces, Reports Prog. Phys., vol. 68, no. 5, p. 1095, 2005.

[21] S. S. Mukrimaa et al., No , vol. 6, no. August. 2016.

[22] https://rb.gy/t74e1q

[23] Y. Liu et al., Optical terahertz sources based on difference frequency generation in nonlinear crystals, Crystals, vol. 12, no. 7, p. 936, 2022.

[24] H. Hellwig, J. Liebertz, and L. Bohatý, Linear optical properties of the monoclinic bismuth borate BiB3O6, J. Appl. Phys., vol. 88, no. 1, pp. 240244, doi: 10.1063/1.373647, 2000.

[25] K. Upadhya et al., Second and third harmonic nonlinear optical process in spray pyrolysed Mg:ZnO thin films, Opt. Mater. (Amst)., vol. 102, doi: 10.1016/j.optmat.2020.109814, 2020.

[26] R. Baumgartner and R. Byer, Optical parametric amplification, IEEE J. Quantum Electron., vol. 15, no. 6, pp. 432444, 1979.

[27] R. C. Shah, R. P. Johnson, T. Shimada, K. A. Flippo, J. C. Fernandez, and B. M. Hegelich, High-temporal contrast using low-gain optical parametric amplification, Opt. Lett., vol. 34, no. 15, pp. 22732275, 2009.

[28] B. Trophème, B. Boulanger, and G. Mennerat, Phase-matching loci and angular acceptance of non-collinear optical parametric amplification, Opt. Express, vol. 20, no. 24, p. 26176, doi: 10.1364/oe.20.026176, 2012.

[29] G. K. Kitaeva and A. N. Penin, Spontaneous parametric down-conversion, J. Exp. Theor. Phys. Lett., vol. 82, pp. 350355, 2005.

[30] C. Zhang, Y. Huang, B. Liu, C. Li, and G. Guo, Spontaneous parametric down-conversion sources for multiphoton experiments, Adv. Quantum Technol., vol. 4, no. 5, p. 2000132, 2021.

[31] https://t.ly/yTdeL

[32] T. Joo, Y. Jia, J. Yu, M. J. Lang, and G. R. Fleming, Thirdorder nonlinear time domain probes of solvation dynamics, J. Chem. Phys., vol. 104, no. 16, pp. 60896108, 1996.

[33] E. Zhu, C. Zhao, and H. Li, Frequency-domain model of optical frequency-comb generation in optical resonators with second-and third-order nonlinearities, Phys. Rev. A, vol. 102, no. 5, p. 53508, 2020.

[34] H. Yildirim and M. Tomak, Intensity-dependent refractive index of a Pöschl-Teller quantum well, J. Appl. Phys., vol. 99, no. 9, 2006.

[35] P. L. Kelley, Self-focusing of optical beams, Phys. Rev. Lett., vol. 15, no. 26, p. 1005, 1965.

[36] https://rb.gy/7i06c0

[37] R. H. Stolen and C. Lin, Self-phase-modulation in silica optical fibers, Phys. Rev. A, vol. 17, no. 4, p. 1448, 1978.

[38] https://rb.gy/qkkx75

[39] C. W. Thiel, Four-wave mixing and its applications, Fac. Washington, Washingt. DC, 2008.

[40] T. Kobayashi, J. Liu, and Y. Kida, Generation and optimization of femtosecond pulses by four-wave mixing process, IEEE J. Sel. Top. Quantum Electron., vol. 18, no. 1, pp. 5465, 2011.

[41] S. Liu, H. Wang, and J. Jing, Two-beam pumped cascaded four-wave-mixing process for producing multiple-beam quantum correlation, Phys. Rev. A, vol. 97, no. 4, p. 43846, 2018.

[42] M. C. Larciprete and M. Centini, Second harmonic generation from ZnO films and nanostructures, Appl. Phys. Rev., vol. 2, no. 3, doi: 10.1063/1.4928032, 2015.

[43] B. Chmielak et al., Pockels effect based fully integrated, strained silicon electro-optic modulator, Opt. Express, vol. 19, no. 18, pp. 1721217219, 2011.

[44] D. A. Nelson and Z. D. Schultz, The impact of optically rectified fields on plasmonic electrocatalysis, Faraday Discuss., vol. 214, pp. 465477, 2019.

[45] M. Tonouchi, Simplified formulas for the generation of terahertz waves from semiconductor surfaces excited with a femtosecond laser, J. Appl. Phys., vol. 127, no. 24, 2020.

[46] J. A. Squier, M. Müller, G. J. Brakenhoff, and K. R. Wilson, Third harmonic generation microscopy, Opt. Express, vol. 3, no. 9, pp. 315324, 1998.

Chapter 3

Semiconductor Nonlinearties

Semiconductor materials are crucial in nonlinear optics due to their ability to generate significant nonlinear optical responses and their suitability for creating integrated devices that combine electronic, semiconductor laser, and nonlinear optical components on a single semiconductor substrate [1]. Semiconductor materials have a distinctive characteristic where their electronic energy states are arranged into broad bands that are separated by forbidden regions [2]. The valence bands are occupied or nearly occupied, while the conduction bands are partially filled or empty. The energy difference between the highest valence band and the lowest conduction band is referred to as the band-gap energy, E_g [3]. Among the kinds of semiconductors which is having highly transparent and conductive materials known as Transparent Conducting Oxides (TCOs) - including but not limited to tin oxide, zinc oxide, zirconium oxide, nickel oxide, and indium oxide - are widely utilized in various fields due to their excellent optical transparency and electrical properties [4]. TCO materials find extensive use in diverse applications such as optoelectronic devices, Low-E windows, Liquid Crystal Displays (LCDs), and plasma screen displays. The materials' remarkable blend of transparency and conductivity is attributed to the inherent oxygen vacancy defects. These defects contribute significantly to the materials' properties increased when doping with suitable dopant atoms [5]. SnO_2 is a semiconductor material, which means that it has properties that are intermediate between those of a conductor and an insulator. Specifically, SnO_2 is an n-type semiconductor, which means that it has an excess of negatively charged electrons that are free to move through the material. This property makes SnO_2 useful in various electronic applications, including as a material for gas sensors, solar cells, and transparent conductive coatings for electronic displays. When SnO_2 is doped with certain impurities, its electrical properties can be further tuned for specific applications [6]. Our current research involves synthesizing highly degenerate n-type semiconductor tin oxide by spry pyrolysis technique with moving nozzle. This de-

generacy is achieved by substituting O^{-2} with a cobalt atom (Co) which acts as an electron donor. The choice of cobalt as a dopant is based on its similarity in ionic radius to tin, which is $R_{(Co^{+2})} = 0.65$Å compared to tin $R_{(Sn^{+4})} = 0.69$Å [7]. A few scientific papers discussed the NLO properties of Co-doped SnO_2 using Semi empirical formula [8].In recent times, there has been a proposal for a nonlinear Lorentz-Duffing oscillator model aimed at forecasting third-order nonlinear optical phenomena [9], [11]. Nonetheless, only a limited number of studies have detailed the process of acquiring third-order nonlinear optical processes from materials using the self-Kerr effect, in which the refractive index variation in due to the intensity of light fields. This is despite the fact that this nonlinear correction is exceptionally minute and challenging to detected. [12].
The aim of this study lies in the utilization of a semi-empirical formula for determining the nonlinear optical parameters of both pure and cobalt-doped tin oxide. It is a widely recognized fact that all materials possess third-order nonlinear processes, as evidenced by the manifestation of the optical Kerr effect, which is observable even in a vacuum. [13]. The selection of tin oxide is primarily based on its ready availability within our laboratory, and it falls within the family of Transparent Conductive Oxides (TCOs), which find extensive applications in the field of modern optics. such as contains high third order nonlinear optical response near plasma frequency because in this domain refractive index of tin oxide thin films very close to zero and also electric permittivity, there are many materials having some effect near plasma frequency knows index near zero (INZ) or epsilon near zero (ENZ) [14]. Furthermore, cobalt is a transition element has three electrons in its outermost orbit, rendering it susceptible to excitation by photons.

3.1 Materials and Methods

The fabrication of the thin films involved the utilization of a spray method decomposition, where a moving nozzle was employed. The spray is generated through gas pressure. Figure 3.1 is illustrate the parts of this device The solution is directed onto a heated aluminum plate in the form of a spray, enabling chemical interaction and leading to the formation of a rigid film once the solution evaporates. This method serves various purposes, including surface treatment and the production of layers with adjustable thickness. It is well-recognized for its simplicity and cost-effectiveness in the manufacturing process [14].

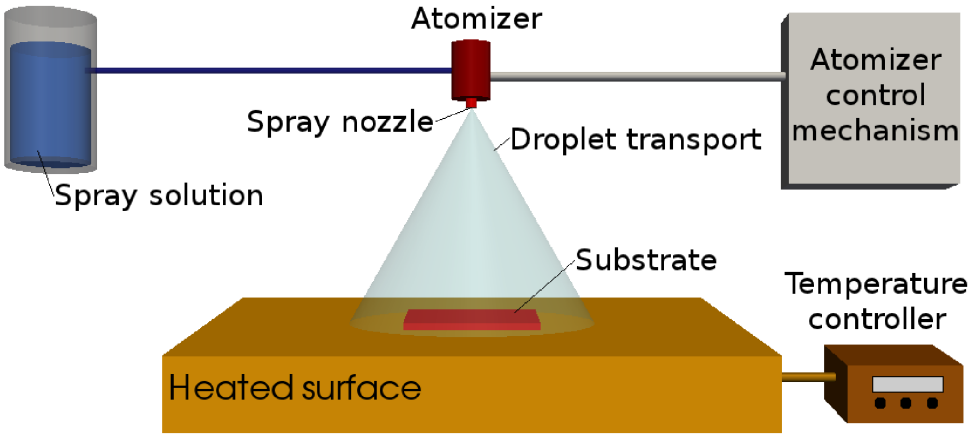

Fig.}3.1: Spray pyrolysis technique

3.1.1 Preparation of samples

Thin films of pure of pure and Co-doped SnO_2 were fabricated using solution evaporation onto a $450^{\circ}C$ heated glass substrates. The spray solution was prepared by dissolving 0.5M tin chloride into a mixture of methanol and double distilled water with ratio of (2/3, 1/3). The mixture was left on the magnetic stirrer until a uniform solution was obtained. Cobalt doping was accomplished by introducing dissolved $Cocl_2$ in double-distilled water. The cobalt molar ratio was from 0 to 5 atomic percent.% (Co/Sn). The ultimate solutions were sprayed onto ultrasonically cleaned glass substrates using a nozzle with a consistent flow rate.The temperature of the substrate was maintained using a digital temperature probe in contact with the aluminum hot plate, as illustrated in figure 3.1.The dimension was fixed between the nozzle and the substrate at 3 cm. Following deposition, the thin films were let to normally cool to ambient temperature. It was visually evident that the deposited films exhibited uniformity and strong rigid to the layers.

3.1.2 Characterization techniques

The structural analysis of both undoped and doped samples was carried out using a PROTO AXRD X-ray diffractometer (30 kV). The instrument scanned an angular range between 20° and 80° with a Cu $K\alpha$ wavelength of 0.15405 nm. To assess the optical transmittance spectrum in the 300-900 nm wavelength range, a Shimadzu Model 1800 UV-visible apparatus was employed. For the evaluation of electrical properties, specifically sheet resistances, a Keithley 2450 instrument was utilized.
Drawing from previous observations where samples with smooth surfaces displayed interference oscillations, the transmittance spectrum of such samples was employed

to estimate film thickness using the following equation. [15].

$$t = \frac{\lambda_1 \lambda_2}{2(n_1\lambda_2 - n_2\lambda_1)} \tag{3.1}$$

Here, n_1 and n_2 represent the refractive indices at λ_1 and λ_2, respectively. The following formula allow to selected this values. [16].

$$n_{1,2} = \sqrt{N_{1,2} + \sqrt{N_{1,2}^2 + S^2}} \tag{3.2}$$

where $N_{1,2}$ are determined from this equation [17]

$$N_{1,2} = \frac{2S(T_M - T_m)}{T_M T_m} + \frac{(S^2 + 1)}{2} \tag{3.3}$$

where T_M is the upper limit of the transmittance at wavelength λ_1 and T_m is lower limit of the transmittance at wavelength λ_2 and S is the refractive index of glass substrate [18]. Samples thicknesses are recapitulated in Table 1 for upcoming use to measure linear optical properties. The thickness increases with cobalt rate doping then decreased at 3 at% and after then it increases at the doping value 5 at%.

3.2 Results and Discussion

3.2.1 Determination of structural properties

The X-ray diffraction spectra of tin oxide films, both pure and doped with varying cobalt concentrations (0-5 at.%.), are presented in figure 3.2. The analysis was conducted using the PROTO AXRD apparatus at 30 kV, scanning an angular range from 20° to 80° with Cu K_α (0.15405 nm) wavelength. The obtained results are summarized in Table 1.

The X-ray analysis revealed that all the tin oxide thin films exhibited a tetragonal crystalline structure of the rutile type, which closely matched the international number card (JCBDS:$N°$.01-072-1147). These films belong to the space group ($N°$.136P42/mnm). Figure 3.2 clearly illustrates the predominant growth orientation of the tin oxide films, which is primarily along the (211) plane. Notably, the intensity of this peak was found to change with varying doping percentages, indicating a sensitivity to doping levels.

Furthermore, the X-ray diffraction patterns exhibited additional peaks corresponding to various crystallographic planes, including (110), (101), (200), (211), and (301). These peaks signify the polycrystalline nature of the samples.

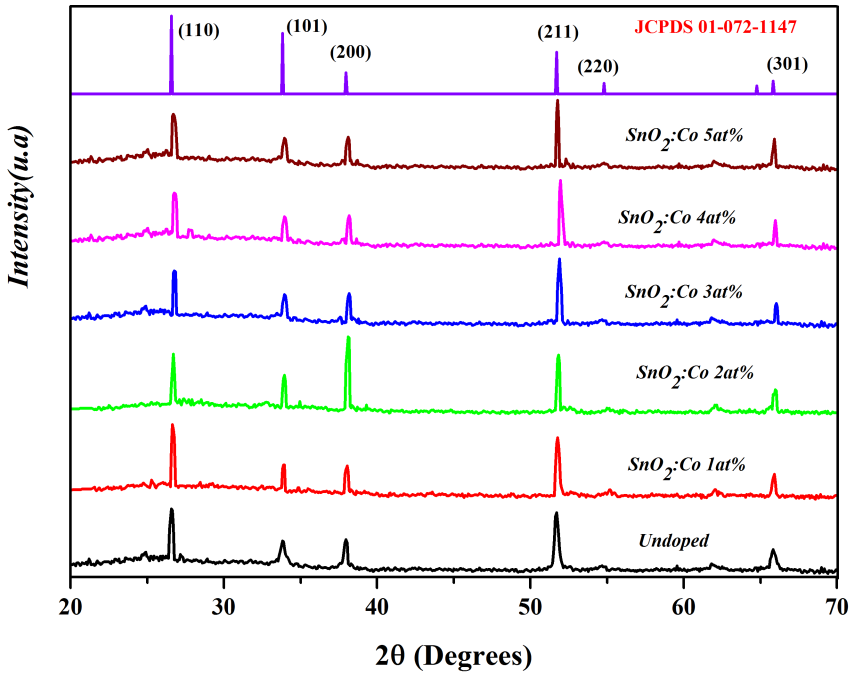

Fig.}3.2: X-ray Diffraction spectra of pure and Co doped SnO_2 thin films.

For further study, the grain sizes, denoted as **D** for all samples, were determined using the relation shown in Equation3.4 [19].

$$\mathbf{D} = \frac{0.9\lambda}{\beta \cos\theta} \tag{3.4}$$

In the provided equations, β represents the full-width at half maximum (FWHM), θ is the diffraction angle, and λ stands for the wavelength of the X-ray radiation, which is the Cu K_α line at 0.15405 nm.

The grid strain and dislocation are quantified as ε and δ, respectively. The magnitudes of these parameters for both undoped and cobalt-doped tin oxide can be computed using the equations as presented in Equation3.5 [20].

$$\varepsilon = \frac{\beta \cos\theta}{4} \tag{3.5}$$

$$\delta = \frac{1}{\mathbf{D}^2} \tag{3.6}$$

Table 1 presents the data for grain size, lattice strain, and dislocation. Notably, when comparing the doped samples with the undoped one, the grain size consistently increases as the cobalt doping level rises, reaching values of approximately 32

nm, whereas the undoped sample maintains a smaller grain size of only 20 nm. This trend may be attributed to the reduction in structural defects, which in turn leads to a decrease in lattice strain and dislocations with higher levels of cobalt doping.

Furthermore, the sheet resistance exhibits an increase in values up to 2% atomic cobalt doping, after which it decreases, reaching its lowest values (30.56) for 4% doping, before increasing once again. This behavior of sheet resistance (R_{sh}) is closely related to the surface dislocation, as indicated in Table 1, suggesting that dislocations may act as electron traps.

Rate of doping at %	**D** [nm]	$\varepsilon/10^3$	$\delta/10^{-3}$ [nm^{-3}]	t [nm]	R_{sh} [Ω]	a [$\mathring{\text{A}}$]	c [$\mathring{\text{A}}$]
0	20.05597	1.88	3.19691	876	34.44	4.74091	3.19083
1	30.83852	1.12991	1.06777	982	50.36	4.71998	3.18000
2	32.68507	1.06345	0.94372	960	44.90	4.71998	3.18000
3	31.83256	1.13977	1.13155	1015	30.88	4.70787	3.18358
4	32.73008	1.12517	1.10871	1030	30.56	4.70787	3.18356
5	32.42054	1.15495	1.18994	997	52.85	4.73042	3.17666

Table}3.1: The characteristics of both pure and $Co - SnO2_2$ thin films include grain size, lattice strain, dislocation density, film thickness, sheet resistance, and structural parameters.

3.2.2 Selection and study the Optical magnitudes

Among the noteworthy characteristics of thin layers, we find their optical attributes, which encompass transmittance T, absorption coefficient α, energy bandgap E_g, and refractive index n among others.

3.2.2.1 Transmittance of Layers

The impact of cobalt doping levels on the transparency of tin oxide thin films was investigated. As shown in figure 3.3b, the transparency of all the samples was examined, revealing that transmittance consistently exceeded 70%. Transparency in tin oxide films is influenced by two key factors: dislocation (δ) and film thickness, as illustrated in figure 3.3a, which delineates the dominant domains.

In the range of 0% to 2% Co-doping, an increase in thickness resulted in reduced dislocation and higher transmittance, defying the Beer-Lambert law. However, in the 2-5% Co-doping range, where dislocation (δ) remained relatively constant, there was

a noticeable decrease in transparency with increasing sample thickness, consistent with the Beer-Lambert law.

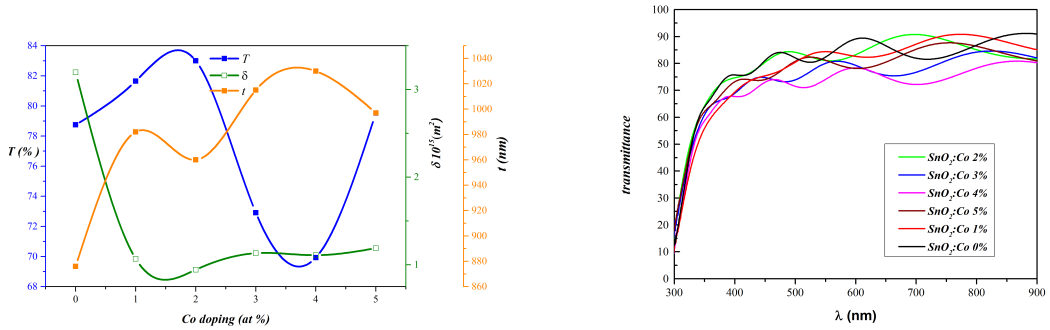

(a) (b)

Fig.}3.3: (a) Variation of transmittance and thickness and dislocation versus doping percentage. (b) UV-visible transmittance versus wavelength

3.2.3 Absorption coefficient

Figure 3.4 displays the changes in the absorption coefficient as a function of wavelength across the range of 300 to 900 nm. The curves reveal a prominent region of high absorption between 300 nm and 350 nm, signifying distinctive material properties associated with band-to-band absorption.

In the wavelength range of 350 nm to 900 nm, all samples exhibit nearly constant absorption coefficient values, suggesting the absence of electronic transitions within the atomic structure of tin oxide or cobalt. Utilizing the Beer-Lambert formula and the transmittance spectrum, it is possible to compute the material's characteristic absorption coefficient. [21].

$$\alpha = \frac{1}{t} \ln \frac{100}{T} \tag{3.7}$$

In the equation, where T stands for transmittance, t denotes the film's thickness, and α represents the absorption coefficient, the absorption coefficient values, as evident from figure 3.4, consistently fall within the range of approximately 1.5×10^3 to $3.5 \times 10^3, \mathrm{cm}^{-1}$.

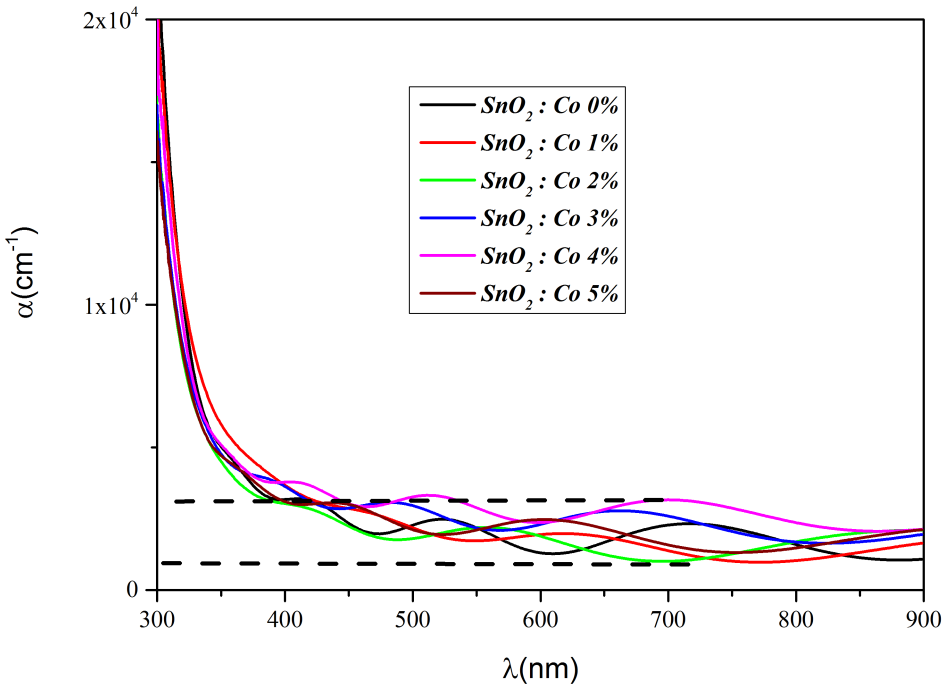

Fig.}3.4: Absorption coefficient versus wavelength

3.2.4 Gap energy

The determination of the energy bandgap (E_g) is a crucial parameter for semiconductor materials, and it is established by employing the Tauc relation [22].

$$f(h\nu) = (\alpha h\nu)^2 = A.(h\nu - E_g) \tag{3.8}$$

In this context, we use the Tauc relation, where E_g signifies the energy bandgap, α stands for the absorption coefficient, A denotes a proportionality constant, and $h\nu$ represents photon energy. The energy bandgap for each sample is determined by locating the point of intersection of the tangent lines with the $h\nu$ axis, as depicted in figure 3.5.

As presented in Table 2, there are discernible alterations in the energy bandgap values corresponding to various doping percentages, which fall within the range of $(3.742 - 3.798eV)$.

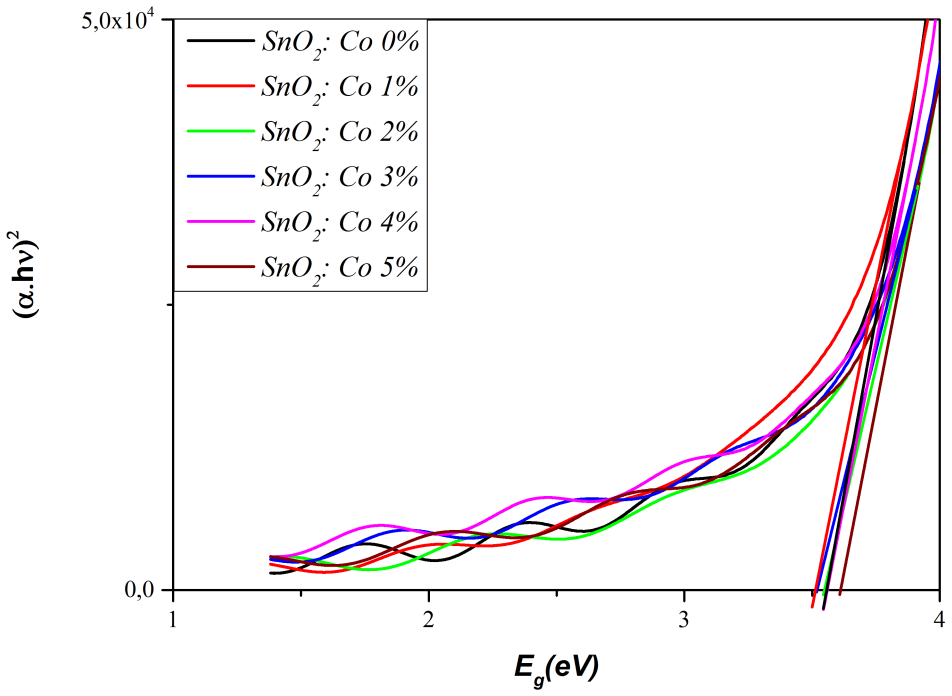

Fig.}3.5: Graphical representation of the Tauc relation as a function of photon energy, comparing pure SnO_2 with Co-doped SnO_2.

3.2.5 Urbach energy

Disorder within the structure of materials, particularly semiconductors, can be elucidated through the concept of Urbach energy, expressed by the following relation.

$$\ln \alpha = \ln \alpha_0 + \frac{h\nu}{E_u} \tag{3.9}$$

where E_u is Urbach energy, $h\nu$ is photon energy, and α is the absorption coefficient. As depicted in figure 3.6, the inverse of the slope of the tangent to each curve serves as the indicator of Urbach energy for each respective sample. The outcomes are tabulated in Table 2.

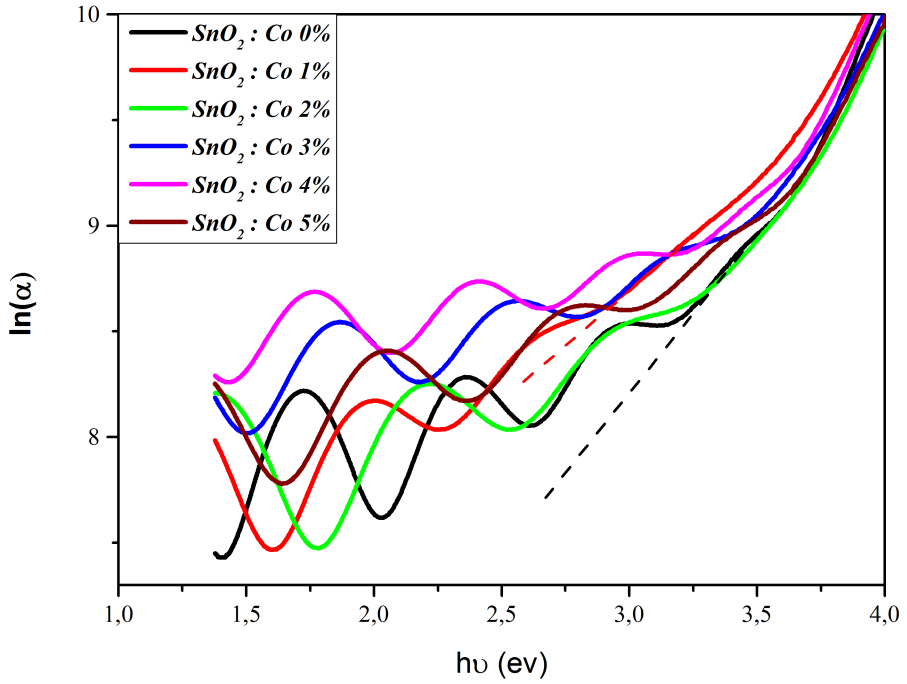

Fig.}3.6: Graphical representation of the Urbach energy relation as a function of photon energy

Doping ratio at%	0	1	2	3	4	5
$E_g(eV)$	3.764	3.7836	3.798	3.776	3.753	3.742
$E_U(eV)$	1.1	0.899	0.64	0.91	0.95	1.019

Table}3.2: Urbach energy and Gap energy values of intrinsic SnO_2 and Co doped SnO_2

Figure 3.7 shows the gap energy and Urbach energy of the samples, confirming the established inverse relationship between these two parameters

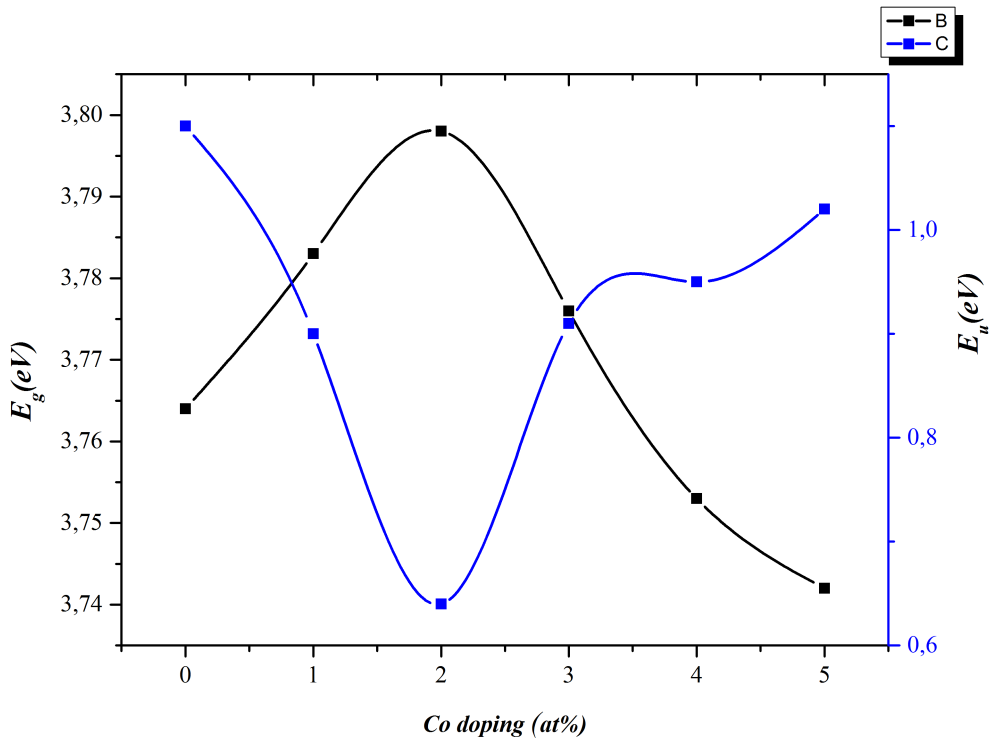

Fig.}3.7: Graphical representation of the Urbach energy and Gap energy as a function of wavelength

3.3 Refraction Index

The refractive index is closely linked to the dispersion and absorption characteristics of materials. It is described as a complex function reliant on the frequency of light. Its real and imaginary components signify dispersion and absorption, respectively, and they are interconnected through Kramers-Kronig relations, as referenced in [23]. The real part (n) of the refractive index can be determined using the following formula.

$$n = \frac{1+R}{1-R} + \left(\frac{2R}{(1-R)^2} - k^2\right)^{\frac{1}{2}} \tag{3.10}$$

In this context, with K representing the extinction coefficient as detailed in [24], R representing reflectance, it's worth noting that k is derived from the formula $k = \alpha\lambda/(4\pi)$, where λ denotes the wavelength and α signifies the absorption coefficient.

The refractive indices of both undoped and cobalt-doped tin oxide for each sample are presented in figure 3.8. Notably, these indices exhibit substantial values

within the absorption regions. This phenomenon can be attributed to the energy loss of photons in these regions ($h\nu$) due to electronic transitions from the valence band to the conduction band.

Minor variations in the refractive index are observable depending on the cobalt doping ratio. It was observed that in samples with 3% and 4% doping, the refractive index reaches its highest values due to chemical constraints. Conversely, in the 1% and 2% doping samples, the refractive index exhibits gradual changes within the visible region, aligning with expectations

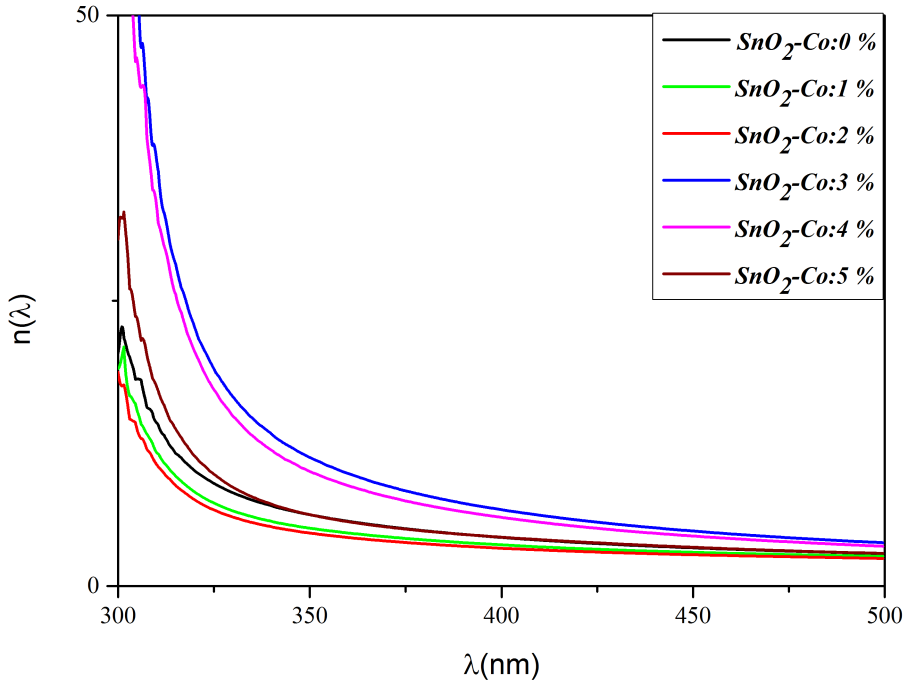

Fig.}3.8: Refractive indexes square versus square wavelength

To clarify the dispersive character of the index of refraction, one could consider the single oscillator model of Sellmeier-Wimple-DiDomenico [25], [26].

$$n^2 - 1 = \frac{E_d E_0}{E_0^2 - (h\nu)^2} \tag{3.11}$$

where E_0 is the energy of effective desperation oscillator and E_d is the desperation energy parameter. The values of E_0 and Ed were calculated from the intersection of the slope with vertical axis. Moreover, the values of spectra moments M_{-1} ,M_{-3},

static refractive index n_0 for ($h\nu$) and $E_{wmp} = E_0/2$ is Wemple energy, for the different rate of Co-doping Sn_2 thin films are given according to references [27], [28].

$$M_{-1} = \frac{E_d}{E_0}; \quad M_{-3} = \frac{M_{-1}}{E_0}; \tag{3.12}$$

$$n_0^2 = 1 + \frac{E_d}{E_0}; \quad E_{wmp} = \frac{E_0}{2} \tag{3.13}$$

Figure 3.9 shows the dispersion of energy in thin films versus photon energy squared.

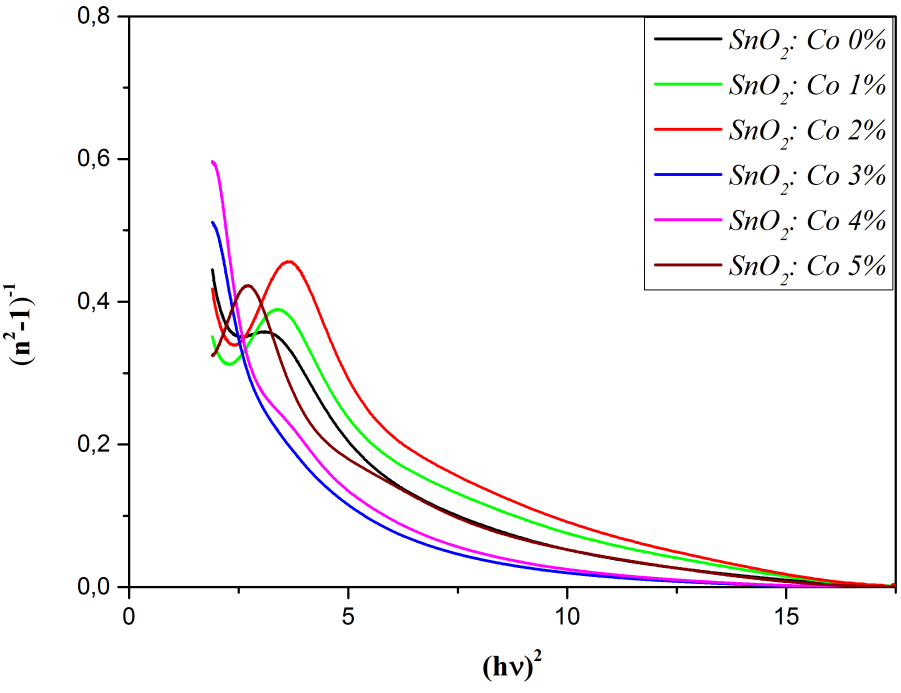

Fig.}3.9: Plot of $(n^2 - 1)^{-1}$ versus $(h\nu)$ for $SnO_2 : Co$ thin films at different rate doping

Rate of doping at.%	$E_0(ev)$	$E_d(ev)$	M_{-1}	M_{-3}	n_0	$E_{wmp}(ev)$	$E_{dir}(ev)$
0	3.715	9.215	2.480	0.180	1.865	1.857	3.764
1	3.9	10.14	2.558	0.170	1.894	1.95	3.7836
2	3.781	8.184	2.164	0.151	1.778	1.890	3.798
3	3.502	9.827	2.8055	0.228	1.950	1.751	3.776
4	3.564	8.973	2.517	0.198	1.875	1.782	3.753
5	3.604	8.875	2.462	0.189	1.860	1.802	3.742

Table}3.3: values of nonlinear optical parameters of pure SnO_2 and Co-doped SnO_2

3.3.1 Photoluminescence properties

Photoluminescence (PL) emission in undoped and $Co : SnO_2$ thin films is attributed to crystal defects in their structure, as shown in figure 3.10b. Pure tin oxide film exhibit four fundamental transitions or emission peaks as we illustrated figure 3.10a, where the excitation wavelength is $260nm$, whereas all other samples display three emission peaks in their PL spectra. These peaks correspond to the transitions between different energetic levels of tin oxide. Oxygen vacancies (V_o) are significant defects that can create a donor band very close to the conduction band edge. The violet and blue emissions observed between 350 to 450 nm in all samples, where the violet emission corresponds to the recombination of electrons and the holes accumulated at the top of the valence band or direct transients of electrons in $Sn - 5p$ levels to holes in $O - 2p$ couldnt appeared , and the blue emission where illustrated for all samples ascribed structural defects that created during the layer growth or by the tin interstitials defect site. The high peaks in green emission observed in the undoped sample 523nm were due to the energetic levels created by singly charged oxygen vacancies, which are crystal defects. In contrast, the weak green emission observed in the other samples is a result of less crystal defects due to the doping percentage Additionally, weak red emission at 604nm is observed in the undoped samples, which can be attributed to the formation of radiative centers by tin (Sn_i) interstitials in the undoped SnO_2 film [29].

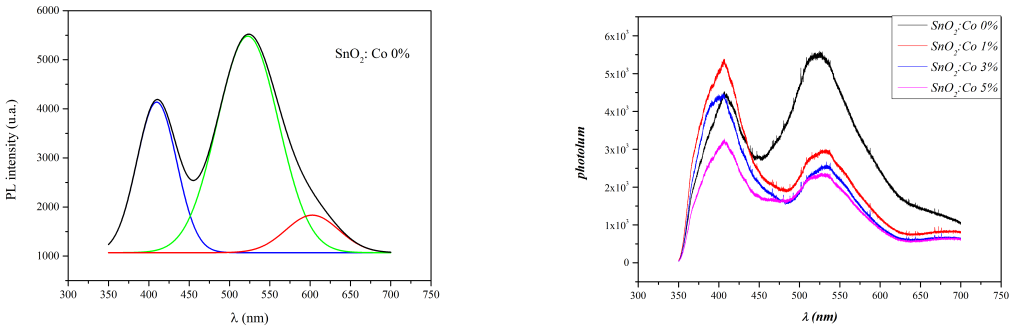

(a) (b)

Fig.}3.10: (a) PL peaks versus Wavelength of all samples. (b) Plot deconvolution of PL spectrum versus Wavelength.

3.4 Nonlinear Optical Properties

Transparent conducting oxides are materials that exhibit nonlinear optical susceptibility parameters and are well-suited for measuring fluctuations in refractive indices through nonlinear optical processes (NP). NP in TCOs primarily hinges on the gap energy value, which must align with the energy of the incident photons. [30]. A semi-empirical approximation formula for the third-order nonlinear optical response is provided as follows [31].

$$\chi^{(3)} = B\left[\frac{n^2-1}{4\pi}\right]^4 \tag{3.14}$$

In the equation, B is a constant with a uniform value for all ionic crystals, specifically 1.7×10^{-10} (esu), and n represents the linear refractive index. The connection between n_2 and $\chi^{(3)}(\omega)$ is outlined in accordance with the reference [32].
As depicted in figure 3.11a, the nonlinear refractive index exhibits a slight decline as the doping percentage increases up to 2%. However, there is a pronounced increase in the nonlinear refractive index in the range of 3% to 4% of doping rates, followed by a significant decrease once again.
figure 3.11b illustrates the variation of the third-order nonlinear susceptibility (TONS) in relation to the doping percentage. Notably, TONS decreases as the doping percentage rises within the 0-2% range, but from 3% to 5%, TONS experiences an ascent due to the expansion of the dielectric volume. A logarithmic scale for TONS is employed to provide enhanced clarity in observing the events occurring in the UV range.

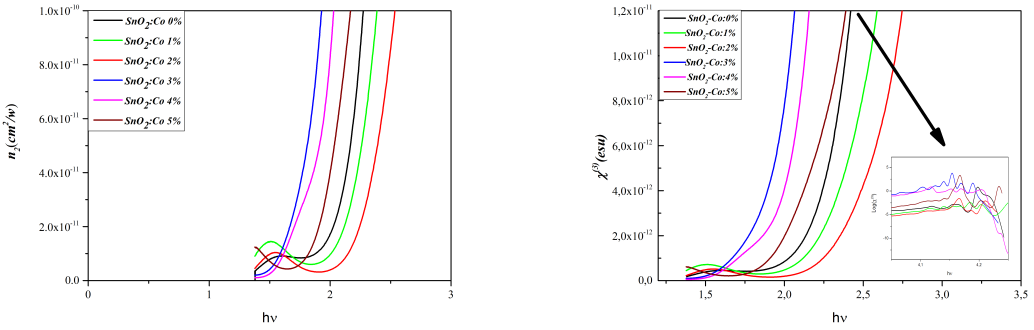

(a) (b)

Fig.}3.11: (a) Plot of nonlinear refractive index versus Wavelength. (b) Graphical representation of the nonlinear optical susceptibility as function of photons energy

The optical Kerr effect is a phenomenon where the refractive index of dielectrics exhibits slight changes in response to variations in light intensity, reflecting a connection between the two.

$$n(\omega, I) = n(\omega) + n_2 I(\omega) \tag{3.15}$$

The linear refractive index, denoted as $n(\omega)$, is defined as the square root of the quantity $n(\omega) = \sqrt{1 + \chi^{(1)}}$, and

$$n_2 = \frac{8}{3n_0}\chi^{(3)}(\omega, \omega, \omega; -\omega) \tag{3.16}$$

is the second-order nonlinear refractive index.

This phenomenon is a part of third-order nonlinear optical processes. It leads to the concentration of light intensity along the propagation axis through self-focusing and alters the phase velocity of the pulse through self-phase modulation. The specific values of the nonlinear refractive indices for each sample are determined at the energy level of half the band gap ($\frac{E_g}{2}$) and are provided in the table shown in figure 3.12.

Rate of doping at.%	0	1	2	3	4	5
$n_2.10^{-11}$	1	0,62	0,328	7,63	4,42	1,67

Table}3.4: values of nonlinear refractive index of pure SnO_2 and Co-doped SnO_2 at $\frac{E_g}{2}$

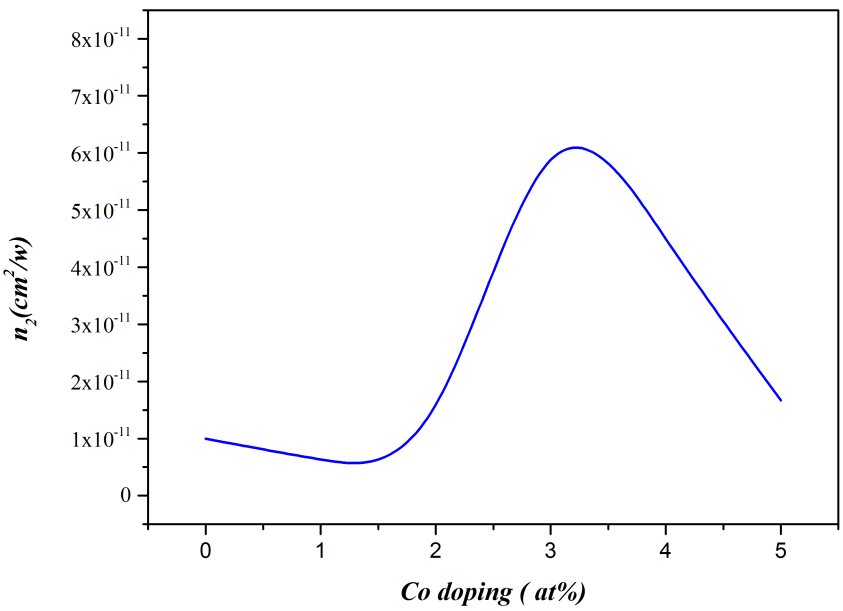

Fig.}3.12: The connection between the doping ratio and nonlinear refractive indices values.

Figure 3.12 illustrates the NRI (Nonlinear Refractive Index) variation. A weak change in NRI is observed for undoped and minimally doped samples, attributed to their high transmittance. Notably, a sharp increase in NRI is observed, reaching its peak at a 3.4% doping ratio, which can be attributed to low transmittance. However,NRI decreases significantly as the doping percentage continues to rise through electronic bonds created by the molecular compound with an increased number of modes.

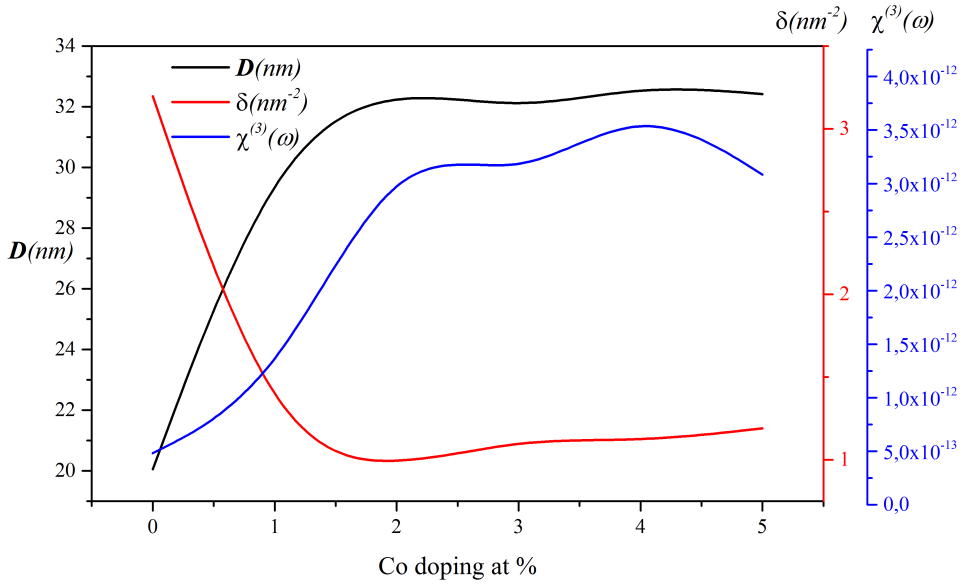

Fig.}3.13: Relation between nonlinear optical response and dislocation and grain size

Thin films are commonly produced with a polycrystalline structure, meaning they consist of spatial domains with different crystal orientations, forming a grain distribution. The nonlinear optical tensor components can be influenced by the mean direction of the optical axis, which may result from the orientation distribution within the grains in certain cases. Grain size is a crucial factor as the generation of a portion of the SH signal occurs at grain boundaries or through defects like stacking faults. The predictability of these circumstances is often challenging, and it heavily relies on both the growth way and the substrate kind. On the other hand, considering these factors, utilizing second harmonic efficiency can serve as a valuable means of indirectly evaluating the crystal quality of a particular thin layer [33]. In addition to nonlinear optical characterization, various treatment techniques, such as x-ray diffraction (XRD) patterns, scanning electron microscopy (SEM), enable the evaluation of grain size distribution. In comparison between characterization methods, nonlinear optical measurements can also serve as a sensitive and appropriate means of examining the textures of thin films produced using different way and conditions. Figure 3.13 illustrates the relationship between cobalt doping percentage, dislocation, grain size, and third-order nonlinear optical susceptibility. The undoped samples exhibit a high dislocation density, resulting in a lower value of nonlinear optical response and grain size. Conversely, samples with lower dislocation density exhibit a higher value of nonlinear optical response and grain size compared to the undoped

samples means that the dislocation and grain size effected on tensor element of third order nonlinear response.

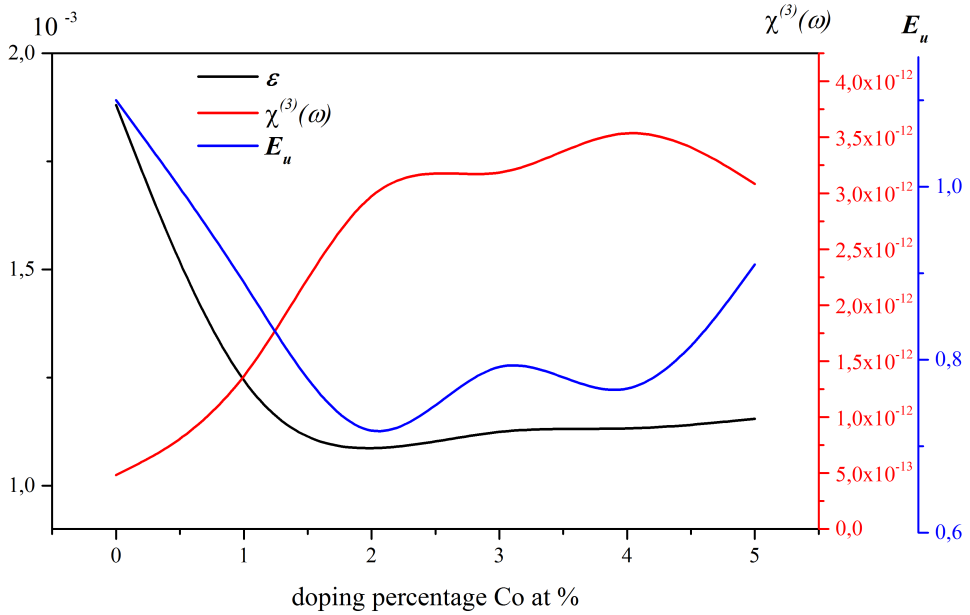

Fig.}3.14: Relation between nonlinear optical response and Urbach energy and grid string

The properties of polycrystalline films, both in terms of electronics and optics, can be impacted by the structure of grain boundaries. Grain boundaries and defects can disrupt the crystalline structure, causing a loss of symmetry that may contribute to second harmonic generation (SHG). Additionally, because neighboring grains have slightly different orientations, changes in crystalline order can occur [34]. Urbach energy is a parameter that characterizes the degree of disorder in the band energy distribution of a material due to crystal defects. This energy is related to the degree of disorder in the material, with higher values indicating greater disorder. It is often used to characterize the quality of thin films. This disorder affects the nonlinear optical susceptibility (NLOS), where the figure 3.14 exhibits the variation between Urbach energy, third order nonlinear optical response, and grid strain versus doping percentage. In undoped samples, high grid strain and Urbach energy values result in low NLOS. However, in other samples with lower values of grid string and Urbach energy, there is a high NLOS, except for 5% doping percentage where there is a slight decrease in NLOS corresponding to an increase in Urbach energy. This confirms that the doping percentage influences the third-order optical tensor elements.

3.5 Mechanisms for the Nonlinear Polarization

In addition to the various mechanisms responsible for linear polarization in matter, there are also several mechanisms responsible for nonlinear polarization. The contribution of these mechanisms to the nonlinear polarization depends on the frequencies of the applied fields and the resulting nonlinear polarizations. At low electromagnetic fields, all of these mechanisms (except the last one) can be considered strictly linear. Nonlinearities become apparent only when the fields are increased [35].
1- **Electronic polarization:** This mechanism refers to the distortion of the outer shell electronic cloud of atoms, ions, and molecules in gases, liquids, or solids, which results in a change in the electronic distribution compared to the undisturbed state. This effect has a very fast response time ($< 10^{-15}s$) and is responsible for several optical frequency mixing phenomena, such as second harmonic and third harmonic generation, sum-frequency mixing, optical parametric oscillation, and four-photon parametric interaction.
2-**Ionic polarization:** This mechanism is based on the optical-field induced relative motion (such as vibrations, rotations in molecules, and optical phonons in solids) between nuclei or ions. Its response time is typically around (10^{-12}) seconds. Examples of effects that use this mechanism include Raman resonance-enhanced four-wave-mixing effects and Raman enhanced refractive index change.
3-**Molecular reorientation:** This mechanism describes the induced electric polarization resulting from the optical-field induced reorientation of anisotropic molecules in a liquid. The response time of this process depends on the rotational viscosity of molecules in the liquid and is typically around (10^{-12}) to (10^{-13}) seconds. Examples of effects that use this mechanism include Stimulated Kerr scattering and the Kerr-effect related refractive index change.
4-**Induced population change:** The polarization contribution from electrons depends on their eigenstates, which can be changed by one-photon or two-photon absorption, as well as other resonant interactions (e.g. in Raman processes). The response time of this mechanism strongly depends on the respective electronic transition but is generally slower than in the previously discussed mechanisms. Examples of this mechanism include all resonance-enhanced nonlinear processes. And there are other mechanisms (Induced acoustic motion, Induced population change, Spatial redistribution of electrons, Spatial redistribution of ions).The fourth mechanism, which appears in semiconductors, can be described by the Sheik-Bahae approximation.

3.5.1 Sheik-Bahae approximation

When examining the nonlinear optical response of tin oxide thin layers, we work under the assumption that $\hbar\omega < E_g$, meaning that the energy of individual photons is sufficiently low to prevent direct transitions between energy bands through single-photon absorption. In such cases, the nonlinear response arises from the absorption of two photons, leading to transitions between virtual levels within the energy gap. This two-photon absorption process (TPA) takes precedence over the one-photon process due to the lower photon energy relative to the band gap. This nonlinear response, often referred to as "photon up-conversion," can be effectively described through a simplified model that focuses solely on the two-photon absorption process. Theoretical investigations conducted by Sheik-Bahae and colleagues (1990, 1991) have demonstrated that the contribution to the imaginary part β of the nonlinear response is significantly influenced by this two-photon absorption process and can be expressed as follows. [36]:

$$\beta = \frac{k\sqrt{E_p}}{n_0^2 E_g^3} F_2\left(\frac{2\hbar\omega}{E_g}\right) \tag{3.17}$$

Where $E_p = 21eV, K$ has value empirically equals to $3, 1.10^3, n_0$ is the linear refractive index, E_g is gap energy, and F_2 is universal function has the following form

$$F_2(2x) = \frac{(2x-1)^{3/2}}{(2x)^5} \quad \text{for} 2x > 1 \tag{3.18}$$

Where $x = \hbar\omega/E_g$. Figure 3.15 illustrates the variation in the TPA coefficient. Below the threshold of $\hbar\omega/E_g$, which is indicative of the absence of virtual energy levels with weak energy in all samples of tin dioxide (SnO_2), the TPA coefficient remains at zero or F_2 is negligible. In the range of $\hbar\omega/E_g = 0.5$ to $\hbar\omega/E_g = 0.71$, there are a peak increase in the TPA coefficient is observed across all samples due to the presence of virtual energy levels in (SnO_2). Beyond $\hbar\omega/E_g = 0.71$, a gradual decline in the TPA coefficient occurs, as this region is in proximity to the energy gap where direct transitions start to emerge. Nevertheless, some distinctions persist due to Urbach energy. These findings are consistent with the results obtained from photoluminescence experiments.

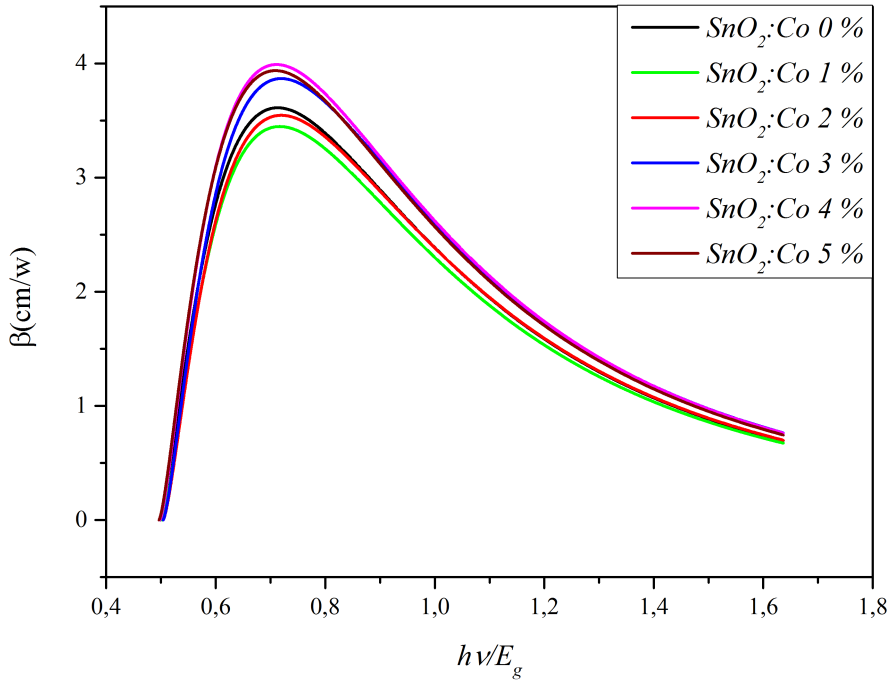

Fig.}3.15: Tow photons absorption coefficient versus $\hbar\omega / E_g$

The coefficient for the NRI can be calculated through the application of the Kramers-Kronig equation:

$$n_2 = \frac{\hbar c \sqrt{E_p}}{2 n_0^2 E_g^4} G_2\left(\frac{2\hbar\omega}{E_g}\right) \tag{3.19}$$

where E_p, k, E_g, n_0 are the previously mentioned values, G_2 is determined using the following formula:

$$G_2(x) = \frac{-2 + 6x - 3x^2 - x^3 - \frac{3}{4}(x^4 + x^5) + 2(1-2x)^{3/2}\theta(1-2x)}{64x^6} \tag{3.20}$$

where θ is the Heaviside step function, to be null when $(1-2x) < 0$.

Figure 3.16 illustrates the nonlinear refractive index (NRI) variation, showcasing its behavior in different energy regimes. Initially, in the weak energy range at $\hbar\omega / Eg = 0.356$, NRI remains quite small, indicating the absence of significant nonlinear processes in this region. Following this, there is a substantial increase in NRI, peaking at $\hbar\omega / Eg = 0.535$, signifying the presence of virtual energy levels within

the energy gap, with an energy of roughly $\hbar\omega = 2.07eV$. These levels contribute significantly to most of the nonlinear processes. However, after reaching its maximum value, NRI sharply decreases until it becomes negligible at $\hbar\omega/Eg = 0.738$. This decline results from the limited number of energy levels in this domain, with electron transitions between virtual levels almost non-existent, except for direct transitions between the valence and conduction bands. Negative values of NRI are associated with optical Stark effect-induced refraction.

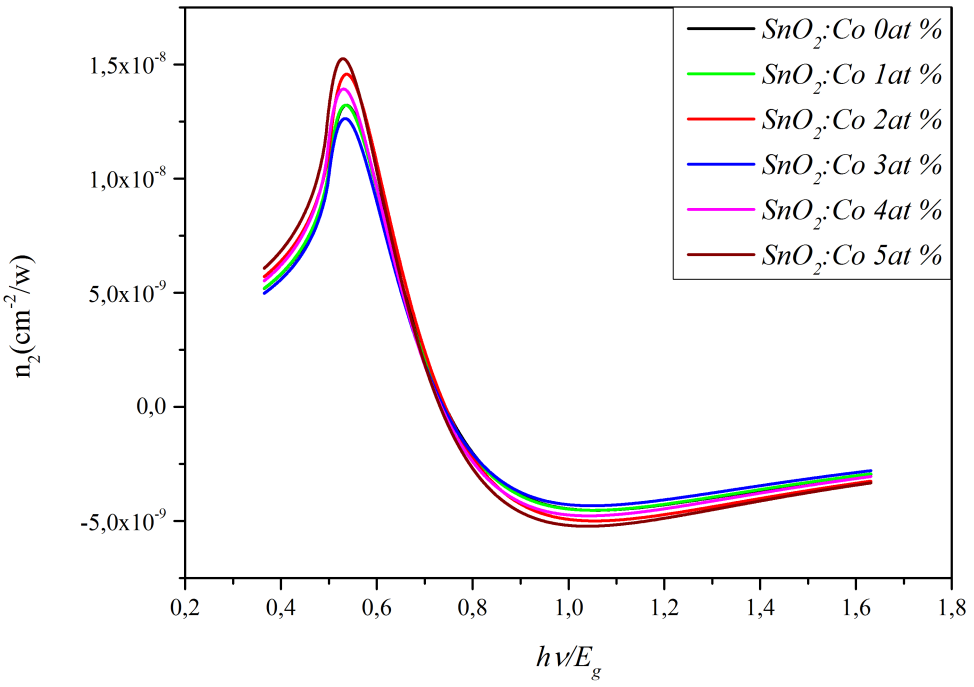

Fig.}3.16: Nonlinear refractive index versus $\hbar\omega/E_g$

3.6 Conclusion

Thin films of cobalt-doped tin oxide were fabricated through the spray pyrolysis technique, with cobalt doping levels ranging from 0% to 5%. The influence of cobalt doping on these films was thoroughly investigated. X-ray diffraction analysis revealed that all tin oxide thin films exhibited a tetragonal crystalline structure consistent with the rutile type, as indicated in the JCBDS card for tin oxide. The preferred orientation for tin oxide film growth was found to be the (211) plane. An interesting observation was made regarding the grain size, which consistently increased with

higher cobalt doping levels, reaching an approximate size of 32 nm, in contrast to the undoped film with a grain size of only 20 nm. The sheet resistance of these films ranged from 30.56 to 52.85. Furthermore, UV-Vis spectrometry results indicated that the transparency of all samples exceeded 70% and was influenced by two factors: film thickness and dislocation (δ). The absorption coefficient values averaged between 1.5 and $3.5 \times 10^3, \mathrm{cm}^{-1}$. Gap energy values for all samples fell within the range of 3.74 to 3.79 eV The study delved into the nonlinear optical response, particularly focusing on the self-Kerr effect, a third-order nonlinear optical effect for a single frequency. The Sheik-Bahae model, with an emphasis on nonlinear refractive index (NRI) and two-photon absorption (TPA), revealed that tin oxide thin films displayed promising nonlinear optical properties, primarily due to the presence of multiple virtual energy levels within the 400-540 nm range. However, it was noted that weak cobalt doping had a minimal impact on the nonlinear optical properties of these tin oxide thin films.

Bibliography

[1] E. Garmire,Nonlinear optics in semiconductors, Phys. Today, vol. 47, no. 5, pp. 42-50, 1994.

[2] A. H. Chin, O. G. Calderón, and J. Kono, Extreme midinfrared nonlinear optics in semiconductors, Phys. Rev. Lett., vol. 86, no. 15, p. 3292, 2001.

[3] V. M. Axt and S. Mukamel, Nonlinear optics of semiconductor and molecular nanostructures; a common perspective, Rev. Mod. Phys., vol. 70, no. 1, p. 145, 1998.

[4] T. Kobayashi, Nonlinear optics of organics and semiconductors. Springer, 1989.

[5] H. J. Queisser and E. E. Haller, Defects in semiconductors: some fatal, some vital, Science (80-.)., vol. 281, no. 5379, pp. 945950, 1998.

[6] A. Benhaoua, A. Rahal, and B. Benhaoua, Superlattices and Microstructures Effect of fluorine doping on the structural , optical and electrical properties of SnO_2 thin films prepared by spray ultrasonic, SUPERLATTICES Microstruct., vol. 70, pp. 6169, doi: 10.1016/j.spmi.2014.02.005, 2014.

[7] M. Mahmoudi, A. Benhaoua, B. Benhaoua,L. Segueni, R. Gheriani, and A. Rahal, study of structural, optical and electrical properties of fluorine, cobalt doped and fluorine-cobalt co-doped tin dioxide SnO_2 , Dig. J. Nanomater. BIOSTRUCTURES, vol. 14, no. 4, pp. 10791086, 2019.

[8] I. M. El Radaf, T. A. Hameed, G. M. El komy, and T. M. Dahy, Synthesis, structural, linear and nonlinear optical properties of chromium doped SnO_2 thin films, Ceram. Int., vol. 45, no. 3, pp. 30723080, doi: 10.1016/j.ceramint.2018.10.189, 2019.

[9] C. C.Wang, Empirical relation between the linear and the third-order nonlinear optical susceptibilities, Phys. Rev. B, vol. 2, no. 6, pp. 20452048, 1970.

[10] M.Scalora, M. A. vincenti, D. DE Ceglia, C. M. Cojocaru, M. Grande, and J. W. Haus Nonlinear Duffing oscillator model for third harmonic generation, J. Opt. Soc. Am. B, vol. 32, no. 10, 2015.

[11] M. Scalora, M. A. vincenti, D. DE Ceglia, C. M. Cojocaru, M. Grande, and J. W. Haus Nonlinear Duffing oscillator model for third harmonic generation, J. Opt. Soc. Am. B, vol. 32, no. 10, 2015.

[12] S. Robertson, Optical Kerr efect in vacuum, Phys. Rev. A, vol. 100, no. 6, 063831, 2019.

[13] D. M. Solís, R. W. Boyd, and N. Engheta, Dependence of the Efficiency of the Nonlinear-Optical Response of Materials on their Linear Permittivity and Permeability, Laser Photonics Rev., vol. 15, no. 12, pp. 111, doi: 10.1002/lpor.202100032, 2021.

[14] J. Matouek and V. Sychra, Atomic Fluorescence Study on Iron, Cobalt, and Nickel, Anal. Chem., vol. 41, no. 3, pp. 518522, doi: 10.1021/ac60272a017, 1969.

[15] I. Kemerchou et al., Processing temperature effect on optical and morphological parameters of organic perovskite CH3NH3PBI3 prepared using spray pyrolysis method, J. nano-and Electron. Phys., no. 11, 3, p. 3011, 2019.

[16] M. Mahmoudi, A. Benhaoua, B. Benhaoua, L. Segueni, R. Gheriani, and A. Rahal, study of structural, optical and electrical properties of fluorine, cobalt doped and fluorine-cobalt co-doped tin dioxide sno2, Dig. J. Nanomater. BIOSTRUCTURES, vol. 14, no. 4, pp. 10791086, 2019.

[17] E. R. Shaaban, I. S. Yahia, and E. G. El-Metwally, Validity of Swanepoels method for calculating the optical constants of thick films, Acta Phys. Pol. A Gen. Phys., vol. 121, no. 3, p. 628, 2012.

[18] R. Swanepoel, Determination of the thickness and optical constants of amorphous silicon, J. Phys. E., vol. 16, no. 12, p. 1214, 1983.

[19] E. Elangovan and K. Ramamurthi, Optoelectronic properties of spray deposited SnO 2: F thin films for window materials in solar cells, J. Optoelectron. Adv. Mater., vol. 5, no. 1, pp. 4554, 2003.

[20] M. Shkir, S. AlFaify, I. S. Yahia, V. Ganesh, and H. Shoukry, Microwave-assisted synthesis of Gd3+ doped PbI2 hierarchical nanostructures for optoelectronic and radiation detection applications, Phys. B Condens. Matter, vol. 508, pp. 4146, 2017.

[21] M. Shkir and S. AlFaify, Tailoring the structural, morphological, optical and dielectric properties of lead iodide through Nd 3+ doping, Sci. Rep., vol. 7, no. 1, pp. 19, 2017.

[22] Z. Y. Banyamin, P. J. Kelly, G. West, and J. Boardman, Electrical and optical properties of fluorine doped tin oxide thin films prepared by magnetron sputtering, Coatings, vol. 4, no. 4, pp. 732746, 2014.

[23] J.Bechhoefer, KramersKronig, Bode, and the meaning of zero Am. J. Phys 79, 1053, 2011.

[24] A. M. Alsaad, A. A. Ahmad, I. A. Qattan, Q. M. Al-Bataineh, and Z. Albataineh, Structural, optoelectrical, linear, and nonlinear optical characterizations of dip-synthesized undoped ZnO and group III elements (B, Al, Ga, and In)-doped ZnO thin films, Crystals, vol. 10, no. 4, p. 252, 2020.

[25] D. J. Borah and A. T. T. Mostako, Investigation on dispersion parameters of Molybdenum Oxide thin films via WempleDiDomenico (WDD) single oscillator model, Appl. Phys. A, vol. 126, no. 10, pp. 113, 2020.

[26] S. H. Wemple and M. DiDomenico Jr, Behavior of the electronic dielectric constant in covalent and ionic materials, Phys. Rev. B, vol. 3, no. 4, p. 1338, 1971.

[27] G. A. Kumar et al., Optical absorption studies of free (H2Pc) and rare earth (RePc) phthalocyanine doped borate glasses, Phys. Chem. Glas., vol. 41, no. 2, pp. 8993, 2000.

[28] S. S. Fouad, I. M. El Radaf, P. Sharma, and M. S. El-Bana, Multifunctional CZTS thin films: structural, optoelectrical, electrical and photovoltaic properties, J. Alloys Compd., vol. 757, pp. 124133, 2018.

[29] Anusha et al., Laser stimulated second and third harmonic optical effects in F: SnO2 nanostructures grown via chemical synthetic route, Opt. Laser Technol., vol. 119, no. May, p. 105636, doi: 10.1016/j.optlastec.2019.105636, 2019.

[30] M. Shkir, V. Ganesh, S. AlFaify, I. S. Yahia, and H. Y. Zahran, Tailoring the linear and nonlinear optical properties of NiO thin films through Cr3+ doping, J. Mater. Sci. Mater. Electron., vol. 29, no. 8, pp. 64466457, doi: 10.1007/s10854-018-8626-y, 2018.

[31] M. A. Islam, J. R. Mou, M. F. Hossain, and M. S. Hossain, Highly transparent conducting and enhanced near-band edge emission of SnO2: Ba thin films and

its structural, linear and nonlinear optical properties, Opt. Mater. (Amst)., vol. 106, p. 109996, 2020.

[32] R. del Coso and J. Solis," Relation between nonlinear refractive index and third-order susceptibility in absorbing media " J. Opt. Soc. Am. B , Vol. 21, No. 3, 2004.

[33] K.-Y. Lo, S.-C. Lo, S.-Y. Chu, R.-C. Chang, and C.-F. Yu, Analysis of the growth of RF sputtered ZnO thin films using the optical reflective second harmonic generation, J. Cryst. Growth, vol. 290, no. 2, pp. 532538, 2006.

[34] C. K. Chen, T. F. Heinz, D. Ricard, and Y. R. Shen, Detection of molecular monolayers by optical second-harmonic generation, Phys. Rev. Lett., vol. 46, no. 15, p. 1010, 1981.

[35] K. Thyagarajan and A. K. Ghatak, Nonlinear optics, Encycl. Mod. Opt., vol. 15, pp. 1026, doi: 10.1016/B978-0-12-809283-5.00700-X, 2018.

[36] H. Garcia and K. Nasiri, Direct and indirect two-photon absorption in Ge within the effective mass approximation, doi: 10.1063/1.3693389,no. May 2016.

General Conclusion

The thesis primarily centered on the optical properties of nonlinear optical materials, with a specific focus on tin oxide doped with cobalt due to its wide-ranging applications in photonics physics. The chapter covered a diverse range of topics, commencing with an exploration of electromagnetic waves in a vacuum and an in-depth examination of polarization, including its three types. The monochromatic nature of light and energy density were subsequently explored, providing the foundational understanding required to delve into Maxwell's equations and their relevance to wave propagation in different media. Particular emphasis was placed on how matter responds to external electromagnetic fields, with the utilization of the dipole oscillator model to extract insights through Kramers-Kronig relations. This analytical approach facilitated comprehension of optical susceptibility in the frequency domain, along with an investigation into the characteristics of laser pulses during their propagation through dispersive media. Throughout this chapter, crucial solutions for wave equations within this context were encountered and analyzed.

The second chapter concentrated on nonlinear optical phenomena and processes. It prominently featured the nonlinear susceptibility of a classical anharmonic oscillator, notably the Lorentz model, elucidating mathematical relationships between polarizability and electron motion. The discussion then shifted to nonlinear optical processes in the frequency domain, including an exploration of second harmonic generation and its representation via energy level diagrams, optical rectification leading to the generation of DC voltage during intense radiation propagation through a nonlinear medium, and the Pockels effect, where a static electric field applied to a nonlinear crystal results in oscillating polarization. The chapter also covered sum and difference frequency generation, emphasizing the importance of phase matching for nonlinear phenomena. The optical parametric oscillation (OPO) effect was introduced, along with applications and the generation of two entangled photons. The chapter concluded with a study of third-order nonlinear processes in the frequency domain, including the Optical Kerr Effect, Intensity-Dependent Refractive Index, and related phenomena such as self-focusing, self-phase modulation, chirp

frequency, and four-wave mixing, third harmoncic generation, all within the context of phase matching condition.

In the third chapter, the focus shifted to semiconductor optical nonlinearity. It began by exploring the origin of nonlinearity in matter. The preparation of cobalt tin oxide thin films, ranging from 0-5% cobalt doping, using the spray pyrolysis technique, was discussed. X-ray diffraction analysis revealed that all tin oxide thin films exhibited a four-angle crystalline structure of a rutile type. The preferred orientation for tin oxide film growth was identified as planar (211), and grain sizes increased with cobalt doping. Sheet resistance ranged from 30.56 to 52.85 Ω for the various doping levels. Using uv-vis spectrometry we study some linear proprieties, where the results indicated high transparency 70% influenced by dislocation σ and film thickness, with average absorption coefficient values in the range of $1.5 - 3.5Œ10^3 cm^{-1}$. Gap energy values for the samples were found to range from 3.74 to 3.79 eV . The nonlinear optical response was investigated in relation to cobalt doping percentage, with a particular focus on the self-Kerr effect as a third-order nonlinear optical effect for a single frequency. The Sheik-Bahae model, biased towards negative refractive index (NRI) and two-photon absorption (TPA), demonstrated the promising nonlinear optical properties of tin oxide thin films in the 400-540 nm region. However, it was noted that weak Co-doping did not significantly impact these properties. The future prospects of our work involves the experimental study of the nonlinear optical response in tin oxide thin films at telecommunication wavelengths, such as 1550 nm, where the refractive index of tin oxide thin films approaches zero (INZ). Because under this condition the materials give high third order nonlinear response.

Scientific Production

International articles

- Effect of weak doping with cobalt over the optical magnitudes of tin oxide thin films.
- Effect of Li doping on the structural, linear and nonlinear optical properties of NiO thin films.
- Nonlinear optical properties of cobalt doped SnO_2 thin films
- Organometallic Perovskite Solar Cell
- Synthesis of Co, Fe co-doped SnO_2: characterization and applications.

International conferences

- Nonlinear optical propreties of pure tin oxide.
- Quantum electrodynamics of arbitrary linear media path integration technique.
- simulation of third order nonlinear susceptibility by using single oscillator model.

national conferences

- semiconductor nonlinear materails.